Wideband Characterisation of UHF Mobile Radio Channels in Urban Areas

by

David Andrew Demery

Thesis submitted in accordance with the requirements of the University of Liverpool for the degree of Doctor in Philosophy.

January 1989

Department of Electrical Engineering & Electronics

ABSTRACT

The presence of multipath propagation in urban environments severely limits the performance of wideband mobile radio communication systems. The characteristics of wideband UHF radio signals at 900MHz are presented for a medium sized UK city.

The complex bandpass impulse response of urban mobile radio channels was measured using a Swept Time-Delay Cross-Correlator channel sounder, having a time resolution of 0.1μs. The implementation of the receiver used in this study incorporated a slightly different configuration to those used in previous studies.

The propagation data were analysed with particular relevance to the development of a representative channel simulation and production of parameters useful to Systems Engineers. In both cases, two-stage characterisations of the data were performed. A Moving Average normalisation method was applied to the processing of the simulation data, whilst a zero-padding technique was used to improve frequency resolution when computing the frequency-domain systems parameters. This is believed to the first time that these techniques have been used in a study of wideband mobile radio channels.

The wideband propagation path is shown to be well modelled by a tapped-delay line, with each tap comprising an uncorrelated Rayleigh modulator, a partially correlated log-normal modulator and a weighting factor. These results lend support to the Gaussian Wide-Sense Stationary Uncorrelated Scattering model which has been proposed for small-scale mobile radio channels. The simplicity in using this model is highlighted by way of an example.

Gross non-stationarity in the channel impulse responses identified the need for formulating cumulative distributions of the small-scale systems parameters. Explanations are presented of how these results may be used in assessing the performance of existing and future mobile radio systems.

ACKNOWLEDGEMENTS

I would like to thank my supervisor, Professor J. D. Parsons, for his continuous support, encouragement and guidance throughout the course of this study. I am extremely grateful to Dr. Adel Turkmani for his humour and enthusiasm during our many invaluable discussions, for which he sacrificed countless hours.

I am indebted to Messrs. Andy(AJ) Richardson, Mike(MTF) Feeney and Steve Mockford, for undertaking the difficult driving duties during the experimental programme; thanks for not complaining guys.

The assistance provided by the members of the Electronics and Mechanical Workshops, with the construction of the channel sounder and rigging of the transmitter sites, is gratefully appreciated.

Acknowledgement is made to the Science and Engineering Research Council and Philips Research Laboratories, Redhill, Surrey for the provision of financial assistance through a C.A.S.E. studentship.

No amount of thanks is sufficient to repay the love, generosity, support and encouragement given to me by my family and friends throughout my education. Last, but by no means least, I would like to say a special thank you to Janet(Are You Going With Me?) Williams for just being there.

This thesis is dedicated to my Mother,
who is more than dedicated to me.
May I someday be, all that she sees in me.

TABLE OF CONTENTS

LIST OF PRINCIPAL SYMBOLS.

APDP	average power delay profile.
ASCII	American national Standards institute Code for Information Interchange.
dB	decibel.
dBc	decibels referenced to the carrier.
DF	double Fourier transform.
DS-SS	direct sequence-spread spectrum.
EBCDIC	extended binary coded decimal interchange code.
F	Fourier transform.
FCF	frequency correlation function.
FDMA	frequency division multiple access.
FFT	fast Fourier transform.
GSM	Groupe Speciale Mobile.
I	inphase component of the channel impulse response.
i.p.s.	inches-per-second.
ISDN	integrated services digital network.
m.p.h.	miles-per-hour.
PABX	private automatic branch exchange.
PMR	private mobile radio.
PN	pseudo-noise.
PRBS	pseudo-random binary sequence.
PRF	pulse repetition frequency.
PRK	phase-reversal keying.
Q	quadrature component of the channel impulse response.
QWSS	quasi-wide-sense stationary.
SAW	surface-acoustic wave.

SCPC	single channel per carrier.
STDCC	swept time-delay cross-correlator.
TACS	total access communications system.
TDMA	time division multiple access.
US	uncorrelated scattering.
VSWR	voltage standing wave ratio.
WSS	wide-sense stationary.
WSSUS	wide-sense stationary uncorrelated scattering.
$A_i(t)$	time-varying amplitude of the i^{th} propagation path.
B_c	coherence bandwidth.
$B\tau$	3dB filter bandwidth-chip rate product.
$B_{0.5}$	coherence bandwidth at 0.5 correlation.
$B_{0.9}$	coherence bandwidth at 0.9 correlation.
c	velocity of electromagnetic waves in free space.
D	average delay.
E[...]	ensemble average.
E_R	average received energy.
f	frequency variable.
f_c	centre or carrier frequency.
$h(\xi)$	impulse response of a linear system.
$h(t, \xi)$	complex envelope of the time-variant channel impulse response - Input Delay-Spread Function.
$H(f, v)$	Output Doppler-Spread Function.
$I_i(t_n)$	discrete time-sequence of the inphase component of the channel impulse response.
k	time scaling factor for a swept time-delay cross-correlator.
$\ell_i(t)$	large-scale amplitude variation.
m	frequency variable/m-sequence length.

N	number of stages in a shift-register/number of records used for spectral estimates/number of points used in a moving average normalisation.
N_0	single-sided noise power spectral density.
$n(t)$	white-noise.
$p(\tau_i)$	individual power delay profile(discrete).
$P(\xi)$	average power delay profile.
$P(\tau_i)$	average power delay profile(discrete).
$P_h(\xi)$	Delay-power spectral density.
$P_h(t,s;\xi)$	Delay cross-power spectral density for a US channel.
$P_h(\tau;\xi)$	Delay cross-power spectral density for a WSSUS channel.
$P_H(f,m;v)$	Frequency-Doppler cross-power spectral density for a WSS channel.
$P_H(\Omega;v)$	Doppler cross-power spectral density for a WSSUS channel.
$P_S(\xi, \eta;v)$	Delay-Doppler cross-power spectral density for a WSS channel.
$P_S(\xi;v, \mu)$	Delay-Doppler cross-power spectral density for a US channel.
$P_S(\xi;v)$	Delay-Doppler cross-power spectral density for a WSSUS channel.
$Q_i(t_n)$	discrete time-sequence of the quadrature component of the channel impulse response.
Re[...]	real part of a complex function.
$R_h(t,s;\xi, \eta)$	autocorrelation function of the Input Delay-Spread Function, $h(t, \xi)$.
$R_h(\tau;\xi, \eta)$	autocorrelation function of $h(t, \xi)$ for a WSS channel.
$R_H(f,m;v, \mu)$	autocorrelation function of the Output Doppler-Spread Function, $H(f, v)$.
$R_H(\Omega;v, \mu)$	autocorrelation function of $H(f, v)$ for a US channel.
$R_m(\xi)$	periodic autocorrelation function of an m-sequence.
$R_n(\xi)$	autocorrelation function of white noise, $n(t)$.

$R_S(\xi, \eta; \nu, \mu)$	autocorrelation function of the Delay Doppler-Spread Function, $S(\xi, \nu)$.
$R_T(f,m;t,s)$	autocorrelation function of the Time-Variant Transfer Function, $T(f,t)$.
$R_T(f,m;\tau)$	autocorrelation function of $T(f,t)$ for a WSS channel.
$R_T(\Omega;t,s)$	autocorrelation function of $T(f,t)$ for a US channel.
$R_T(\Omega;\tau)$	autocorrelation function of $T(f,t)$ for a WSSUS channel.
$R_T(\Omega)$	frequency correlation function for a WSSUS channel.
$R_v(t,s)$	autocorrelation function of the channel output, $v(t)$, for a point-scatterer model.
$R_w(t,s)$	autocorrelation function of the channel output, $w(t)$.
$R_x(t - T)$	autocorrelation function of a matched filter.
s	time variable.
$s_i(t)$	small-scale amplitude variation.
S	delay spread.
S_i	output of i^{th} shift register stage.
$S_m(f_c)$	power spectral density of an m-sequence.
S_S	serial input to shift register.
$S(\xi, \nu)$	Delay Doppler-Spread Function.
t	time variable.
t_n	discrete time-sequence.
t_0	time-delay for the shortest echo path.
T	time variable.
$T(f,t)$	Time-Variant Transfer Function.
$T(t)$	time-variant propagation time-delay.
v	vehicle velocity.
W	profile width.
$z^*(t)$	complex conjugate of $z(t)$.
$\delta(\bullet)$	Dirac delta function.

$d\xi$	perturbation delay.
Δf	frequency difference between two atomic standards.
ζ	initial propagation time-delay.
$\dot{\zeta}$	rate of change of propagation time-delay.
η	time-delay variable.
μ	Doppler-shift variable.
μ_i	mean of the large-scale amplitude variations in the i^{th} time-delay cell.
ν	Doppler-shift variable.
ξ	time-delay variable.
ρ_{jk}	correlation coefficient between the j^{th} and k^{th} time-delay cells.
ρ^2	scatterer cross-section.
σ_i	standard deviation of the large-scale amplitude variations in the i^{th} time-delay cell.
$\sigma(\xi;\nu)$	scattering function for a WSSUS channel/normalised density of cross-section.
$\tilde{\sigma}(\xi;\nu)$	average scatterer cross-section.
τ	time variable.
$\tau_i(t)$	time-varying time-delay of the i^{th} propagation path.
τ_0	clock period of an m-sequence.
$\phi_i(t)$	time-varying phase of the i^{th} propagation path.
ω_c	angular centre(carrier) frequency.
Ω	frequency variable.

CHAPTER 1. INTRODUCTION.

The 1980s have witnessed a dramatic upsurge in the demand for mobile radio services, with currently some two million users in the UK alone. Present mobile communication services are provided by four incompatible systems, namely, Private Mobile Radio(PMR), Wide-Area Paging, Cordless Telephones and Cellular Mobile Radio Telephony. These systems perform subtly different tasks, with no one system being 'ideal', however, they must all compete with each other for a limited frequency spectrum. Despite being the most sophisticated, and hence expensive, system, the interest in cellular radio, introduced to the UK in 1985, has been so great that demand has consistently outstripped even the most optimistic forecasts of subscriber numbers.

In view of these factors, it has been proposed that future mobile radio systems should seek to integrate all these services under a single specification[1.1]. Furthermore, it should also be able to incorporate a number of new features as they become available, e.g., a wireless Private Automatic Branch eXchange(PABX). This has become known as the concept of Personal Communications[1.2].

With the rapid developments taking place in digital technology, it seems almost certain that future systems will be wholly digital. Fortunately this provides two benefits, firstly, it will be possible to provide a wide variety of services over a single mobile network, just as the Integrated Services Digital Network(ISDN) does for fixed networks. Secondly, digital transmissions can operate satisfactorily in the presence of lower carrier-to-interference(C/I) ratios than their analogue counterparts[1.3].

Some of these goals will be achieved with the introduction of the pan-European Digital Cellular Mobile Radio Network in 1991. This system, also known as GSM(Groupe Speciale Mobile) after the organising committee that specified it, will provide digital cellular mobile communications in a single specification for the whole of Europe. In contrast to the present UK TACS(Total Access Communications System) cellular system which uses a Single Channel Per Carrier/Frequency Division Multiple Access(SCPC/FDMA) technique with 25KHz channels, the GSM

scheme will use a 270Kb/s Time Division Multiple Access(TDMA) strategy[1.4]. Since TDMA generally requires a significantly wider operating bandwidth than FDMA, the GSM system can be termed wideband.

A major prerequisite to the specification and design of any future digital mobile radio system is a thorough knowledge of the wideband propagation characteristics of the mobile radio channel. This requirement was the primary motivating factor behind the work presented in this thesis.

Although wideband studies had been undertaken in the United States as early as 1950[1.5], it is the work of Cox[1.6] at 910MHz in New York City around 1972 that can be regarded as the seminal study for wideband mobile radio channels. Using a spread-spectrum type channel sounder, adapted from a study of tropospheric propagation[1.7], he became the first experimentalist to measure the complex bandpass impulse response of the base-station to mobile(receiver) propagation path.

Drawing upon the extensive work of Bello[1.8] on the statistical characterisation of randomly time-variant linear filters, Cox was able to fully characterise the mobile radio channel in terms of parameters that provided a physical insight into the problems caused by multipath propagation. This work was shortly followed by that of Bajwa[1.9] in Birmingham, which was the first such study in the UK.

Both of these studies concentrated heavily on presenting examples of the variability in propagation conditions by way of average power delay profiles(APDP), Frequency Correlation Functions(FCF) and two-dimensional delay-Doppler scattering functions[1.6,1.9]. The latter was employed extensively, since it can be used to identify paths of single scattering from calculation of the propagation time-delays and Doppler spectra(correspondingly angles-of-arrival)[1.9]. Consequently, assumptions were made about the likely modes of propagation in US and UK cities.

By relating the measured scattering functions to the local environments, it is possible to develop a model for multipath channels assuming only single scattering takes place. However, for such a model to produce

accurate results, a detailed environmental database is mandatory. Such databases though are extremely rare.

An alternative approach, proposed by Turin[1.10], was to ascribe statistical distributions to the observed features of the channel, e.g., echo amplitudes, time-delays, phases, etc. Then, provided measurements are undertaken in sufficiently diverse locations, the model becomes essentially independent of the environment.

This approach has gained some favour for software simulations[1.11,1.12] of both mobile and indoor radio propagation. However, one of the fundamental principles of this method is that the echo time-delays form a Poisson sequence[1.13]. Regardless of whether this hypothesis is correct, or not, generating the time-delays from Poisson-distributed random numbers inevitably restricts this model to computer simulations.

In view of these facts, the main emphasis of this study was placed upon the generation of a simple, realistic channel simulation that could be implemented in both hardware and software. The second part of this investigation concentrated on the production of parameters relevant to Systems Engineers seeking to design communication systems that can counteract the impairments of multipath propagation. Since neither of these studies required calculation of the scattering function, in contrast to previous works[1.6,1.9], it is omitted from this study. A brief review of the contents of each chapter, however, now follows.

Chapter 2 contains a complete statistical characterisation of a general class of randomly time-variant linear channels. Simplifications for restricted classes of channels are introduced. A simple point-scatterer model of the mobile radio channel is developed, and is shown to be identical to the more strict statistical model provided the channel conforms to Wide-Sense Stationary Uncorrelated Scattering statistics. The concept of applying two-stage characterisations to channel behaviour is introduced in terms of both simulation and systems studies.

Chapter 3 reviews the various methods of channel sounding. Both narrowband and wideband techniques are discussed, and the advantages

and limitations of each method are highlighted. The reasons for selecting the Swept Time-Delay Cross-Correlator technique in preference to all others are presented.

A detailed description of the main features of the experimental channel sounder are contained in Chapter 4. Factors that are considered essential to good system performance are discussed, and the interrelationships between all the sounder parameters are emphasised. Measures of the back-to-back laboratory tests are presented. Although the Doppler information, contained in the phases of the time-delayed echo paths, was not processed in this study, the channel sounder was designed from the outset to facilitate Doppler measurement. This enables the measured data to be suitable for other wideband studies which may require the phase information. Moreover, during the design stage, no single reference could be found that contained a thorough treatment of the interaction between the parameters of a swept-correlator system. Therefore, sections on Doppler-shift resolution, etc., are included in Chapter 4 for completeness.

Chapter 5 contains a brief description of how the experimental programme was conducted and how the measured data were digitised for mainframe computer analysis.

The methods of experimental data processing are explained in Chapter 6. This chapter is essentially composed of two sections, the first relating to simulation and the second relating to Systems Engineering. Two-stage processing of the data was relevant in both cases, and the small and large-scale techniques are discussed independently.

The results of the experimental field trials in the City of Liverpool are presented in Chapter 7. This chapter follows the layout of Chapter 6, and discusses the small and large-scale characteristics of both the simulation and systems studies. Emphasis is placed upon the simulation results, and the ease of using the proposed model is highlighted by way of an example. The systems results concentrate on cumulative distributions of the small-scale channel descriptors, and comparisons with previous studies are made wherever possible.

Finally, overall conclusions and recommendations for future work are presented in Chapter 8.

REFERENCES

[1.1] MacNamee, R. J. G., Vadgama, S. K. and Gibson, R. W., "Universal mobile telecommunication system - a concept", Presented at IERE Fourth International Conference on Land Mobile Radio, University of Warwick, Coventry, 15-17 December, 1987, Publication No.78.

[1.2] Cox, D. C, "Universal digital portable radio communications", Proc. IEEE, Apr. 1987, Vol. 75, No. 4, pp 436-477.

[1.3] Lindell, F., Swerup, J. and Uddenfeldt, J., "Digital cellular radio for the future", Ericsson Review, No. 3, 1987, pp 160-168.

[1.4] Balston, D. M., "Pan-European cellular radio: or 1991 and all that", Electronics & Commun. Eng. J., Jan./Feb. 1989, pp 7-13.

[1.5] Young, W. R. and Lacy, L. Y., "Echoes in transmission at 450 megacycles from land-to-car radio units", Proc. IRE, March 1950, Vol. 38, pp 255-258.

[1.6] Cox, D. C., "Delay .doppler characteristics of multipath propagation at 910-MHz in a suburban mobile radio environment", IEEE Trans. Antennas Propagat., Sept. 1972, Vol. AP-20, No. 5, pp 625-635.

[1.7] Bailey, C. C., "Characterisation of tropospheric scatter channels by impulse reponse measurements", 16th. Symposium AGARD electromagnetic wave propagation panel(NATO), Dusseldorf, Germany, 31st. Aug. - 4th. Sept. 1970, Part II, pp 39-1 to 39-11.

[1.8] Bello, P. A., "Characterization of randomly time-variant linear channels", IEEE Trans. Commun. Syst., Dec. 1963, Vol CS-11, pp 360-393.

[1.9] Bajwa, A. S., "Wideband characterisation of UHF mobile radio propagation in urban and suburban areas", Ph.D. Thesis, Department of Electronic and Electrical Engineering, University of Birmingham, 1979.

[1.10] Turin, G. L., Clapp, F. D., Johnston, T. L., Fine, S. B. and Lavry, D., "A statistical model of urban multipath propagation", IEEE Trans. Veh. Technol., Feb. 1972, Vol. VT-21, No. 1, pp 1-9.

[1.11] Hashemi, H., "Simulation of the urban radio propagation channel", IEEE Trans. Veh. Technol., Aug. 1979, Vol. VT-28, No. 3, pp 213-225.

[1.12] Saleh, A. A. M. and Valenzuela, R. A., "A statistical model for indoor multipath propagation", IEEE J. Selected Areas Commun., Feb. 1987, Vol. SAC-5, No. 2, pp 128-137.

[1.13] Papoulis, A., "Probability, Random Variables and Stochastic Processes", McGraw-Hill, 1965.

CHAPTER 2. CHARACTERISATION OF MOBILE RADIO CHANNELS.

The mobile radio propagation environment places fundamental limitations on the performance of mobile radio communication systems. Since there is seldom a line-of-sight path between transmitter and receiver, due to blocking by natural, or man-made obstacles, signals arrive at a receiver via scattering from such obstacles. The existence of multiple propagation paths(multipath), with different time-delays, attenuations and phases, gives rise to a highly complex, time-varying multipath transmission channel.

In order for Systems Engineers to be able to determine optimum methods of mitigating the impairments caused by multipath propagation, it is essential for the transmission channel to be satisfactorily characterised. Additionally, the characterisation should take into account the intended application of the channel, i.e, for narrowband or wideband transmissions.

2.1 NARROWBAND PROPAGATION CHARACTERISTICS.

Transmissions where the inverse of the signal bandwidth is very much greater than the propagation path delays are termed narrowband.[1] For narrowband transmissions in a mobile environment, the multipath results in rapid fading of the received signal envelope as the receiver is spatially displaced, see Fig.(2.1), with an associated Doppler spread in the received spectrum[2.1]. The signal strength variations are a result of the random phase additions of the radio waves arriving via many paths. A Rayleigh distribution is usually a good approximation for the statistics of the envelope variations.

However, the distribution departs significantly from Rayleigh when a strong direct path is present. The envelope statistics are better described by a Rician distribution in this case. Nevertheless, areas with strong direct paths typically experience higher signal levels than those with blocked paths, but, low signal areas dominated by multipath fading are of

[1] The statistics appropriate to narrowband transmissions are usually determined from measurements carried out at a single frequency.

most concern in determining mobile radio system performance. Therefore, departures from Rayleigh for higher signal strength areas will not adversely affect the usefulness of a Rayleigh model for most system analysis applications.

Superimposed upon the fast fading is a much slower variation in the average received signal strength(shadow fading). This is due to differences in local terrain, range and/or number of scatterers. The variation in the average signal strength is usually described as a log-normally distributed random variable with a distance-dependent mean.

A description of the channel in terms of Rayleigh distributed fast fading and log-normally distributed shadow fading is usually adequate for the evaluation of narrowband systems.

2.2 WIDEBAND PROPAGATION CHARACTERISTICS.

In addition to the multipath and shadow fading encountered in narrowband systems, the performance of wideband transmissions is also limited by dispersion in the channel due to delay spread[2.1]. For digital systems, the time-delayed echoes, see Fig.(2.2), produce intersymbol interference. Increasing the signal-to-noise ratio will not effect a decrease in error performance, and so, the delay spread sets the lower bound in error performance for a specified data rate.[2]

The delay spread gives rise to frequency-selective fading, which means that two (sufficiently)spaced frequencies fade in an uncorrelated manner. This lack of correlation between message frequency components results in a distorted frequency spectrum. Thus, there is a variation in received signal strength as a function of frequency, similar to the variation in signal strength with location. In analogue frequency modulation systems, the frequency-selectivity limits the maximum useable frequency deviation. Therefore, it is necessary that the characterising functions used to describe the wideband transmission channel explicitly show its fading and dispersive properties.

---

[2] This is often termed the irreducible error rate, however, the error performance can be improved using channel equalisation techniques.

2.2.1 Characterisation Of Multipath Propagation Channels In Terms Of Linear Time-Variant Channels.

The characterisation of the mobile radio propagation channel will be developed from the general description of linear time-variant channels[2.2]. The behaviour of the channel will be described in terms of system functions which give an insight into the physical mechanisms which dominate the channel behaviour.

The first general analytical treatment of time-variant linear filters was presented by Zadeh[2.3]. Kailath[2.4] produced further work, with an emphasis on channel characterisation. He developed various symmetrical mathematical relationships between the filter system functions in time and frequency domains, the relationships being in the form of duality and Fourier transformations. Kailath also proposed canonical channel models by exploiting the finite number of degrees of freedom which all real channels possess due to restrictions on time-duration and bandwidth. Bello[2.2] further developed the work of his predecessors and presented it in a form which readily showed the compactness, symmetry and application of the characterisation approach to general and restricted classes of channels. Bajwa[2.5] reduced the work by Bello by primarily concentrating on the characterisation of practical channels. Alternative descriptions for restricted classes of channels have also been presented[2.6]. These works have principally been used to obtain the statistics presented in the subsequent sections.

2.3 CHARACTERISATION OF DETERMINISTIC CHANNELS.

The propagation channel may be thought of as a device which transforms input signals into output signals. It is, therefore, analogous to a linear filter, but, since the channel behaviour is generally time-variant, the transmission characteristics of the equivalent filter must also be time-varying. Since inputs and outputs to the linear filter can be described in both time and frequency domains, there will be four possible transmission system functions.

2.3.1 Time-domain Function.

Throughout the discussion to follow, real bandpass signals will be represented by their complex envelopes for convenience. The relationship between real and complex signals is expressed as,

$$x(t) = \mathrm{Re}[z(t)\exp\{j2\pi f_c t\}] \tag{2.1}$$

where, Re[...] is the real part of a complex function, $z(t)$ is the complex envelope of $x(t)$ and f_c is a nominal carrier frequency.

The time-domain description of a linear system is specified by the time-impulse response of the system. Application of the superposition principle then expresses the system output, for a known input signal, in the time-domain. Since the channel is time-variant, then the impulse response is also a time-varying function. If the complex envelope of the time-variant impulse response of the channel equivalent filter is given by $h(t, \xi)$, then the complex envelope of the filter output, $w(t)$, is related to the complex envelope of the input, $z(t)$, by the following convolution relationship,[3]

$$w(t) = \int z(t-\xi)h(t, \xi)\, d\xi \tag{2.2}$$

Equation (2.2) provides a physical representation of the channel as a continuum of non-moving, scintillating scatterers, with each elemental scatterer having a gain fluctuation $h(t, \xi)\, d\xi$ and providing delays in the range $(\xi, \xi + d\xi)$. Such a physical representation is shown in Fig.(2.3) in the form of a densely-tapped delay line, composed of differential delay elements and modulators[2.3,2.4,2.6]. It should be noted that equation (2.2) leads to a model where the input is first delayed and then modulated by the differential scattering gain.

It is possible to interpret $h(t, \xi)$ as the channel response at time t to an impulse input ξ seconds in the past. Since a physical channel cannot have an output before the input has arrived, there must be the constraint

---

[3] The limits for all integrals should be assumed to be $(-\infty, \infty)$ unless otherwise indicated.

placed on $h(t, \xi)$ that it vanishes for $\xi < 0$. Therefore, for a physically realisable channel, observed over a finite time, T, the limits of integration for equation (2.2) become (0,T). However, for simplicity, the limits will remain as $(-\infty, \infty)$ with the constraint that the integrand becomes zero outside the range (0,T), thereby ensuring physical realisability.

In his discussion of channel characterisation using system functions, Bello[2.2] called the time-variant impulse response, $h(t, \xi)$, the Input Delay-Spread Function.

2.3.2 Frequency-domain Function.

A general channel characterisation is possible in terms of frequency variables through the use of a function which is the dual of the time-variant impulse response. This dual channel function, $H(f, \nu)$, relates the channel output spectrum to the channel input spectrum in an identical manner to the way $h(t, \xi)$ relates the input-output time functions. This dual characterisation involves representing the output spectrum, $W(f)$, as a superposition of elemental Doppler-shifted and filtered replicas of the input spectrum, $Z(f)$. The transmission characteristics are then described in terms of frequency and frequency-shift variables by the following input-output relationship,

$$W(f) = \int_{f-\nu}^{Z} Z(f - \nu) H(f, \nu)\, d\nu \tag{2.3}$$

Although the Input Delay-Spread Function, $h(t, \xi)$, provides an insight to the contributions from scatterers having different path lengths, i.e., multipath, it does not provide an illustration of the time-varying behaviour of the channel. However, this is possible through a characterisation in terms of $H(f, \nu)$, where the frequency-shift variable, ν, can be thought of as the Doppler-shift experienced in such channels. A differential circuit model representation of equation (2.3) is possible in the form of a dense frequency conversion chain, analogous to the tapped-delay line model used to represent equation (2.2). Figure(2.4) represents equation (2.3) through the use of a bank of filters having transfer functions $H(f, \nu)\, d\nu$, followed by Doppler-shifting frequency converters, producing

Doppler-shifts in the range $(v, v + dv)$ Hz. Bello[2.2] referred to $H(f, v)$ as the Output Doppler-Spread Function.

2.3.3 Time-Variant Transfer Function.

The characterisation of a time-variant channel in terms of the Input Delay-Spread Function, $h(t, \xi)$, relates the output time function to the input time function, whilst a characterisation in terms of the Output Doppler-Spread Function, $H(f, v)$, relates the output spectrum to the input spectrum. Another characterisation approach is possible which relates the output time function in terms of the input spectrum to the channel equivalent filter[2.2]. This function is known as the Time-Variant Transfer Function, $T(f,t)$, and was first introduced by Zadeh[2.3]. The input-output relationship in this case is given by,

$$w(t) = \int Z(f)T(f,t) \exp\{j2\pi ft\}\, df \tag{2.4}$$

Bello[2.2] showed that the Time-Variant Transfer Function equals the Fourier transform of the Input Delay-Spread Function with respect to the delay variable, and also equals the inverse Fourier transform of the Output Doppler-Spread Function with respect to the Doppler-shift variable. That is,

$$T(f,t) = \int h(t, \xi) \exp\{ -j2\pi f\xi\}\, d\xi = \int H(f, v) \exp\{j2\pi vt\}\, dv \tag{2.5}$$

$T(f,t)$ can be considered as a transmission frequency characteristic of the channel and can be determined by direct measurement of the channel cissoidal response. Each of the system functions provides a description of the channel behaviour as a function of two variables, and so, $T(f,t)$ describes the frequency transfer function of the channel as a function of time.

2.3.4 Delay Doppler-Spread Function.

In Sections 2.3.1 and 2.3.2 it was shown that any linear time-variant channel could be represented as a continuum of stationary scintillating scatterers through the use of the Input Delay-Spread Function, or, as a continuum of filters and hypothetical Doppler-shifting elements through use of the Output Doppler-Spread Function. The two functions, therefore, provided a description of only one aspect of the channel dispersive behaviour, either time-delay, or Doppler-shift. A system function will now be introduced that simultaneously provides a description of the multipath behaviour in both time-delay and Doppler-shift domains.

The system functions in the preceding sections were classified according to whether the channel model had its delay operation, or Doppler-shift operation, at the input, or output. Since both time-delays and Doppler-shifts occur in this new characterisation, one of the two operations has to be constrained to the input, and the other to the output. A characterisation which has the time-delay operation at the input, and the Doppler-shift operation at the output can be termed a delay-Doppler domain characterisation of the channel.

The delay-Doppler domain system function is determined by representing the Input Delay-Spread Function, $h(t, \xi)$, as the inverse Fourier transform of its spectrum, $S(\xi, \nu)$, i.e.,

$$h(t, \xi) = \int S(\xi, \nu) \exp\{j2\pi\nu t\}\, d\nu \tag{2.6}$$

Substitution of equation (2.6) in equation (2.2) yields,

$$w(t) = \int\int z(t - \xi) S(\xi, \nu) \exp\{j2\pi\nu t\}\, d\nu\, d\xi \tag{2.7}$$

Inspection of equation (2.7) shows that the output is represented as the sum of delayed and then Doppler-shifted signals. Signals corresponding to delays in the range $(\xi, \xi + d\xi)$, and Doppler-shifts in the range $(\nu, \nu + d\nu)$ Hz have a differential scattering amplitude $S(\xi, \nu)\, d\nu\, d\xi$. The Delay Doppler-Spread Function[2.2], $S(\xi, \nu)$, therefore, explicitly describes the

dispersive behaviour of the channel in terms of both time-delays and Doppler-shifts.

2.3.5 Relationships Between System Functions In Different Domains.

To conclude this discussion on characterisation of deterministic time-variant linear channels it will be worthwhile illustrating the interrelationships between the various system functions[2.2]. These are shown diagrammatically in Fig.(2.5). The lines labelled **F** connecting any two system functions indicate that they are related via single Fourier transforms. It can be seen that the system functions involve two variables, and that any two system functions connected by an **F** have one common variable. This should be regarded as a fixed parameter when employing the Fourier transform relationships involving the other two variables, one of which will be a time variable, and the other a frequency variable. In order to make the **F** notation unique, the following convention is applied; when transforming from a time to a frequency variable a negative exponent is used, whilst in transforming from a frequency to a time variable a positive exponent is used.

2.4 CHARACTERISATION OF RANDOMLY TIME-VARIANT LINEAR CHANNELS.

When the behaviour of the channel is randomly time-variant the system functions in Section 2.3 become stochastic processes. Therefore, in order to describe the statistical characterisation of such a channel exactly, a knowledge of the multidimensional joint probability density distributions of all the system functions is required. While this approach may appear necessary for a precise assessment of the channel behaviour in some instances, it is unlikely to be achieved in practice. A less accurate, but more realistic, approach is based upon a statistical characterisation in terms of correlation functions for the various system functions[2.2,2.6]. This approach is adopted since it enables the autocorrelation function of the channel output to be determined. Furthermore, if the output is a Gaussian process, then a description in terms of the mean and autocorrelation function is statistically complete[2.7].

In the discussion that follows, it is assumed that each of the system functions has a zero ensemble average, so that the deterministic component in the random system function is not included.

2.4.1 Channel Correlation Functions.

In using complex envelopes to represent real bandpass processes a problem arises when attempting to define the autocorrelation function of the original real process, since, in general, two autocorrelation functions are required to uniquely specify it[2.2]. This can be shown from calculation of the autocorrelation function of the real process, $x(t)$, i.e.,

$$\begin{aligned} \mathrm{E}[x(t)x(s)] = \frac{1}{2}\mathrm{Re}\big[\mathrm{E}[z^*(t)z(s)]\exp\{j2\pi f_c(s-t)\}\big] + \\ \frac{1}{2}\mathrm{Re}\big[\mathrm{E}[z(t)z(s)]\exp\{j2\pi f_c(s+t)\}\big] \end{aligned} \tag{2.8}$$

where, E[...] is the ensemble average and $z^*(t)$ is the complex conjugate of $z(t)$. Therefore, two autocorrelation functions defined as,

$$R_z(t,s) = \mathrm{E}[z^*(t)z(s)] \tag{2.9}$$

$$\tilde{R}_z(t,s) = \mathrm{E}[z(t)z(s)] \tag{2.10}$$

are required to specify the autocorrelation function of the real process. However, real random processes that are wide-sense stationary[2.2] require only the autocorrelation function defined in equation (2.9), and in the following discussion, only this form of the autocorrelation function will be used.

The correlation functions for the system functions, defined in Section 2.3, will be defined as,

$$\mathrm{E}[h^*(t,\xi)h(s,\eta)] = R_h(t,s;\xi,\eta) \tag{2.11}$$

$$\mathrm{E}[H^*(f,\nu)H(m,\mu)] = R_H(f,m;\nu,\mu) \tag{2.12}$$

$$\mathrm{E}[T^*(f,t)T(m,s)] = R_T(f,m;t,s) \tag{2.13}$$

$$\mathrm{E}[S^*(\xi,\nu)S(\eta,\mu)] = R_S(\xi,\eta;\nu,\mu) \tag{2.14}$$

Through use of the channel input-output relationships, defined in equations (2.11) to (2.14), it is possible to determine the relationships between the autocorrelation function of the output, and the autocorrelation functions of the system functions. The Input Delay-Spread Function will be considered as an example; the input-output correlation function relationships for the other system functions can be derived in a similar manner.

Using equation (2.2), the autocorrelation function of the channel output, $R_w(t,s)$, can be expressed as,

$$R_w(t,s) = \mathrm{E}[w^*(t)w(s)] = \mathrm{E}\left[\int\int z^*(t-\xi)z(s-\eta)h^*(t,\xi)h(s,\eta)\,d\xi\,d\eta\right] \qquad (2.15)$$

When the input, $z(t)$, is deterministic, equation (2.15) becomes,

$$R_w(t,s) = \int\int z^*(t-\xi)z(s-\eta)\mathrm{E}[h^*(t,\xi)h(s,\eta)]\,d\xi\,d\eta \qquad (2.16)$$

The term $\mathrm{E}[h^*(t,\xi)h(s,\eta)]$ has been defined previously, in equation (2.11), as the autocorrelation function of the Input Delay-Spread Function, $R_h(t,s;\xi,\eta)$. So, equation (2.16) reduces to,

$$R_w(t,s) = \int\int z^*(t-\xi)z(s-\eta)R_h(t,s;\xi,\eta)\,d\xi\,d\eta \qquad (2.17)$$

Therefore, equation (2.17) shows that the autocorrelation function of the channel output, $R_w(t,s)$, can be determined provided that the autocorrelation function, $R_h(t,s;\xi,\eta)$, of the Input Delay-Spread Function, $h(t,\xi)$, is known. For physical channels, $R_h(t,s;\xi,\eta)$ can be measured in the form $\mathrm{E}[h^*(t,\xi)h(t,\eta)]$ via impulse sounding techniques.

2.4.2 Relationships Between Channel Correlation Functions.

In Section 2.3.5 the relationships between the four system functions were shown in terms of single Fourier transforms. It is easily shown[2.2] that the autocorrelation functions of the system functions are related through double Fourier transforms. These relationships are shown di-

agrammatically in Fig.(2.6). The lines marked **DF** indicating a double Fourier transform relationship between the connected correlation functions, and the subscripts, h, H, T and S, indicating the appropriate system function.

Since the channel correlation functions comprise four variables, any two correlation functions linked by a **DF** must have two common variables which should be considered as fixed parameters when employing the double Fourier transform involving the remaining variables. So that the Fourier transform relationships are made unique, the following convention is applied; when transforming from a pair of time(or time-delay) variables to a pair of frequency(or frequency-shift) variables a positive exponent is used to connect the first pair of variables, and a negative exponent to connect the second pair, whilst in transforming from a pair of frequency variables to a pair of time variables the opposite signing procedure is used.

2.5 CLASSIFICATION OF PRACTICAL CHANNELS.

2.5.1 The Wide-Sense Stationary Channel.

Many physical channels possess fading statistics that can be assumed stationary over short periods of time. Whilst these channels are not necessarily stationary in the strict sense, they can be categorised as stationary in the wide-sense(or weakly stationary). Wide-Sense Stationary(WSS) channels have the property that the channel correlation functions are invariant under a translation in time, i.e., the fading statistics do not change over an interval of time, τ. This means that the autocorrelation functions for a WSS channel depend on the variables t and s only through the difference between them, i.e., $\tau(\tau = s - t)$. Therefore, for a WSS channel the autocorrelation functions of the Input Delay-Spread Function, $h(t, \xi)$, and the Time-Variant Transfer Function, $T(f,t)$, become,

$$R_h(t, t + \tau;\xi, \eta) = R_h(\tau;\xi, \eta) \tag{2.18}$$

$$R_T(f,m;t,t + \tau) = R_T(f,m;\tau) \tag{2.19}$$

It will now be shown that WSS channels give rise to uncorrelated Doppler-shift scattering. Using the double Fourier transform relationships in Fig.(2.6), the autocorrelation function of the Delay Doppler-Spread Function, $S(\xi, \nu)$, in terms of the autocorrelation function of the Input Delay-Spread Function, $h(t, \xi)$, is given by,

$$R_S(\xi, \eta;\nu, \mu) = \int\int R_h(t,s;\xi, \eta) \exp\{j2\pi(\nu t - \mu s)\}\, dt\, ds \tag{2.20}$$

Noting that $\tau = s - t$ for a WSS channel, and using equation (2.18), equation (2.20) becomes,

$$R_S(\xi, \eta;\nu, \mu) = \int\int R_h(\tau;\xi, \eta) \exp\{j2\pi(\nu t - \mu t - \mu\tau)\}\, dt\, d\tau \tag{2.21}$$

Rearranging equation (2.21) gives,

$$R_S(\xi, \eta;\nu, \mu) = \int \exp\{j2\pi t(\nu - \mu)\}\, dt \int R_h(\tau;\xi, \eta) \exp\{-j2\pi\mu\tau\}\, d\tau \tag{2.22}$$

The first integral in equation (2.22) can be recognised as a unit impulse at $\nu = \mu$[2.8]. The second integral can be expressed in terms of the Delay-Doppler cross-power spectral density, $P_S(\xi, \eta;\nu)$, by noting that $P_S(\xi, \eta;\nu)$ is the Fourier transform of $R_h(\tau;\xi, \eta)$ with respect to the variable τ, i.e.,

$$P_S(\xi, \eta;\nu) = \int R_h(\tau;\xi, \eta) \exp\{-j2\pi\nu\tau\}\, d\tau \tag{2.23}$$

Therefore, equation (2.22) reduces to,

$$R_S(\xi, \eta;\nu, \mu) = \delta(\nu - \mu) P_S(\xi, \eta;\nu) \tag{2.24}$$

The singular behaviour of the channel correlation function $R_S(\xi, \eta;\nu, \mu)$ in equation (2.24) suggests the following physical interpretation. In terms of the channel model composed of a number of differential scatterers, each producing delays and Doppler-shifts, the contributions from elemental scatterers are uncorrelated if they produce different Doppler-shifts.

In a similar manner, it can be shown that,

$$R_H(f,m;v,\mu) = \delta(v-\mu)P_H(f,m;v) \tag{2.25}$$

where, $P_H(f,m;v)$ is the Fourier transform of $R_T(f,m;\tau)$ with respect to the delay variable, τ, i.e.,

$$P_H(f,m;v) = \int R_T(f,m;\tau)\exp\{-j2\pi v\tau\}\,d\tau \tag{2.26}$$

In terms of a circuit model representation, the singular behaviour of $R_H(f,m;v,\mu)$ implies that the transfer function of the random filters associated with different Doppler-shifts are uncorrelated.

2.5.2 The Uncorrelated Scattering Channel.

Several physical channels(e.g., troposcatter and moon reflection) have been modelled approximately as a continuum of uncorrelated scatterers[2.2]. In an Uncorrelated Scattering(US) channel the contributions from elemental scatterers with different path delays are uncorrelated. So, in a manner analogous to equation (2.24), the autocorrelation of the channel functions will be singular in the time-delay variable. The autocorrelation functions may, therefore, be expressed in terms of delta functions in the time-delay domain as,

$$R_h(t,s;\xi,\eta) = \delta(\eta-\xi)P_h(t,s;\xi) \tag{2.27}$$

$$R_S(\xi,\eta;v,\mu) = \delta(\eta-\xi)P_S(\xi;v,\mu) \tag{2.28}$$

where,

$$P_h(t,s;\xi) = \int R_T(\Omega;t,s)\exp\{j2\pi\xi\Omega\}\,d\Omega \tag{2.29}$$

$$P_S(\xi;v,\mu) = \int R_H(\Omega;v,\mu)\exp\{j2\pi\xi\Omega\}\,d\Omega \tag{2.30}$$

Equations (2.29) and (2.30) define the Delay and Delay-Doppler cross-power spectral densities respectively.

Bello[2.2] discovered that US and WSS channels are time-frequency duals. Consequently, the US channel can be regarded as possessing WSS statistics in the frequency variable, so, the autocorrelation functions depend only on the frequency difference between the variables, e.g., f and m, i.e., $\Omega(\Omega = m - f)$. Therefore, the autocorrelation functions of the Output Doppler-Spread Function, $H(f, \nu)$, and the Time-Variant Transfer Function, $T(f,t)$, become,

$$R_H(f,f+\Omega;\nu,\mu) = R_H(\Omega;\nu,\mu) \tag{2.31}$$

$$R_T(f,f+\Omega;t,s) = R_T(\Omega;t,s) \tag{2.32}$$

It is now possible to show that the expressions in equations (2.27) and (2.28) are correct by way of an example. From Fig.(2.6) the relationship between the autocorrelation of the Input Delay-Spread Function, $R_h(t,s;\xi,\eta)$, and the Time-Variant Transfer Function, $R_T(f,m;t,s)$, is,

$$R_h(t,s;\xi,\eta) = \int\int R_T(f,m;t,s)\exp\{-j2\pi(f\xi - m\eta)\}\,df\,dm \tag{2.33}$$

Noting that $\Omega = m - f$ for a US channel, and using equation (2.32), equation (2.33) becomes,

$$R_h(t,s;\xi,\eta) = \int\int R_T(\Omega;t,s)\exp\{-j2\pi(f\xi - f\eta - \Omega\eta)\}\,df\,d\Omega \tag{2.34}$$

Rearranging equation (2.34) gives,

$$R_h(t,s;\xi,\eta) = \int \exp\{j2\pi f(\eta-\xi)\}\,df \int R_T(\Omega;t,s)\exp\{j2\pi\eta\Omega\}\,d\Omega \tag{2.35}$$

The first integral in equation (2.35) can be recognised as a unit impulse at $\eta = \xi$. The second integral can be expressed in terms of the Delay cross-power spectral density, $P_h(t,s;\xi)$, by noting that $P_h(t,s;\xi)$ is the Fourier transform of $R_T(\Omega;t,s)$ with respect to the variable Ω, i.e.,

$$P_h(t,s;\xi) = \int R_T(\Omega;t,s)\,\exp\{j2\pi\xi\Omega\}\,d\Omega \tag{2.36}$$

It can be seen that this agrees with equation (2.29). Therefore, equation (2.35) reduces to,

$$R_h(t,s;\xi,\eta) = \delta(\eta-\xi)P_h(t,s;\xi) \tag{2.37}$$

This agrees with equation (2.27): equation (2.28) can be proved in a similar manner.

The singular behaviour of the channel correlation function $R_S(\xi,\eta;\nu,\mu)$ has the following interpretation for a physical channel. In terms of the channel model composed of a number of differential scatterers, producing delays and Doppler-shifts, the complex scattering amplitudes of elemental scatterers are uncorrelated if they produce different time-delays.

2.5.3 The Wide-Sense Stationary Uncorrelated Scattering Channel.

A class of channel which simultaneously combines Wide-Sense Stationarity in the time variable, and Uncorrelated Scattering in the time-delay variable is designated a Wide-Sense Stationary Uncorrelated Scattering(WSSUS) channel. This is the simplest non-degenerate class of channel, displaying uncorrelated dispersiveness in both the time-delay and Doppler-shift domains, that can be described in terms of channel correlation functions[2.2]. Fortunately, many radio channels can be characterised as WSSUS channels.

From the discussions on WSS and US channels it can be inferred that the simultaneous constraints placed on a WSSUS channel result in singular behaviour in both the time-delay and Doppler-shift variables. Therefore, the autocorrelation functions of the channel system functions have the following form,

$$R_h(t,t+\tau;\xi,\eta) = \delta(\eta-\xi)P_h(\tau;\xi) \tag{2.38}$$

$$R_H(f,f+\Omega;\nu,\mu) = \delta(\nu-\mu)P_H(\Omega;\nu) \tag{2.39}$$

$$R_T(f,f+\Omega;t,t+\tau) = R_T(\Omega;\tau) \tag{2.40}$$

$$R_S(\xi,\eta;\nu,\mu) = \delta(\eta-\xi)\delta(\nu-\mu)P_S(\xi;\nu) \tag{2.41}$$

Equations (2.38) to (2.41) lead to the following physical pictures for the WSSUS channel.

The autocorrelation function of the Input Delay-Spread Function, $R_h(t,t+\tau;\xi,\eta)$, indicates wide-sense stationarity in the time variable and uncorrelated scattering in the time-delay variable. In terms of a differential circuit model as a densely-tapped delay line, the channel can be represented as a continuum of uncorrelated randomly scintillating scatterers having wide-sense stationary statistics.

The autocorrelation function of the Output Doppler-Spread Function, $R_H(f,f+\Omega;\nu,\mu)$, exhibits wide-sense stationarity in the frequency variable and uncorrelated scattering in the Doppler-shift variable. In terms of a circuit model, the channel appears as a continuum of uncorrelated filtering-Doppler-shifting elements, with the filter transfer functions having wide-sense stationary statistics in the frequency variable.

The autocorrelation function of the Time-Variant Transfer Function, $R_T(f,f+\Omega;t,t+\tau)$, displays wide-sense stationarity in both time and frequency variables. Previously this has been used to determine the correlation between two signals which are separated by $\Omega/2\pi$ Hz[2.1,2.9,2.10]. A correlation function of practical interest is the spaced frequency correlation function[2.11], given by,

$$R_T(\Omega;0) = R_T(\Omega) \tag{2.42}$$

It has been shown that the frequency coherence for the variable Ω can be determined by pulse sounding techniques[2.9].

The autocorrelation function of the Delay Doppler-Spread Function, $R_S(\xi,\eta;\nu,\mu)$, reveals uncorrelated scattering in both time-delay and Doppler-shift variables. In terms of a differential circuit model, the channel can be depicted as a continuum of non-scintillating, uncorrelated scatterers causing both time-delays and Doppler-shifts. Such a represen-

tation is closer to the phenomenological description of dispersive radio channels[2.6]. For WSSUS channels the delay-Doppler cross-power spectral density, $P_S(\xi;\nu)$, is identical to the radar target scattering function, $\sigma(\xi;\nu)$, and although $\sigma(\xi;\nu)$ was defined for radar targets[2.11], it has more general applications[2.2], and can be incorporated into a study of propagation in mobile radio channels[2.6].

2.5.4 Relationships between Channel Correlation Functions For WSSUS Channels.

The relationships between the channel correlation functions for WSSUS channels are shown diagrammatically in Fig.(2.7), and take the form of single Fourier transforms. To make the Fourier transform notation unique the same convention as described in Section 2.3.5 is used.

2.6 CHANNEL CHARACTERISATION USING THE SCATTERING FUNCTION.

The statistics presented in Section 2.5.3 showed how a characterisation in terms of the Delay Doppler-Spread Function explicitly revealed the dispersive behaviour of the channel. It was also stated that the Delay Doppler-Spread Function, $P_S(\xi;\nu)$, and the Target Scattering Function, $\sigma(\xi;\nu)$, were identical. In order to present a simple physical introduction to the scattering function, a simple channel model will now be considered[2.6].

2.6.1 The Point-Scatterer Description.

Assuming that propagation through the mobile radio channel takes place purely through single scattering, then the channel can be represented as a set of independent scatterers[2.6] as shown in Fig.(2.8). Energy arriving at the receiver from the i^{th} scatterer is related to its scattering cross-section, ρ_i^2, where ρ_i determines the amplitude of the scattered waveform. Each scatterer also has an associated propagation time-delay, T_i, however, since the position of scatterers changes due to vehicle motion, the propagation time-delay must be a function of time, i.e, $T_i(t)$. Considering $T_i(t)$ as a linear function of time gives,

$$T_i(t) = \zeta_i + \dot{\zeta}_i t \tag{2.43}$$

where, ζ_i is the initial propagation delay, and $\dot{\zeta}_i$ is the rate of change of delay(i.e., the first differential of ζ_i with respect to t).

The transmitted waveform, $x(t)$, expressed in terms of its complex envelope, $z(t)$, is given by,

$$x(t) = \mathrm{Re}[z(t) \exp\{j\omega_c t\}] \tag{2.44}$$

which can be seen to be identical to equation (2.1). Hence, the contribution of the i^{th} scatterer, $x_i(t)$, to the received waveform, $v_i(t)$, is merely a delayed and attenuated replica of the transmitted signal, i.e,

$$v_i(t) = A\rho_i \,\mathrm{Re}\Big[z(t - \zeta_i - \dot{\zeta}_i t) \exp\Big\{j\omega_c(t - \zeta_i - \dot{\zeta}_i t)\Big\}\Big] \tag{2.45}$$

where, A is an unimportant constant.

If the variation in $\dot{\zeta}_i t$ is small compared to the reciprocal bandwidth of $z(t)$ then its variation in the argument of z may be ignored. Also, provided the signal is narrowband, i.e., the bandwidth of $z(t)$ is much smaller than the carrier frequency, then differences of π/ω_c in the value of ζ_i will not significantly change the value of $z(t - \zeta_i)$, however, they will appreciably affect the value of $\not{x}_i(t)$, because they alter the exponent by π radians[2.6].

Since each value of ζ_i is rarely known exactly, and since small perturbations are important, it seems reasonable to represent each ζ_i as the sum of a gross delay, ξ_i, and a perturbation delay, $\delta\xi_i/\omega_c$, i.e.,

$$\zeta_i = \xi_i + \frac{\delta\xi_i}{\omega_c} \tag{2.46}$$

where, $\delta\xi_i$ is specified as being a variable which takes values in the range $[-\pi, \pi]$.

Applying the above conditions, and using equation (2.46), equation (2.45) can be rewritten as,

$$v_i(t) = A\rho_i \,\mathrm{Re}\Big[z(t-\xi_i)\exp\Big\{j\Big(\omega_c(t-\xi_i-\dot{\zeta}_i t)-\delta\xi_i\Big)\Big\}\Big] \tag{2.47}$$

Rewriting equation (2.47) to show the Doppler-shift, v_i, associated with the contribution from the i^{th} scatterer gives,

$$v_i(t) = A\rho_i \,\mathrm{Re}[z(t-\xi_i)\exp\{j(2\pi(f_c - v_i)t - 2\pi f_c\xi_i - \delta\xi_i)\}] \tag{2.48}$$

where,

$$2\pi v_i = \omega_c\dot{\zeta}_i \tag{2.49}$$

and v_i is in Hz.

Summation of the individual contributions, from all the scatterers comprising the channel, produces the total received waveform due to single scattering, which is,

$$v(t) = \sum_i v_i(t) = A\,\mathrm{Re}\left[\sum_i \rho_i z(t-\xi_i)\exp\{j(2\pi(f_c - v_i)t - 2\pi f_c\xi_i - \delta\xi_i)\}\right] \tag{2.50}$$

Although an expression has been obtained for the received waveform, the parameters ρ_i, ξ_i, $\delta\xi_i$ and v_i are all random variables, therefore, a statistical description of equation (2.50) is required.

2.6.2 Statistical Point-Scatterer Model.

It would be possible to obtain a statistical description of the channel by considering the joint probability distributions of the variables ρ_i, ξ_i, $\delta\xi_i$ and v_i. However, a simpler approach is possible through consideration of the individual probability distributions.

The perturbation term, $\delta\xi_i$, corresponds to a maximum phase ambiguity of π radians, i.e., a delay uncertainty of half a wavelength, and since the total delay is many thousands of wavelengths at UHF, the percentage uncertainty is sufficiently small that it is reasonable to assume that $\delta\xi_i$ is uniformly distributed over the range $(-\pi, \pi)$. In addition, it is presumed that the $\delta\xi_i$ are statistically independent, and, therefore, uncorrelated[2.6].

The cross-sections, ρ_i^2, account for such factors as aspect of scatterers, and consequently they can be regarded as random variables. It is also reasonable to assume that the values of ρ_i^2 are uncorrelated, and independent of the other parameters. A uniform distribution is sometimes assumed for the Doppler-shifts, v_i. These assumptions suffice for an elementary channel model.

The assumptions made above imply that the mean value of $v(t)$ is zero. They also imply that, using equation (2.50), the autocorrelation function, $R_v(t,s)$, of $v(t)$ can be expressed as,

$$R_v(t,s) = \mathrm{Re}\left[\sum_i \frac{A^2}{2}\, \mathrm{E}\left[\rho_i^2 z(t-\xi_i)z^*(s-\xi_i)\right] \exp\{j2\pi(f_c - v_i)(t-s)\}\right] \qquad (2.51)$$

However, since the complex envelope of the input, $z(t)$, is deterministic, then $z(t-\xi_i)$ is also deterministic, so, equation (2.51) simplifies to,

$$R_v(t,s) = \mathrm{Re}\left[\sum_i \frac{A^2}{2}\, \mathrm{E}\left[\rho_i^2\right] z(t-\xi_i)z^*(s-\xi_i) \exp\{j2\pi(f_c - v_i)(t-s)\}\right] \qquad (2.52)$$

In equation (2.52) the dispersive behaviour of the channel is displayed by the average cross-sections, $\mathrm{E}[\rho_i^2]$, for each delay, ξ_i, and Doppler-shift, v_i. However, it is rather awkward to manipulate and interpret this correlation function as it stands, and so, a more suitable form will be arrived at in the following section.

2.6.3 The Scattering Function.

The expression on the right hand side of equation (2.52) depends only on the total average cross-section associated with each pair of values of ξ_i and v_i, and is independent of the number of scatterers involved. Hence, it is possible to introduce an average scatterer cross-section[2.6], $\tilde{\sigma}(\xi;v)$, for each pair of ξ_i and v_i, i.e.,

$$\tilde{\sigma}(\xi;v) = \sum_i \mathrm{E}[\rho_i^2] \tag{2.53}$$

where, the summation is for all cross-sections that correspond to delays $\xi_i = \xi$, and Doppler-shifts $v_i = v$.

The autocorrelation function, $R_v(t,s)$, can now be expressed as,

$$R_v(t,s) = \mathrm{Re}\left[\sum_i \frac{A^2}{2} z(t-\xi)z^*(s-\xi)\tilde{\sigma}(\xi;v)\exp\{j2\pi(f_c - v)(t-s)\}\right] \tag{2.54}$$

where, the summation is over all pairs of ξ and v for which $\tilde{\sigma}(\xi;v)$ is nonzero.

Owing to practical limitations on $z(t)$, there will be times when it is impossible to differentiate between contributions from individual scatterers. That is, time-delays, ξ, which differ by less than the reciprocal bandwidth of $z(t)$, and Doppler-shifts, v, which differ by much less than the reciprocal time duration of $z(t)$ are unresolvable. When this occurs, the contributions merge together to produce an average contribution. Therefore, the discrete form of $\tilde{\sigma}(\xi;v)$ can be replaced by a continuous function, and the summation can be replaced by an integral. Equation (2.54) then becomes,

$$R_v(t,s) = \mathrm{Re}\left[\int\int \frac{A^2}{2} z(t-\xi)z^*(s-\xi)\tilde{\sigma}(\xi;v)\exp\{j2\pi(f_c - v)(t-s)\}\, d\xi\, dv\right] \tag{2.55}$$

In its continuous form the scattering function, $\tilde{\sigma}(\xi;v)$, can be thought of as a scatterer cross-section density for all values of ξ and v. The cross-section corresponding to delays in the range $(\xi, \xi + d\xi)$ and Doppler-shifts in the range $(v, v + dv)$ is then given by $\tilde{\sigma}(\xi;v)\, d\xi\, dv$.

The function $\tilde{\sigma}(\xi;v)$ describes both the distribution of average cross-section, and also the total amount of such cross-section; whilst $z(t)$ describes both the structure of the transmitted waveform, and its energy

level. In both cases, the former attribute relates to the general structure of the received process, while the latter attribute merely determines the average received energy[2.6].

It is possible to assume that $z(t)$ can be scaled to a unit norm, since this is easily satisfied by redefining A, so that,

$$\int |z(t)|^2 \, dt = 1 \tag{2.56}$$

The normalised density of cross-section, $\sigma(\xi;v)$, will now be introduced; it is defined as,

$$\sigma(\xi;v) = \frac{\tilde{\sigma}(\xi;v)}{\int\int \tilde{\sigma}(\xi;v) \, d\xi \, dv} \tag{2.57}$$

$\sigma(\xi;v)$ is more usually called the channel scattering function[2.2,2.6,2.12]. It is obvious from equation (2.57) that,

$$\int\int \sigma(\xi;v) \, d\xi \, dv = 1 \tag{2.58}$$

Also, the average received energy, E_R, is defined by each of the following,

$$E_R = \int \mathrm{E}[v(t)]^2 \, dt = \int R_v(t,t) \, dt = \frac{A^2}{2} \int\int \tilde{\sigma}(\xi;v) \, d\xi \, dv \tag{2.59}$$

Using equations (2.57) and (2.59) in equation (2.55) gives,

$$R_v(t,s) = \mathrm{Re}\left[E_R \int\int z(t-\xi) z^*(s-\xi) \sigma(\xi;v) \exp\{j2\pi(f_c - v)(t-s)\} \, d\xi \, dv \right] \tag{2.60}$$

Finally, for the condition that the channel is Wide-Sense Stationary, the time variables t and s are related through their difference, i.e., $\tau = s - t$. So, equation (2.60) reduces to,

$$R_v(t,t+\tau) = \mathrm{Re}\left[E_R \int z(t-\xi) z^*(t+\tau-\xi) \sigma(\xi;\nu) \exp\{-j2\pi(f_c-\nu)\tau\}\, d\xi\, d\nu \right] \quad (2.61)$$

Therefore, an expression for the autocorrelation function of the Wide-Sense Stationary channel output, $R_v(t,t+\tau)$, has been obtained in terms of the scattering function, $\sigma(\xi;\nu)$.

Alternatively, a similar expression can be arrived at through the relationships between autocorrelation functions described in Section 2.4.1. The autocorrelation function of the channel output was given in equation (2.17), it can also be expressed as,

$$R_w(t,s) = \int\int z(t-\xi) z^*(s-\eta) R_h(t,s;\xi,\eta)\, d\xi\, d\eta \quad (2.62)$$

From Section 2.4.2, the double Fourier transform relationship relating $R_h(t,s;\xi,\eta)$ to $R_S(\xi,\eta;\nu,\mu)$ is given by,

$$R_h(t,s;\xi,\eta) = \int\int R_S(\xi,\eta;\nu,\mu) \exp\{-j2\pi(\nu t - \mu s)\}\, d\nu\, d\mu \quad (2.63)$$

Substitution in equation (2.62) gives,

$$\begin{aligned} R_w(t,s) = & \int\int z(t-\xi) z^*(s-\eta) \times \\ & \int\int R_S(\xi,\eta;\nu,\mu) \exp\{-j2\pi(\nu t - \mu s)\}\, d\nu\, d\mu\, d\xi\, d\eta \end{aligned} \quad (2.64)$$

In the case of a WSSUS channel, the function $R_S(\xi,\eta;\nu,\mu)$ can be replaced by the Delay-Doppler cross-power spectral density, $P_S(\xi;\nu)$, as given in equation (2.41), so $R_w(t,s)$ becomes,

$$\begin{aligned} R_w(t,s) = & \int\int z(t-\xi) z^*(s-\eta) \times \\ & \int\int \delta(\nu-\mu)\delta(\eta-\xi) P_S(\xi;\nu) \exp\{-j2\pi(\nu t - \mu s)\}\, d\nu\, d\mu\, d\xi\, d\eta \end{aligned} \quad (2.65)$$

Simplifying equation(2.65) produces,

$$R_w(t,s) = \int\int z(t-\xi)z^*(s-\xi)P_S(\xi;v)\exp\{-j2\pi v(t-s)\}\,dv\,d\xi \qquad (2.66)$$

The autocorrelation of the real bandpass signal $R_v(t,s)$ can be obtained from $R_w(t,s)$ through use of the equivalence relationship given in equation (2.1). Therefore, $R_v(t,s)$ is given by,

$$R_v(t,s) = \mathrm{Re}\Big[\int\int z(t-\xi)z^*(s-\xi)P_S(\xi;v)\times \exp\{-j2\pi v(t-s)\}\exp\{j2\pi f_c(t-s)\}\,dv\,d\xi\Big] \qquad (2.67)$$

Now noting from Section 2.5.3 that $P_S(\xi;v)$ is equivalent to the scattering function, $\sigma(\xi;v)$, and that for WSS channels the variables t and s are related through their difference, i.e, $\tau = s - t$, equation (2.67) becomes,

$$R_v(t,t+\tau) = \mathrm{Re}\Big[\int\int z(t-\xi)z^*(t+\tau-\xi)\sigma(\xi;v)\exp\{j2\pi(f_c-v)\tau\}\,dv\,d\xi\Big] \qquad (2.68)$$

Apart from the constant E_R, equations (2.61) and (2.63) are identical, showing how the scattering function description based on a simple physical model can be derived from the more strict channel characterisation of Section 2.4.

It has, therefore, been shown how knowledge of $\sigma(\xi;v)$ allows a description of the received process for a given input signal. Additionally, a statistical channel characterisation in terms of $\sigma(\xi;v)$ provides an insight to the physical mechanisms of multipath propagation. Finally, if the statistics of the received process are Gaussian, then a description in terms of $\sigma(\xi;v)$ is statistically complete[2.2,2.6].

2.7 MOBILE RADIO CHANNEL CHARACTERISATION.

Practically all mobile radio communication channels can be characterised as linear in regard to the effect they have on message signals transmitted through them. Therefore, it seems reasonable to consider mobile radio channels as special cases of random time-variant linear filters[2.2]

Mobile radio links, e.g., cellular, usually require communication between fixed base-stations and mobile transceivers. As discussed in Sections 2.1 and 2.2, radio waves in a mobile environment suffer from multipath, resulting in rapid fluctuations of the received signal envelope due to motion through the fading field distribution. Superimposed on this fast fading is a much slower variation in the mean received signal strength due to changes in local terrain, range and/or number of scatterers. Consequently, it would appear that the mobile radio channel is non-stationary. However, characterisation of mobile radio channels proves extremely difficult unless stationarity can be assumed over short intervals of time.

In order to obtain a fairly complete statistical description of the channel, a two-stage characterisation is proposed. Firstly, the channel is characterised over a period of time which is small in comparison to the period of the slow channel variations, so that the mean received signal strength appears virtually constant. It is further assumed that over this small interval the prominent features of the environment remain unchanged, i.e., the significant scattering centres do not change. Then the large-scale behaviour of the channel is obtained by averaging the small-scale statistics. This two-stage model was first proposed by Bello[2.2], and was subsequently used by Cox[2.9] in his study at 910MHz in New York City, and by Bajwa[2.5] in his study at 436MHz in Birmingham. This class of channel has been called Quasi-Wide-Sense Stationary(QWSS).

A further simplification in the characterisation of mobile radio channels can be effected by assuming that contributions from scatterers with different path delays are uncorrelated. Therefore, the channel can be described in terms of WSSUS statistics, and it can be depicted as a continuum of uncorrelated scatterers, in both time-delays and Doppler-shifts, having elemental cross-sections $\sigma(\xi;\nu)\,d\xi\,d\nu$. The channel is specified here in terms of the scattering function, $\sigma(\xi;\nu)$[2.6]. Useful characterisation of mobile radio channel behaviour can be provided by application of the various correlation functions, and their interrelationships.

2.7.1 Small-scale Channel Characterisation.

The primary small-scale channel transmission characteristics of interest are the Input Delay-Spread Function, and the Time-Variant Transfer Function. In Section 2.4.1 it was shown how the autocorrelation function of the complex envelope of the received signal, $R_w(t,s)$, could be obtained from the autocorrelation function of the Input Delay-Spread Function, $R_h(t,s;\xi,\eta)$. As shown in Section 2.5.3, certain simplifications in the characterisation arise when the channel is WSSUS. A sufficient characterisation of the WSSUS channel, in terms of its dispersive behaviour, is possible through knowledge of $R_h(t,s;\xi,\eta)$. This will now be shown for both the time and frequency domain descriptors.

2.7.1.1 Time-domain Description.

The time-domain description of the channel is obtained by expressing the autocorrelation function of the channel output, $R_w(t,s)$, in terms of the autocorrelation function of the Input Delay-Spread Function, $R_h(t,s;\xi,\eta)$. This was given in equation (2.17) as,

$$R_w(t,s) = \int\int z^*(t-\xi)z(s-\eta)R_h(t,s;\xi,\eta)\,d\xi\,d\eta \tag{2.69}$$

In equation (2.38) of Section 2.5.3 it was shown that, for WSSUS channels, the autocorrelation function $R_h(t,s;\xi,\eta)$ can be expressed in terms of the Delay cross-power spectral density function, $P_h(\tau;\xi)$, as,

$$R_h(t,t+\tau;\xi,\eta) = \delta(\eta-\xi)P_h(\tau;\xi) \tag{2.70}$$

Therefore, for a WSSUS channel equation (2.69) becomes,

$$R_w(t,t+\tau) = \int\int z^*(t-\xi)z(t+\tau-\xi)\delta(\eta-\xi)P_h(\tau;\xi)\,d\xi\,d\eta \tag{2.71}$$

When the time separation of the observation is zero, i.e., $\tau = 0$, $P_h(\tau;\xi)$ becomes,

$$P_h(0;\xi) = P_h(\xi) \tag{2.72}$$

that is, the cross-power spectral density, $P_h(\tau;\xi)$ becomes a simple delay-power spectral density, $P_h(\xi)$. Thus, equation (2.71) simplifies to,

$$R_w(t,t) = \int |z(t-\xi)|^2 P_h(\xi)\, d\xi \tag{2.73}$$

Now, if $|z(t)|^2$ is an impulse function then equation (2.73) becomes,

$$R_w(t,t) = P_h(t) \tag{2.74}$$

Equation (2.74) shows that, for WSSUS channels, the autocorrelation function of the channel output is described by the profile of the time distribution of received power. The expression in equation (2.74) is valid on condition that $|z(t)|^2$ appears to be impulsive with respect to $P_h(t)$, this is satisfied provided that the time duration of $z(t)$ is much smaller than the multipath delay spread(to be defined later) of the channel. Stated more precisely, equation (2.74) holds as long as the Fourier transform of $|z(t)|^2$ is constant over the frequency interval where the Fourier transform of $P_h(t)$ is nonzero[2.6].

For convenience, $P_h(t)$ normally has its time origin redefined so as to position the earliest received echo at $t = 0$, and the function is then defined in terms of the excess time-delay variable, ξ, i.e.,

$$P_h(\xi) = P_h(t - t_0) \tag{2.75}$$

where, t_0 is the time-delay for the shortest echo path. Provided the received signal has Gaussian statistics then the channel behaviour will be completely described by $P_h(\xi)$. A knowledge of $P_h(\xi)$ will typically specify some gross features of the channel; these are obtained by regarding $P_h(\xi)$ as a statistical distribution of echo strengths. Two statistical moments of $P_h(\xi)$ of practical interest are the average delay, D, and the delay spread,[4] S. The average delay is the first central moment, i.e., mean, of $P_h(\xi)$, and the delay spread is the second central moment, i.e., variance, of $P_h(\xi)$. These are expressed as,

---

[4] This has also been referred to as σ[2.1,2.10,2.13], and Δ[2.14]. An alternative parameter, which is equal to twice S, has also been used called the total multipath spread, T_M[2.15].

$$D = \frac{\int \xi P_h(\xi)\, d\xi}{\int P_h(\xi)\, d\xi} \tag{2.76}$$

$$S = \sqrt{\frac{\int (\xi - D)^2 P_h(\xi)\, d\xi}{\int P_h(\xi)\, d\xi}} \tag{2.77}$$

Although these parameters are estimates, they constitute relevant design parameters for WSSUS channels. The average delay is related to ranging error in phase ranging systems, and the delay spread places limits on communication system performance[2.15], as outlined in Section 2.2.

2.7.1.2 Frequency-domain Description.

The frequency-selective behaviour of the mobile channel is readily obtained by observing the correlation between two signals, at different frequencies, at the receiver. The existence of different time-delays, for the constituent propagation paths, causes the statistical properties of two spaced carrier frequencies to become essentially independent, if their frequency separation is sufficiently large. The maximum frequency difference for which the signals are still strongly correlated is called the coherence bandwidth of the channel. The coherence bandwidth is a useful parameter in assessing the performance, and limitations, of various modulation and diversity-reception techniques.

In Section 2.3.3 it was shown how the Time-Variant Transfer Function, $T(f,t)$, characterises a channel in response to a cissoidal time function. Random time-variant channels require a characterisation in terms of the autocorrelation function of the Time-Variant Transfer Function, $R_T(f,m;t,s)$, as detailed in Section 2.4.1. For WSSUS channels the autocorrelation function reduces to,

$$R_T(f,f+\Omega;t,t+\tau) = R_T(\Omega;\tau) \tag{2.78}$$

and $R_T(\Omega;\tau)$ has been called the Time Frequency Correlation Function[2.2].

Use of the interrelationships between autocorrelation functions for WSSUS channels(see Section 2.5.4) shows that $R_T(\Omega;\tau)$ is related to $P_h(\tau;\xi)$ via a Fourier transform, i.e.,

$$R_T(\Omega;\tau) = \int P_h(\tau;\xi) \exp\{ -j2\pi\Omega\xi\} \, d\xi \tag{2.79}$$

Therefore, a separate measurement of $R_T(\Omega;\tau)$ is not required in order to provide a frequency-domain description of the channel.

When the time separation of the observation is zero, i.e., $\tau = 0$,

$$R_T(\Omega;0) = R_T(\Omega) \tag{2.80}$$

$$P_h(0;\xi) = P_h(\xi) \tag{2.81}$$

and,

$$R_T(\Omega) = \int P_h(\xi) \exp\{ -j2\pi\Omega\xi\} \, d\xi \tag{2.82}$$

$R_T(\Omega)$ is known as the Frequency Correlation Function[2.2], and the coherence bandwidth, B_c, is the smallest value of $\Omega/2\pi$ for which $R_T(\Omega)$ equals some suitable correlation coefficient, e.g., 0.5.

The interrelationships between the channel correlation functions for WSSUS channels were shown in Section 2.5.4, and it can be seen that the scattering function, $\sigma(\xi;\nu)$, the delay-power spectral density, $P_h(\xi)$, and the frequency correlation function, $R_T(\Omega)$, are simply related through Fourier transforms. Therefore, alternative channel descriptions can be easily obtained from practical channel measurements performed in either time, or frequency, domains.

2.7.2 Large-scale Channel Characterisation.

For small spatial distances, of the order of a few wavelengths, the dispersive behaviour of the channel can be modelled as Quasi-Wide-Sense Stationary in the time-domain. However, over larger distances the changes

in terrain and local environment give rise to temporal non-stationarity in the statistical characterisation of the multipath. Therefore, while it is not possible to directly apply the small-scale statistics to the characterisation of multipath over areas where non-local scattering can be observed, it is possible to use the scattering function over consecutive Wide-Sense Stationary, and spatially homogeneous, sections in order to investigate the scattering behaviour for large areas.

Direct data reduction of the statistical moments of the small-scale characteristics provides average distributions of the delay spread, coherence bandwidth, etc. for the larger area[2.2,2.5,2.9]. This method has proved popular in previous studies[2.2,2.5,2.9], since it gives rise to parameters that are useful for Systems Designers. Complete descriptions of the data reduction techniques employed in this study are contained in Chapter 6.

Although this method yields useful design parameters, they represent 'static' measures of the channel performance. A more powerful characterisation would enable the production of an accurate channel simulation. In attempting to achieve this aim, several studies[2.5,2.13,2.17,2.18] have concentrated on fitting global probability distributions to the echo amplitudes, path delays, carrier phases and Doppler-shifts. Whilst representative simulators have been developed[2.17,2.18], the basis for each model has been that the time-delays conform to a Poisson-sequence. This fact restricts the models to computer simulations, since the time-delays must be generated from random numbers. To overcome this drawback, a simple channel simulation based upon a tapped-delay line model was developed for this study, and will be described in detail in Chapter 6.

REFERENCES

[2.1] Jakes, W. C. (Ed.), "Microwave Mobile Communications", John Wiley 1974.

[2.2] Bello, P. A., "Characterization of randomly time-variant linear channels", IEEE Trans. Commun. Syst., Dec. 1963, Vol CS-11, pp 360-393.

[2.3] Zadeh, L. A., "Frequency analysis of variable networks", Proc. IRE, March 1950, Vol. 38, pp 291-299.

[2.4] Kailath, T., "Sampling models for linear time-variant filters", M.I.T. Research Lab. of Electronics, Cambridge, Mass., May 1959, Rept. No. 352.

[2.5] Bajwa, A. S., "Wideband characterisation of UHF mobile radio propagation in urban and suburban areas", Ph.D. Thesis, Department of Electronic and Electrical Engineering, University of Birmingham, 1979.

[2.6] Kennedy, R. S., "Fading Dispersive Communication Channels", Wiley-Interscience, 1969.

[2.7] Lathi, B. P., "An Introduction to Random Signals and Communication Theory", International Textbook Company, 1968.

[2.8] Papoulis, A., "The Fourier Integral and its Applications", McGraw-Hill, 1962.

[2.9] Cox, D. C. and Leck, R. P., "Correlation bandwidth and delay spread multipath propagation statistics for 910-MHz urban mobile radio channels", IEEE Trans. Commun., Nov. 1975, Vol. COM-23, No. 11, pp 1271-1280.

[2.10] Gans, M. J., "A power-spectral theory of propagation in the mobile-radio environment", IEEE Trans. Veh. Technol., Feb. 1972, Vol. VT-21, No. 1, pp 27-38.

[2.11] Price, R. and Green, P. E., "Signal processing in radar astronomy", M.I.T. Lincoln Lab., Lexington, Mass., Oct. 1960, Rept. No. 234.

[2.12] Schwartz, M., Bennett, W. R., and Stein, S., "Communication Systems and Techniques", McGraw-Hill, 1966.

[2.13] Turin, G. L., Clapp, F. D., Johnston, T. L., Fine, S. B. and Lavry, D., "A statistical model of urban multipath propagation", IEEE Trans. Veh. Technol., Feb. 1972, Vol. VT-21, No. 1, pp 1-9.

[2.14] Lee, W. C. Y., "Mobile Communications Engineering", McGraw-Hill, 1982.

[2.15] Lorenz, R. W., "Impact of frequency-selective fading on binary and quadrature phase modulation in mobile radio communication demonstrated by computer simulations using the WSSUS channel model", COST 207 technical document, TD(86)#1(Jan. 1986).

[2.16] Cox, D. C., "Delay doppler characteristics of multipath propagation at 910-MHz in a suburban mobile radio environment", IEEE Trans. Antennas Propagat., Sept. 1972, Vol. AP-20, No. 5, pp 625-635.

[2.17] Suzuki, H., "A statistical model for urban radio propagation", IEEE Trans. Commun., July 1977, Vol. COM-25, No. 7, pp 673-680.

[2.18] Hashemi, H., "Simulation of the urban radio propagation channel", IEEE Trans. Veh. Technol., Aug. 1979, Vol. VT-28, No. 3, pp 213-225.

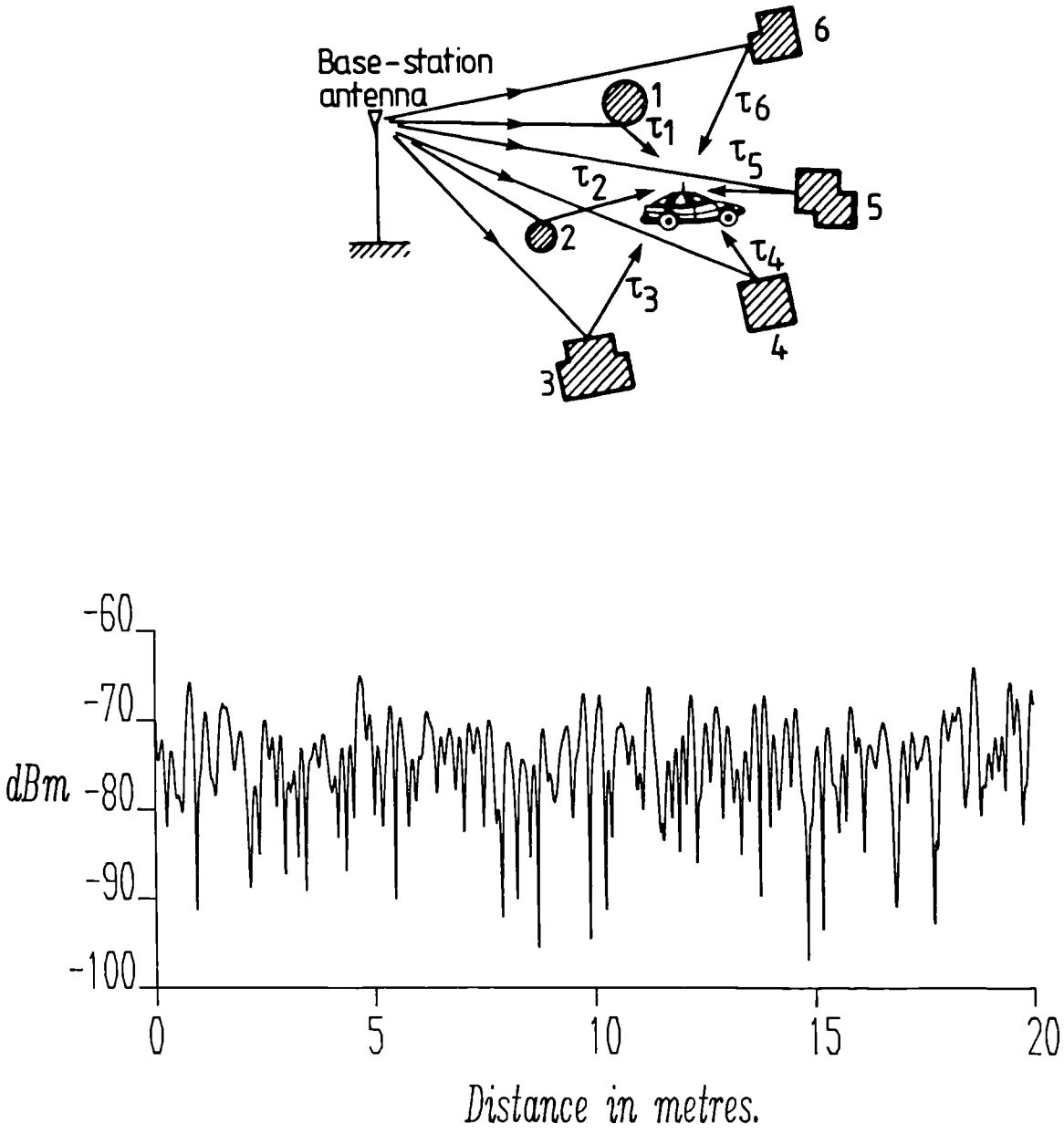

Fig. 2.1. Multipath phenomenon in the narrowband case.

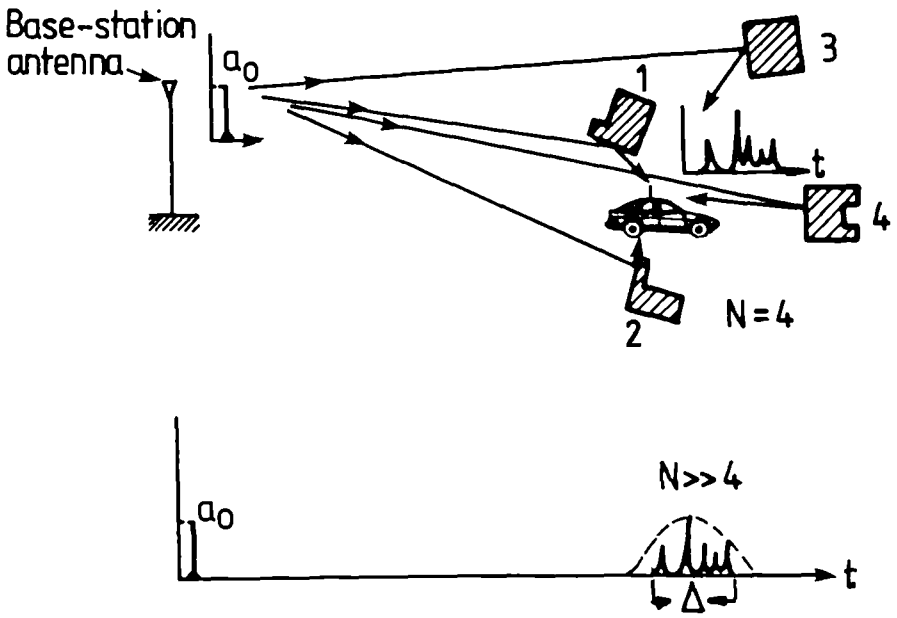

Fig. 2.2. Multipath phenomenon in the wideband case.

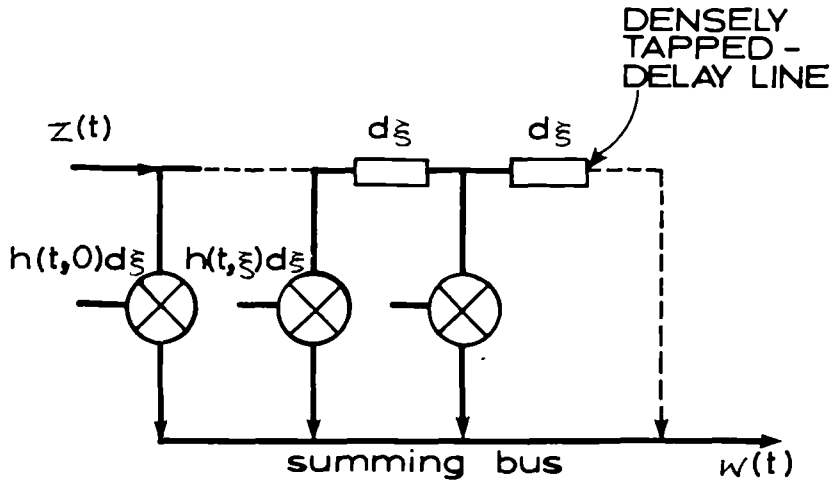

Fig. 2.3. Tapped-delay line model of a multipath channel.

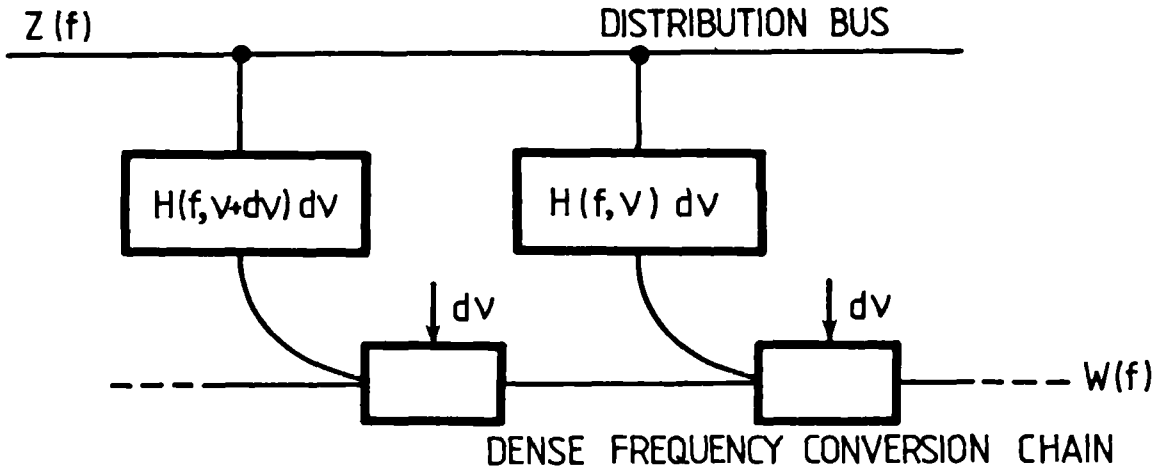

Fig. 2.4. Frequency-shifting converter model of a multipath channel.

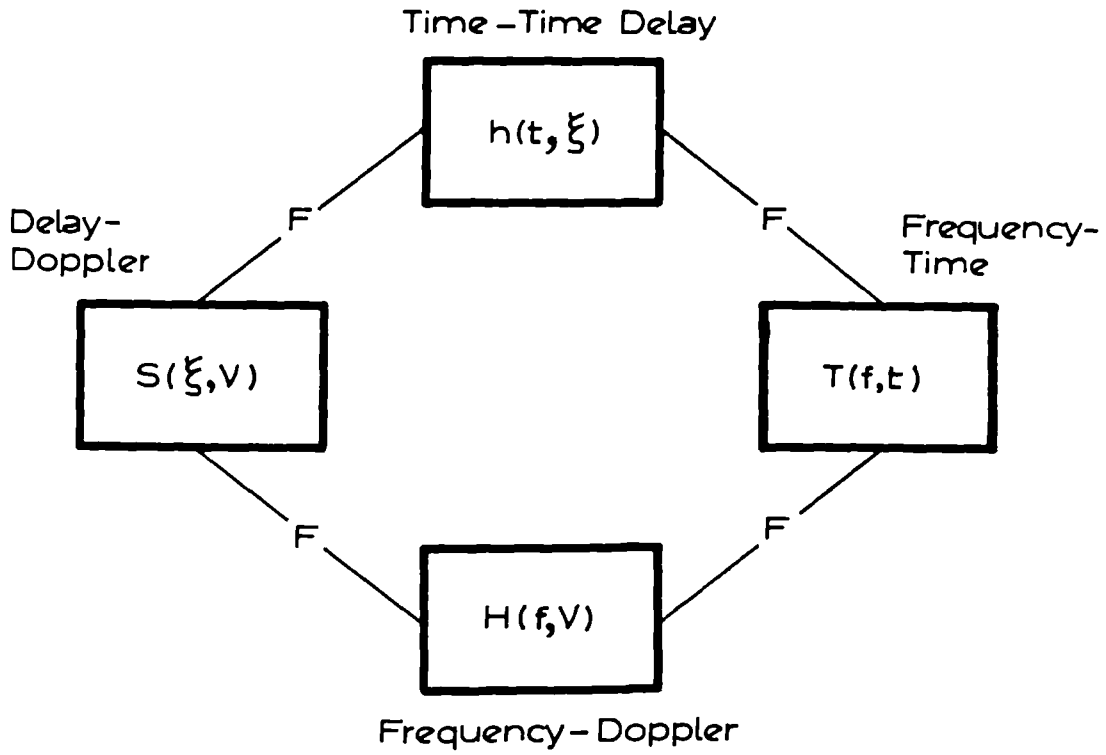

Fig. 2.5. Relationships between system functions.

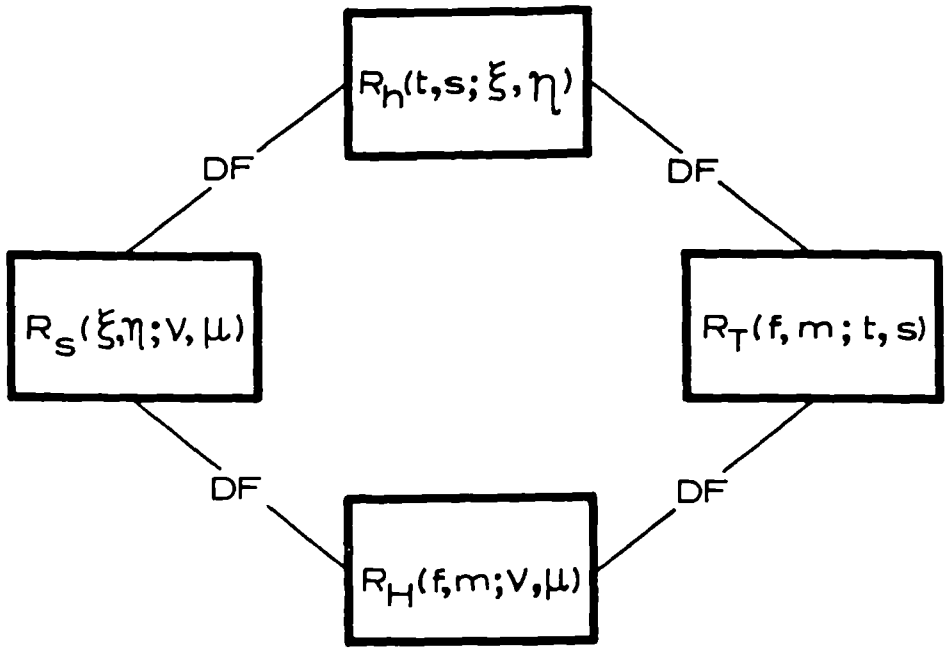

Fig. 2.6. Relationships between channel correlation functions.

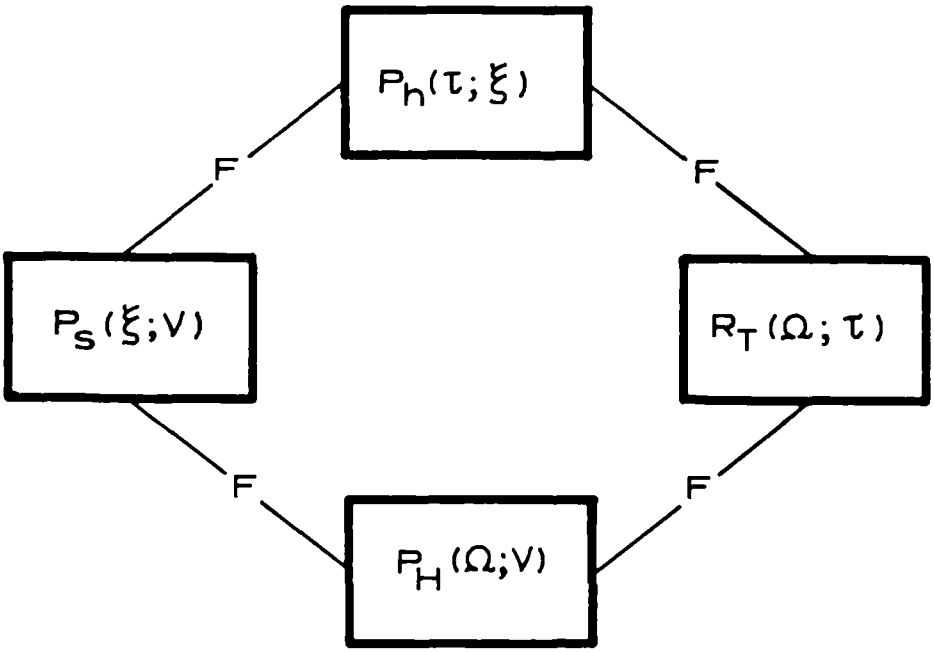

Fig. 2.7. Relationships between correlation functions for WSSUS channels.

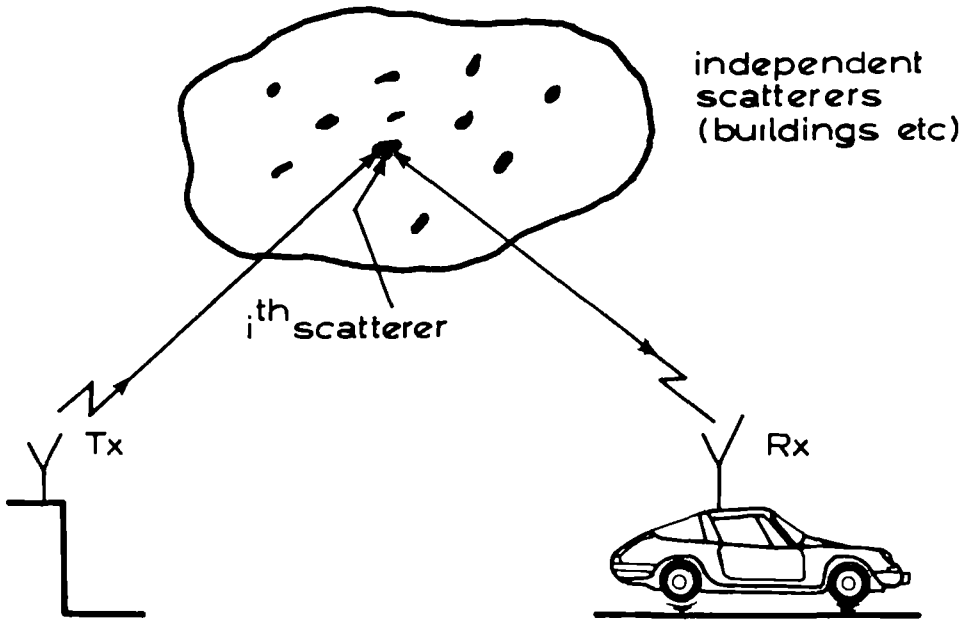

Fig. 2.8. Point-scatterer representation of a multipath mobile radio channel.

CHAPTER 3. A REVIEW OF CHANNEL SOUNDING TECHNIQUES.

A detailed discussion of the statistical characterisation of mobile radio propagation channels was presented in Chapter 2. The symmetric interrelationships between the characterising functions, in the time-time delay, time-frequency, frequency-frequency shift and time delay-frequency shift domains, were then demonstrated. Consequently, a complete characterisation of the channel can be effected through use of a channel sounding technique that provides a suitable two-dimensional descriptor for any of these domains.

The choice of channel sounding technique will usually depend upon the application foreseen for the propagation data. Essentially, a choice has to be made between using narrowband or wideband transmissions, and whether a time or frequency-domain characterisation is required. In the following sections, a brief assessment of narrowband sounding techniques is presented, prior to a more detailed review of the various wideband sounding methods. The advantages and limitations of the different approaches are discussed, and the reasons are given for the choice of channel sounder used in this study.

3.1 NARROW BANDWIDTH CHANNEL SOUNDING TECHNIQUES.

3.1.1 The Single Tone Method.

When the mobile radio channel is excited by an unmodulated RF carrier(single tone), large variations are observed in the amplitude and phase of the received signal. These variations are a result of the random phase additions of signals arriving over many scattered paths.

A considerable number of mobile radio propagation studies have been undertaken, in the VHF, UHF and microwave frequency bands, utilising this technique[3.1-3.3]. From these studies, descriptions of the propagation channel, in terms of statistical parameters related to the fading envelope of the transmitted tone, have been presented. The small-

scale[5] variations of the envelope have been seen to have approximately Rayleigh distributed amplitude statistics. Departures from Rayleigh for areas with a strong specular component have been better described in terms of Rician statistics, however, as detailed in Section 2.1, these are of little consequence when evaluating system performance. The phase has been assumed to be uniformly distributed over $(0, 2\pi]$ radians[3.2]. Therefore, the received signal constitutes a narrowband complex Gaussian process when the channel is excited by a single tone.

The power spectral density of the envelope can be obtained by Fourier transforming its autocorrelation function[3.2], which is easily derived from the measurements. The fact that the transmission of a single tone gives rise to a received signal with a spectrum of non-zero width implies that the channel behaves like a continuum of frequency-shifters. From the description of channel models in Chapter 2, it is known that these are the Doppler-shifts associated with individual scatterers.

In addition to the small-scale variations, there is a perturbation in the mean received signal strength due to gross changes in the environment. These large-scale variations are approximately log-normally distributed, with a distance-dependent mean. However, it is usually the small-scale statistics that are of most importance to the systems designer.

Several small-scale models have been proposed[3.2,3.4-3.7] to describe the behaviour of the channel, and all showed reasonable agreement with single tone measurements of the fading envelope. Hardware and software simulators, based on these models, have been developed[3.2,3.8,3.9], and have proved extremely useful in the assessment of various narrowband transmission schemes.

Although Jakes[3.2], Clarke[3.6] and Gans[3.7] extended their models to consider the correlation between two spaced frequencies in the presence of time-delayed multipath, it is obvious that, in order to verify the models, the single-tone measurements have to be repeated over the frequency band, or an alternative sounding technique used. Therefore, a primary limitation

---

[5] That is, spatial distances of a few tens of wavelengths, where the mean signal strength is approximately constant.

of the single-tone sounding technique is its inability to explicitly illustrate the frequency selective behaviour of the channel. In order to surmount this problem, the spaced tone sounding method was devised.

3.1.2 The Spaced Tone Method.

In Section 2.7.1.2 the Frequency Correlation Function, $R_T(\Omega)$, which is a measure of the degree of correlation between two frequencies spaced ΩHz apart, was introduced. In this sounding technique, two sufficiently spaced carrier frequency tones are used as the probing signal, in an attempt to observe the frequency selective behaviour of the multipath channel.

The earliest measurements employing this technique were carried out by Hoffman(1961)[6] in suburban areas of the USA at 836MHz. Although unpublished, this work formed the basis of support for Jakes's[3.2], Clarke's[3.6] and Gans's[3.7] theoretical scattering models for predicting the frequency coherence of time-delay spread multipath channels. Comparisons with Frequency Correlation Functions obtained from wideband measurements[3.10] in urban New York City were also used to further substantiate the theoretical models. However, the echo-power delay profiles were assumed to have a smooth exponential distribution as a function of time-delay. Although this assumption is valid in some instances, there are times when the echo-power profile contains echoes with significant energy arriving at large excess time-delays. When this occurs the Frequency Correlation Function becomes highly oscillatory, and constitutes a multivalued function[3.11,3.12]. As a result, ambiguities in determining the frequency coherency of the channel could arise, depending on the separation of the transmitted tones. Obviously, this limitation can be overcome by repeating the experiment for various frequency separations.

A recent study in the UK[3.13] has been carried out for separations between 50KHz and 200KHz. By sequentially stepping the tones across a band of frequencies, measurements of the wideband channel frequency

---

[6] There appears to be some confusion in the literature as to who carried out these measurements, Jakes[3.2] credits Hoffman and Ossanna, Clarke[3.6] credits Ossanna, and Gans[3.7] credits Hoffman, with Ossanna carrying out computational work.

transfer function were obtained. Whilst this method provided a wideband measurement, utilising relatively simple, and inexpensive, narrowband equipment, it has two major drawbacks. Firstly, stepping a synthesiser over a large bandwidth in small steps is time consuming, even using modern fast switching designs. Secondly, it is impossible to make mobile measurements using such a system due to the stepping frequency technique. Therefore, no Doppler-shift, and hence angle-of arrival, information can be obtained, which precludes identification of significant single scatterers.

Alternatively, a swept frequency(chirp) or wideband method could be used to excite the mobile channel. Although chirps are quite popular in high resolution radars and HF ionospheric links[3.14], they have not been used in any study of mobile radio channels, and are, therefore, excluded from this discussion. However, wideband sounding techniques will be described in the following sections.

3.2 WIDE BANDWIDTH CHANNEL SOUNDING TECHNIQUES.

3.2.1 Periodic Pulse Sounding Method.

When an impulse(i.e., short duration pulse) is used to excite the mobile propagation channel, the received signal represents the convolution of the sounding pulse with the channel impulse response. In order to observe the time-varying behaviour of the channel, periodic pulse sounding must be employed. The pulse repetition period has to be sufficiently rapid to allow observation of the time-varying response of individual propagation paths, whilst also being long enough to ensure that all multipath echoes have decayed between successive impulses. The width of the pulse determines the minimum echo-path resolution, i.e, the minimum discernible path difference between echo contributions, while the repetition rate determines the maximum unambiguous echo-path time-delay, i.e., the maximum distance for which an echo contribution can be unambiguously resolved. The periodic pulse sounding of the channel provides a series of 'snapshots' of the multipath structure, with successive snapshots forming a 'motion-picture' representation of the multipath propagation between transmitter and receiver(either of which is mobile).

The first study of the impulse response of the mobile radio propagation channel was conducted by Young and Lacy[3.10] in urban New York City. A 100W peak power RF pulse at 450MHz, 0.5μs in duration, transmitted from a fixed base station, was used as the sounding waveform. The 0.5μs pulse width corresponds to a minimum echo-path resolution of $\simeq$150m. At the mobile receiver, the pulsed RF carrier and the time-delayed echoes due to multipath were received on a quarter-wavelength whip antenna, and then fed to a conventional RF front end. Following translation to a 30MHz IF, the received signal was envelope detected to obtain the video response of the channel. An automatic gain control was used for the IF amplifier so as to maintain the amplitude of the largest echo at a predetermined level. The video response of the channel was then displayed on a CRO. The CRO was also triggered by the video response, therefore, in order to avoid missing its beginning, the video response was passed through a 5μs delay-line on its way to the CRO, whereas it passed directly to the trigger circuit.

A record of the impulse response of the channel was obtained by photographing the CRO display with a 16mm cine-camera. Photographic records of the video response were acquired at half-mile intervals for various locations in Manhattan. In order to illustrate the time-variant behaviour of the multipath, some sequences of photographs were taken at a rate of 16 per second. With a vehicle speed of 10 to 15 m.p.h., this meant that successive pictures contained impulse responses corresponding to locations spaced approximately one foot apart.

A more recent study was carried out by Turin[3.15] in San Francisco using essentially the same method as Young and Lacy. Impulse response measurements were obtained using a 0.1μs duration pulse(i.e., $\simeq$30m spatial resolution) at carrier frequencies of 488MHz, 1280MHz and 2920MHz. Peak transmitter powers varied depending on frequency and location, for the less dense East Bay area the peak powers were 390W, 2.76KW and 206W respectively, and for urban San Francisco they were 650W, 3.24KW and 1.16KW respectively. Use of logarithmic IF(log-IF) amplifiers, with 60dB dynamic range, in the receiver obviated the need for automatic gain con-

trols. A three trace CRO was used to display the video responses, and an attached camera allowed photographic recording of the data.

Accurate timing measurements, with respect to the line-of-sight time-delay, were obtained through the use of rubidium atomic frequency standards at both the transmitter and mobile receiver, these being synchronised prior to the start of an experimental run. The transmitter clock was connected so as to pulse the transmitter once a second, while the receiver clock was connected so as to trigger the CRO a short time, τ seconds, later; where τ is less than the expected line-of-sight time-delay. The traces were adjusted to provide $10\mu s$ of video response of the multipath behaviour.

The most recent study of this kind has been undertaken by Van Rees[3.16,3.17] in Leidschendam, The Hague. Impulse response measurements have been obtained by transmitting a 10W peak power pulse, at 910MHz, every $100\mu s$ from a moving vehicle. Pulse durations of 50ns, 100ns[3.16] and 200ns[3.17], corresponding to spatial resolutions of 15m, 30m and 60m respectively, have been used.

The receiver system was housed on a 50m high tower, and employed a directional antenna for signal reception, pointed in the direction of the vehicle. As a result, this may have some influence on the measured data. The remainder of the receiver was essentially identical to Turin's, employing a 60dB dynamic range log-IF amplifier, and an envelope detector. However, data collection was achieved with a high speed waveform digitiser, instead of a camera. The digitising rate was set 10 times higher than the reciprocal of the pulse duration, and the frame size set to enable the observation of $10\mu s$ of path-delay. Each frame of data was stored on a 10MByte hard disk attached to a microcomputer. Therefore, although the pulse repetition rate is $100\mu s$, the data collection rate is set by the data transfer to the hard disk. This varies between 20ms and 50ms depending on the pulse duration. The trigger level for the digitiser was set just above the noise floor of the receiving system, and so, in a similar manner to Young and Lacy's system, the video response itself initiates triggering.

There are, however, several major weaknesses in the periodic pulse sounding measurement technique. The presence of an automatic gain control[3.10] destroys the true relationship between echo levels in successive responses; this can be overcome by the use of log-IF amplifiers[3.15-3.17]. In using the video response to trigger data collection[3.10,3.16,3.17], it is impossible to distinguish between a line-of-sight, or delayed obstructed path which appears as the first observable echo. Since absolute timing information is essential for schemes such as automatic vehicle location monitoring, this problem can be remedied by the use of a common time reference based on highly accurate clocks[3.15]. Photographic data collection[3.10,3.15] enables only a limited number of observations to be made, and leaves the data in a difficult form for post-processing. Use of an analogue instrumentation tape recorder, or a direct digital technique[3.16,3.17] alleviates this short-coming.

All three systems described above used an envelope detection technique, therefore, the phase information, containing the angles-of-arrival of echo-paths in the form of Doppler-shifts, was discarded. Thus, it was impossible to identify the sources of significant single scattering. The Doppler-shifts could be determined by coherently demodulating the quadrature components of the received signal. Possibly the major limitation, however, of the periodic pulse sounding technique is its requirement of a high peak-to-mean power ratio to provide adequate detection of weak echoes. Since, in general, pulsed transmitters are peak power limited, a possible way of overcoming this constraint is to use a sounding method which provides pulse compression. Systems employing pulse-compression techniques will be described in the following sections.

3.2.2 Pulse Compression Techniques.

As stated in Section 3.2.1, one of the principal drawbacks of the periodic pulse sounding method is its requirement of a high peak-to-mean transmitter power ratio. Consequently, schemes have been sought which obviated this need, and they have been termed pulse compression techniques.

The basis for all pulse compression systems is the theory of linear systems[3.18]. It is well known that, if white noise, $n(t)$ is applied to the input of a linear system, and if the output, $w(t)$, is cross-correlated with a delayed replica of the input, $n(t-\xi)$ then the resulting cross-correlation coefficient is proportional to the impulse response of the system, $h(\xi)$, evaluated at the delay time. This can be shown as follows,

$$\mathrm{E}[n(t)n^*(t-\xi)] = R_n(\xi) = N_0\delta(\xi) \tag{3.1}$$

where, $R_n(\xi)$ is the autocorrelation function of the noise, and N_0 is the single-sided noise power spectral density. The system output is given by the convolution relationship,

$$w(t) = \int h(\tau)n(t-\tau)\,d\tau \tag{3.2}$$

so, the cross-correlation of the output and the delayed input is given by,

$$\begin{aligned}\mathrm{E}[w(t)n^*(t-\xi)] &= \mathrm{E}\left[\int h(\tau)n(t-\tau)n^*(t-\xi)\,d\tau\right] \\ &= \int h(\tau)R_n(\xi-\tau)\,d\tau \\ &= N_0h(\xi)\end{aligned} \tag{3.3}$$

Therefore, the impulse response of a linear system can be evaluated using white noise, and some method of correlation processing.

In practice, however, it is impossible to generate white noise, and, as a result, experimental systems must employ deterministic waveforms which have a noise-like character. Possibly the most widely known examples of such waveforms are the maximal length pseudo-random binary sequences(m-sequences).[7] These have proved extremely popular in communications, navigation and ranging systems[3.19-3.21], since they are easily generated using linear feedback shift-registers, and possess excellent periodic autocorrelation properties.

---

[7] Alternatively known as pseudo-noise(PN) sequences, m-sequences and PRBS's, however, it should be noted that not all pseudo-random sequences are of maximal length.

The period, T, of an m-sequence is determined by the number of stages in the shift-register, N, and its clock period, τ_0. The length of an m-sequence is,

$$m = 2^N - 1 \tag{3.4}$$

therefore, its period, T, is,

$$T = m\tau_0 = (2^N - 1)\tau_0 \tag{3.5}$$

The periodic autocorrelation function, $R_m(\xi)$, of an m-sequence can be expressed mathematically as,

$$R_m(\xi) = \begin{cases} m - \dfrac{(m+1)|\xi|}{\tau_0} & |\xi| \le \tau_0 \\ -1 & \tau_0 \le |\xi| \le (T - \tau_0) \end{cases} \tag{3.6}$$

and will repeat at intervals of T seconds. As can be seen from Fig.(3.1), the maximum value of $R_m(\xi)$ equals m, and occurs for zero delay. Outside the interval $|\xi| \le \tau_0$, $R_m(\xi)$ has a residual bias value of -1.

Very often $R_m(\xi)$ is normalised such that the peak value equals 1, and the bias equals $-1/m$. As a result, it is clearly seen that,

$$\lim_{\substack{m\to\infty \\ \tau_0 \to 0}} R_m(\xi) \to \delta(\xi) \tag{3.7}$$

Therefore, these waveforms will provide reasonable accuracy in the measurement of the impulse response of the channel, depending on the values of m and τ_0 used.

The sequence length, m, determines both the dynamic range of the measuring system, i.e., the sensitivity to weak echoes, and the maximum unambiguous echo-path time-delay, while the clock period establishes the minimum detectable echo-path difference. Therefore, for a fixed echo-path resolution, the sensitivity to weak echoes can be improved by increasing m. This is assuming that the overall system noise does not become a limiting factor. Two methods of implementing practical pulse compression channel sounders will be discussed in the following sections.

3.2.3 Convolution Matched-Filter Technique.

One method of effecting pulse compression is to use a filter which is matched to the sounding waveform. This is known as the convolution matched-filter technique, and has been used in a study at 436MHz in Birmingham[3.12].

The principle of operation of the matched-filter method can be explained as follows. Let $x(t)$ represent the maximal length pseudo-random waveform, then, for a physically realisable matched-filter, its impulse response must be given by $x(T-t)$[3.22]. Therefore, if $x(t)$ forms the input to a linear channel, which has an impulse response $h(t)$, the output from the matched-filter, $w(t)$, is given by the convolution relationship[3.12],

$$w(t) = h(t) \circledast x(t) \circledast x(T-t) \tag{3.8}$$

The convolution of $x(t)$ and $x(T-t)$ can be expressed as,

$$y(t) = \int x(\beta)x(T-t+\beta)\,d\beta \tag{3.9}$$

and the convolution of $h(t)$ and $y(t)$ as,

$$w(t) = \int h(\alpha)y(t-\alpha)\,d\alpha \tag{3.10}$$

Therefore, using equation (3.9) in equation (3.10) gives,

$$w(t) = \int h(\alpha) \int x(\beta-\alpha)x(T-t+\beta)\,d\beta\,d\alpha \tag{3.11}$$

The inner integral can be expressed as the autocorrelation function of the sounding waveform within the period of observation, i.e.,

$$\int x(\beta-\alpha)x(T-t+\beta)\,d\beta \simeq AR_x(t-T-\alpha) \tag{3.12}$$

where, A is a constant of proportionality. Using the result of equation (3.12) in equation (3.11) gives,

$$w(t) \simeq A\int h(\alpha)R_x(t-T-\alpha)\,d\alpha \tag{3.13}$$

which can be rewritten as,

$$w(t) \simeq Ah(t-T)\circledast R_x(t-T) \tag{3.14}$$

Therefore, if $R_x(t-T)$ is a delta function, or a close approximation to one, then the output of the matched-filter becomes,

$$w(t) \simeq Ah(t-T) \tag{3.15}$$

i.e., the filter output is the impulse response of the channel as a function of real time.

For the study in Birmingham[3.12], an experimental Surface Acoustic Wave(SAW) device was used to realise the matched-filter. In these experiments a 76.5MHz carrier was phase-reversal modulated with a 127-bit m-sequence clocked at 12.75MHz, thus providing a minimum time-delay resolution of better than 0.1μs. This signal was then translated to the UHF band by mixing with a 360MHz LO frequency. A wideband linear power amplifier was used to provide a 1W RF signal level into an omnidirectional transmitting antenna, mounted atop a fixed base station. All frequencies used were derived from a high stability 5MHz crystal oscillator.

In the receiver, an identical 5MHz crystal oscillator was also used to derive all the required frequencies. After front end amplification and filtering, the received signal was translated to a 76.5MHz IF, and applied to the input of the experimental SAW device. This constituted a matched-filter for a 76.5MHz carrier, phase-reversal modulated by a 127-bit m-sequence. Thus, pulse compression was achieved as successive bursts of the 76.5MHz carrier were obtained at the filter output for each multi-path time-delayed component of the received signal.

The filter output was then divided into two cophasal components, and demodulated to baseband using quadrature carriers. The bandwidth of the quadrature baseband video responses was 12.75MHz, and necessi-

tated suitable bandwidth reduction to facilitate data collection. This was achieved using sample-and-hold gates operating in a similar manner to a high frequency sampling oscilloscope. Using a scaling factor of 2000 resulted in a reduced bandwidth of 6.375KHz, which was compatible with a conventional analogue tape recorder.

Accurate timing information, at the receiver, was provided by a timing circuit which was synchronised to the transmitter clock prior to each experimental run. Therefore, it was possible to distinguish between line-of-sight, and obstructed paths arriving as the first discernible echo. Following suitable data processing, all the information concerning echo time-delays, Doppler-shifts, etc., could be obtained using this technique.

Unlike the cross-correlation method, to be described in the next section, the convolution matched-filter sounding technique does not require local regeneration of the m-sequence at the receiver to produce the pulse-compression, and can, therefore, be thought of as an asynchronous sounding technique. However, it has two severe limitations which, it is felt, limits its appeal for channel sounding. Firstly, the requirement of bandwidth reduction of the impulse response data prior to recording, and secondly, the performance of practical SAW devices is limited by deficiencies in the devices themselves. Specifically, the generation of spurious acoustic signals gives rise to phenomena such as multiple reflection, bi-directional re-radiation and scattering of the surface acoustic waves. Also, since the devices are fabricated using standard photolithographic techniques, the placement accuracy in the mask making process produces errors in the positioning of the interdigitated transducers. As excitation of the transducers is dependent on the accurate spatial position of the interdigitated structures, a degradation in performance arises. The combination of these effects causes time sidelobes to appear in the output of the matched-filter, and results in a reduced sensitivity to weak echoes.

3.2.4 The Swept Time-Delay Cross-Correlation Method.

In Section 3.2.2, it was shown that the cross-correlation of the input and output of a linear system can be expressed by the following convolution relationship,

$$R_{wx}(\xi) = \int h(\tau) R_x(\xi - \tau)\, d\tau = h(\xi) \circledast R_x(\xi) \qquad (3.16)$$

It was further shown that if $R_x(\xi)$ is a good approximation to a delta function, as is the case with a suitable m-sequence, then the cross-correlation coefficient $R_{wx}(\xi)$ is effectively a sample of the impulse response of the system at the delay value ξ.

The relationship in equation (3.16) clearly illustrates the principle of the cross-correlation sounding technique. However, comparison of equation (3.16) with equation (3.14), for the convolution matched-filter method, highlights the subtle difference between the two techniques. The output of the matched-filter provides the impulse response as a function of real time, whereas the output of the cross-correlator is a sample of the impulse response at the single delay value ξ. The cross-correlator technique can be made equal to the matched-filter method by using a densely tapped-delay line composed of infinitesimal delay elements, and a bank of correlators producing samples of the impulse response for all values of delay. Summation of the individual outputs will then produce the impulse response in real time. Obviously a practical system will be limited by the finite number of correlators and delay elements which it is feasible to use. Price and Green employed this technique in implementing their famous RAKE receiver[3.21(Vol. 1),3.23].

An alternative approach, which requires only a single cross-correlation stage, is to vary the relative delay between the two m-sequences. This can be done in two ways, either the m-sequence is discretely stepped(randomly or linearly) through each of its m-phases, or the clock frequencies of the two m-sequences are slightly offset, causing the relative delay between the transmitted and received m-sequences to vary linearly with time. As a result, the parallel form of processing found in the RAKE system, is transformed into a serial form, with the penalty that instantaneous impulse responses can no longer be observed. Therefore, inherent in both these techniques is time-scaling(i.e., bandwidth reduction) of the cross-correlator output.

The stepping cross-correlator method has been used in microwave line-of-sight propagation studies[3.24], and a study of multipath mobile radio propagation in Japan[3.25]. The swept time-delay cross-correlation method was first proposed for the characterisation of tropospheric scatter channels[3.26], and was subsequently used in an investigation of mobile radio channels[3.27].

The earliest impulse response measurements of the mobile radio channel made using a swept time-delay cross-correlation sounder, were obtained by Cox[3.27] in New York City at 910MHz. In these experiments a 511-bit m-sequence clocked at 10MHz, was used to phase-reversal modulate a 70 MHz carrier. This modulated signal was then translated to the sounding frequency by mixing with an 840MHz LO, and was amplified to produce an average radiated power of 10W. The signal was radiated from an omnidirectional antenna mounted atop a fixed base-station. All frequencies used in the transmitter were derived from a stable 5MHz frequency standard.

In the mobile receiver an identical 5MHz standard was also used to derive all frequencies. Following front-end amplification and filtering, the received signal was translated down to 70MHz by mixing with an 840MHz LO. The 70MHz IF signal was then split in a wideband quadrature hybrid, and applied to two correlators.

In each correlator, an identical m-sequence to that formed in the transmitter, but clocked at the slightly slower rate of 9.998MHz, was used to phase-reversal modulate a 70MHz carrier. This signal was then multiplied with the IF signal from the quadrature hybrid. A low-pass integrating filter completed the cross-correlator.

The difference in the clock rates for the two m-sequences determines the bandwidth of the cross-correlation function, in this case 2KHz(i.e., 10MHz - 9.998MHz). This corresponds to a time scaling factor of 5000, which means that the features of 5000 individual responses are contained within each delay profile obtained at the output of the cross-correlator. However, it was not anticipated that path delays would exceed 15μs, therefore, the slow m-sequence was reset every 75ms(5000 $\times$ 15μs). At a

constant speed of 1.4m/s, the vehicle would have travelled a spatial distance of approximately one third of a wavelength of the transmitted RF in this time. As a result, the 5000 individual responses are unlikely to have appreciably altered in their multipath structure. The validity of this argument was confirmed by Bajwa[3.12] in his real time observation of the output of his matched-filter receiver. The inherent bandwidth reduction of this system easily allowed data recording with conventional analogue tape recorders, for later analysis.

Demodulating the received signal in quadrature demodulators enabled extraction of the Doppler-shifts associated with each time-delayed echo. Accurate timing information was obtained by synchronising identical 10MHz m-sequences in the transmitter and receiver, and by using stable frequency standards. This enabled, for the first time, the simultaneous measurement of time-delays and Doppler-shifts in multipath mobile radio channels.

There have been several further studies made, in the mobile radio[3.28-3.31] and microwave[3.32] fields, using the swept time-delay cross-correlator method. All the measuring equipment in these studies were replicas of the system used by Cox,[8] although some sounders[3.29,3.31] employed envelope detectors instead of quadrature demodulators, because only investigations of the received envelope were required.

3.3 SUMMARY OF CHANNEL SOUNDING TECHNIQUES.

The advantages and limitations of the various sounding techniques have been outlined above. It would appear that the swept time-delay cross-correlator method is nearest to an optimum sounding technique. For this reason, it was the method chosen for the study presented here. However, there was a subtle difference between the implementation of the receiver used in this study, and those used by Cox, etc. This will be described, along with the rest of the sounding equipment, in the next chapter.

---

[8] The sounders used in the studies by Sass[3.30] and Linfield et. al[3.32] were, in fact, based on Cox's original equipment.

REFERENCES

[3.1] Bodson, D. and McClure, G. F., "Land-mobile Communications Engineering", IEEE Press, New York, 1984.

[3.2] Jakes, W. C. (Ed.), "Microwave Mobile Communications", John Wiley 1974.

[3.3] Atefi, A., "An investigation of radio wave propagation in mobile radio frequency bands", Ph.D. Thesis, Department of Electrical Engineering & Electronics, University of Liverpool, 1985.

[3.4] Ossanna, J. F., "A model for mobile radio fading due to building reflections: theoretical and experimental fading waveform power spectra", Bell Syst. Tech. J., Nov. 1964, Vol. 43, pp 2935-2971.

[3.5] Gilbert, E. N., "Energy reception for mobile radio", Bell Syst Tech. J., Oct. 1965, Vol. 44, No.8, pp 1779-1803.

[3.6] Clarke, R. H., "A statistical theory of mobile radio reception", Bell Syst. Tech. J., July-Aug. 1968, Vol. 47, pp 951-1000.

[3.7] Gans, M. J., "A power-spectral theory of propagation in the mobile-radio environment", IEEE Trans. Veh. Technol., Feb. 1972, Vol. VT-21, No. 1, pp 27-38.

[3.8] Arredondo, G. A., Chriss, W. H. and Walker, E. H., "A multipath fading simulator for mobile radio", IEEE Trans. Veh. Technol., Nov. 1973, Vol. VT-22, No. 4, pp 241-246.

[3.9] Ball, J. R., "A real-time fading simulator for mobile radio", The Radio and Electronic Engineer, Oct. 1982, Vol. 52, No. 10, pp 475-478.

[3.10] Young, W. R. and Lacy, L. Y., "Echoes in transmission at 450 megacycles from land-to-car radio units", Proc. IRE, March 1950, Vol. 38, pp 255-258.

[3.11] Cox, D. C. and Leck, R. P., "Correlation bandwidth and delay spread multipath propagation statistics for 910-MHz urban mobile radio channels", IEEE Trans. Commun., Nov. 1975, Vol. COM-23, No. 11, pp 1271-1280.

[3.12] Bajwa, A. S., "Wideband characterisation of UHF mobile radio propagation in urban and suburban areas", Ph.D. Thesis, Department of Electronic and Electrical Engineering, University of Birmingham, 1979.

[3.13] Matthews, P. A. and Molkdar, D., "Wideband measurements of the UHF mobile radio channel", IEE Fifth Intl. Conf. on Antennas Propagat., ICAP87, 1987, IEE Conf. Publication No. 274, Pt. 2, pp 73-76.

[3.14] Salous, S., 'FMCW channel sounder with digital processing for measuring the coherence of wideband HF radio links', IEE Part F, Aug. 1986, Vol. 133, No. 5, pp 456-462.

[3.15] Turin, G. L., Clapp, F. D., Johnston, T. L., Fine, S. B. and Lavry, D., "A statistical model of urban multipath propagation", IEEE Trans. Veh. Technol., Feb. 1972, Vol. VT-21, No. 1, pp 1-9.

[3.16] Van Rees, J., "Measurements of impulse response(sic) of a wideband radio channel at 910MHz from a moving vehicle", Electronics Letters, Feb. 1986, Vol. 22, No. 5, pp 246-247.

[3.17] Van Rees, J., "Measurements of the wideband radio channel characteristics for rural, residential, and suburban areas", IEEE Trans. Veh. Technol., Feb. 1987, Vol. VT-36, No. 1, pp 2-6.

[3.18] Papoulis, A., "Probability, Random Variables and Stochastic Processes", McGraw-Hill, 1965.

[3.19] Golomb, S. W., "Shift Register Sequences", Holden-Day, San Francisco, 1967.

[3.20] Sarwate, D. V. and Pursley, M. B., "Crosscorrelation properties of pseudorandom and related sequences", Proc. IEEE, May 1980, Vol. 68, No. 5, pp 593-619.

[3.21] Simon, M. K., Omura, J. K., Scholtz, R. A. and Levitt, B. K., "Spread Spectrum Communications", Computer Science Press, Rockville, MD, 1985(3 Volumes).

[3.22] Urkowitz, H., "Signal Theory and Random Processes", Artech House, Inc., 1983.

[3.23] Price, R. and Green, P. E., "A communication technique for multipath channels", Proc. IRE, Mar. 1958, Vol. 46, pp 555-570.

[3.24] Vilar, E., Moulsley, T. J., Austin, J., Hewitt, A., Norbury, J. R. and Barton, S. K., "A system to measure LOS atmospheric transmittance at 19GHz", presented at AGARD Conf. Proc. No. 346, Spatind, Norway, Oct. 1983.

[3.25] Saruwatari, T., Mizuno, M., Iwama, T., Sekizawa, S., Ryuko, H., Ando. H. and Nilson, M., "Large area characterisation of impulse responses on(sic) 775MHz in mountainous terrain", COST 207 TD(87)36, May 1987.

[3.26] Bailey, C. C., "Characterisation of tropospheric scatter channels by impulse reponse measurements", 16th. Symposium AGARD electromagnetic wave propagation panel(NATO), Dusseldorf, Germany, 31st. Aug. - 4th. Sept. 1970, Part II, pp 39-1 to 39-11.

[3.27] Cox, D. C., "Delay doppler characteristics of multipath propagation at 910-MHz in a suburban mobile radio environment", IEEE Trans. Antennas Propagat., Sept. 1972, Vol. AP-20, No. 5, pp 625-635.

[3.28] Nielson, D. L., "Microwave propagation measurements for mobile digital radio application", IEEE Trans. Veh. Technol., Aug. 1978, Vol. VT-27, No. 3, pp 117-131.

[3.29] Devasirvatham, D. M. J., "Time delay spread and signal level measurements of 850MHz radio waves in building environments", IEEE Trans. Antennas Propagat., Nov. 1986, Vol. AP-34, No. 11, pp 1300-1305.

[3.30] Sass, P. F., "Propagation measurements for UHF spread spectrum mobile communications", IEEE Trans. Veh. Technol., May 1983, Vol. VT-32, No. 2, pp 168-176.

[3.31] Huish, P. W. and Gurdenli, E., "Radio channel measurement and predictions for future mobile radio systems", Br. Telecom. Technol. J., Jan. 1988, Vol. 6, No. 1, pp 43-53.

[3.32] Linfield, R. F., Hubbard, R. W. and Pratt, L. E., "Transmission channel characterisation by impulse response measurements", U.S. Dept. Commerce, Office Telecommunications(OT) Rep. 76-96, Aug. 1976.

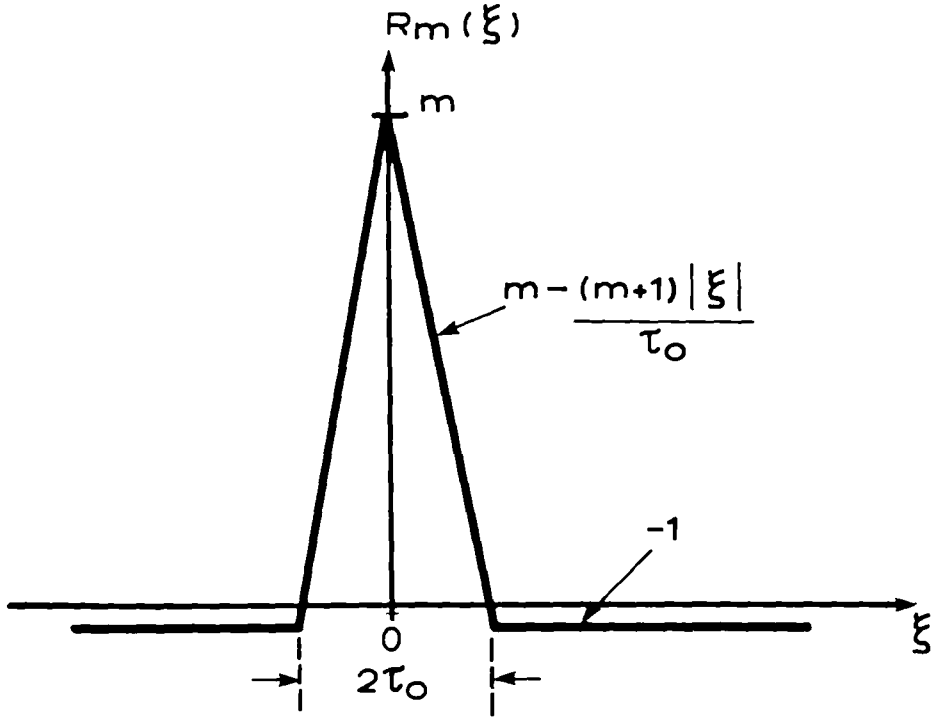

Fig. 3.1. Periodic autocorrelation function of a maximal length pseudo-random binary sequence(m-sequence).

CHAPTER 4. THE EXPERIMENTAL MEASURING EQUIPMENT.

The relative merits of the various channel sounding techniques were discussed in Chapter 3, and a preference was made for the linear Swept Time-Delay Cross-Correlator(STDCC) method. As a result, it was chosen as the sounding technique for this study.

Since no commercial sounding system was available, the measuring equipment was primarily purpose-built. Following a description of the channel sounder requirements, details of the transmitter and receiver systems will be presented.

4.1 SYSTEM REQUIREMENTS.

The recent rapid growth in private mobile radio schemes, and particularly cellular radio-telephony, has spurred the need for accurate methods of assessing, and/or predicting, the performance of these radio systems. From a Systems Engineering standpoint, propagation information which quickly allows the evaluation of modulation schemes, data-rates, diversity techniques, coding formats and equalisation techniques are of principal concern, whereas, from the standpoint of radio propagation modelling, information that relates multipath phenomena to the local environment is required. The ideal channel sounder would be able to satisfy all these criteria simultaneously, however, due to the method of operation of the STDCC, there is an interrelationship between the measured parameters(e.g., delays and Doppler-shifts) such that to effect an improvement in one parameter may cause a degradation in another. This will become clearer in the following sections.

4.1.1 Dynamic Range.

The dynamic range requirement of the system depends on how large a difference needs to be observed between the largest and smallest received echoes. For a STDCC, and ignoring the effect of system noise, the dynamic range is purely a function of the m-sequence length, and equals $20 \log_{10} m$.

For example, if a 30dB dynamic range is considered to be the minimum requirement, then the value of m has to be greater than, or equal to, 31.

4.1.2 Transmission Frequency.

At the outset, a characterisation of the UHF mobile radio channel at a frequency close to 900MHz was intended. However, due to the granting of licences to the cellular services, citizens' band, etc. at frequencies around 900MHz, the choice of operating frequency was limited to a gap in the spectrum between the television and cellular bands(854 to 890MHz), if interference to other users was to be minimised. Consequently, a centre frequency of 879.93MHz was chosen for transmission.

4.1.3 Multipath Resolution.

The multipath resolution capability of the sounder comprises two parts, spatial resolution and maximum unambiguous echo-path time-delay resolution.

4.1.3.1 Spatial Resolution.

Spatial resolution is a measure of the minimum discernible path difference between echo contributions, and is a function of the m-sequence clock rate. The clock rate has to be high enough to enable observation of the multipath echoes, which lead to intersymbol interference, and is limited only by the highest operating rates of available logic gates. Within these bounds, i.e., a few MHz to a few hundred MHz, the choice of clock rate(i.e., resolution) should depend upon the location of the experiment, e.g., a high resolution will be required for an indoor study(small scatterers), whilst a much lower resolution would probably suffice for a study in rural, mountainous areas(large scatterers).

As a result, for this survey in urban locations, a 10MHz clock rate was selected, which corresponds to a spatial resolution of $\simeq$30m. Although Cox[4.1] has reported rapid fading of echo contributions within a time-delay cell, due to unresolved paths differing by less than 30m in path delay,

it is felt that a 10MHz clock rate will still provide an adequate channel characterisation.

4.1.3.2 Maximum Unambiguous Echo-path Time-delay.

The maximum unambiguous echo-path time-delay which can be measured with a STDCC system is given by, the product of the length, in bits, and clock period of the m-sequence. This must be sufficiently long to ensure that no echoes are detectable after this time.

A minimum value of 10μs would appear reasonable for studies in urban areas[4.1]. Consequently, a value of 127 was chosen for m, allowing the observation of 12.7μs of the channel response.

4.1.4 Scaling Factor for the STDCC.

As stated in Section 3.2.4, the STDCC works by correlating two identical m-sequences that are produced at slightly different clock rates. This difference produces time-scaling(bandwidth compression) of the cross-correlation function, where the scaling factor is the ratio of the highest clock rate to the frequency difference.

The choice of time-scaling factor(k) may be thought to be arbitrary, and only depends upon the final bandwidth required for data recording. However, Cox[4.1] found that severe distortion was produced in the cross-correlation function if k was set too low. Therefore, k was chosen to be 5000, equalling Cox's value for his study with a 10MHz m-sequence clock rate.

4.1.5 Doppler-shift Resolution.

In order to identify the location of scatterers, the angles-of-arrival of echo-paths in the form of Doppler-shifts need to be determined. Although the Doppler information was not extracted for this particular study, other investigations of the measured data may require it. Therefore, the channel sounder was designed from the outset to be able to measure the Doppler-shifts. Furthermore, no single reference could be found that provides a complete description of the interaction between all the param-

eters of a STDCC system. Consequently, these features are discussed in this chapter for completeness.

The limits to which Doppler-shift information can be resolved depends upon the following factors,

(i) vehicle velocity(v) and stability

(ii) carrier frequency(f_c) and stability

(iii) m-sequence length(m) and clock period(τ)

(iv) the scaling factor(k) of the swept correlator

(v) the number of records(N) used for spectral estimates

The maximum Doppler-shift experienced by a mobile receiver is given by,

$$F_D = \frac{vf_c}{c} \tag{4.1}$$

where, v equals the vehicle velocity, f_c equals the carrier frequency and c equals the velocity of electromagnetic waves in free space. However, the maximum Doppler-shift that can be measured using a STDCC is given by,

$$F_D = \frac{1}{2km\tau} \tag{4.2}$$

where, k equals the STDCC scaling factor, m equals the m-sequence length and τ equals the m-sequence clock period. Comparing equations (4.1) and (4.2) gives,

$$v = \frac{c}{2km\tau f_c} \tag{4.3}$$

Equation (4.3) shows that, for k, τ and f_c fixed, v is inversely proportional to m. Therefore, whilst doubling m may be beneficial to resolve long time-delays, it would mean halving the vehicle speed to still permit Doppler-shift measurement. This may prove impractical due to the lower vehicle speed required. For $k = 5000$, $m = 127$, $\tau = 0.1\mu$s and $f_c = 900$MHz

the vehicle velocity would have to be less than, or equal to, 2.62m/s($\simeq$6 m.p.h.). However, increasing the m-sequence length to 255, would require a vehicle speed of less than 3 m.p.h.

The minimum Doppler-shift measurable is given by,

$$F_{\min} = \frac{1}{Nkm\tau} \tag{4.4}$$

where, N equals the number of data records used for spectral analysis. The overall frequency resolution, however, will depend upon the stability of the frequency sources, and the ability to maintain a constant vehicle speed throughout the measurement period.

4.1.6 Accuracy of Frequency Standards.

The accuracy of time/frequency generation and measurement depends upon the performance of the frequency standards employed in the transmitter and receiver systems. Furthermore, for a coherent system it is their performance in relation to each other that is of primary importance.

For perfect coherent signal demodulation, the injected carrier must be identical in both phase and frequency to that of the received signal. However, phase synchronism is impossible due to the random location of the mobile receiver, and hence there is a need for quadrature detection. Assuming identical frequency multipliers are employed at the transmitter and receiver, the degree to which frequency synchronism can be achieved depends upon the magnitude of any frequency offset between the transmitter and receiver standards, and their stability.

The stability of frequency standards[4.2] is usually expressed in terms of drift measured relative to a primary master source.[9] Although such a source was not available during this study, and so absolute performance measures could not be made, this was of little consequence since it was the performance of the standards in relation to each other that was of interest.

---

[9] Generally a system of caesium atomic standards.

Any fractional frequency difference between the standards causes a slow drift between the transmitter and receiver systems, and this sets two performance bounds for the channel sounder. Firstly, the drift causes a relative shift in timing, so that echoes with the same path delays no longer occupy the same time-resolution cell. Therefore, there will be a maximum time of field trial operation before re-synchronisation of the sounder is required. Secondly, the slow drift determines the lowest Doppler-shift frequency that can be unambiguously resolved. This has a bearing on how accurately the sounder can measure echo contributions arriving with angles close to 90° relative to the direction of motion.

A measurement period can be defined as the time it takes for a drift of a single time resolution bin, i.e., 0.1μs. If this is to be on the order of 30 minutes, then the frequency difference between the standards has to be on the order of 5.6×10^{-11}, and the stability has to be good enough to maintain this difference over the 30 minute period.

4.1.7 Phase Noise in Signal Sources.

Assuming that perfect frequency synchronism existed between transmitter and receiver, the outputs of two quadrature demodulators would define a received vector with a constant amplitude and a fixed, arbitrary phase angle. However, this statement assumes that all frequency sources are ideal, and produce outputs that are constant in both amplitude and frequency, i.e., their spectra are delta functions in the frequency domain. In practice, all signal sources exhibit random perturbations in both amplitude and phase. The spurious amplitude modulation is typically much smaller than the random phase modulation(phase noise), and is generally ignored[4.3], but the phase noise is important since it leads to a degradation in system performance, particularly in low data-rate communications and Doppler-radars.

The effect of phase noise in a STDCC system is to induce random amplitude fluctuations in the quadrature signal components. This can be best understood by considering the system to be both phase and frequency synchronous, such that all the received energy appears in the inphase channel. The effect of any phase jitter is to cause random perturbations

in the phase of the received vector. For narrowband phase-modulation, the amplitude of the inphase component will 'appear' fixed, however, a small component now appears in the quadrature channel. The result of this jitter will be to cause slight broadening of the measured Doppler spectra components.

4.1.8 Changes to Sounder Layout.

Although several studies have been undertaken using the STDCC method[4.1,4.4-4.6], the sounders used in each instance have generally been identical in form to Cox's[4.1]. For this study, however, two changes to the sounder layout were implemented which resulted in a reduction in both circuit complexity and the number of components used.

The first change was in the transmitter, and involved removing the IF stage and directly modulating the RF carrier with the pseudo-random code. This has the advantages of obviating the need to synthesise the IF and eliminating the need to filter the RF signal, in order to remove the unwanted sideband at LO plus, or minus, IF, following up-conversion.

The second change was in the receiver. Cox's sounder was essentially a direct implementation of the cross-correlator idea. That is, the received signal was translated to IF, then split in a wideband quadrature hybrid, and finally demodulated in two correlators. An alternative approach is to multiply the received signal by the slower m-sequence at the same time as translation to IF.* Demodulating two cophasal components of the IF signal with quadrature sinusoids, and applying the products to two low-pass integrators results in identical outputs to Cox's.

This second approach, however, requires the multiplicative part of the cross-correlation process to be performed in a single place. Also, and more importantly, carrying out the multiplication coincident with RF to IF translation results in a reduced IF bandwidth from twice the clock rate to twice the difference in clock rates, i.e., from 20MHz to 4KHz. Therefore, wideband components in the IF stage are eliminated, and accuracy improved since only the IF carrier needs to be split into quadrature com-

*- A. S. Bajwa - private communication.

ponents. A detailed description of the complete channel sounder now follows.

4.2 TRANSMITTER.

A simplified block diagram of the transmitter is shown in Fig.(4.1). A 127 bit m-sequence, having a chip rate of 10Mb/s, was used to phase-reversal modulate an 879.93MHz carrier. This coded signal has a constant RF envelope, with 180° phase reversals occurring at the transitions of the m-sequence. The RF signal was then amplified, and radiated from a wide-band discone antenna.

The various modules making up the transmitter will be discussed individually in the following sections.

4.2.1 The m-sequence Generator.

Pseudo-random binary sequences(PRBS) are easily generated using shift registers and linear feedback elements, see Fig(4.2). To produce a PRBS the outputs from the last delay stage, and one, or more, intermediate stages are combined in a modulo-2 adder, and fed back to the input of the first shift register stage. The cyclic code sequences generated by this means have a maximum period of $2^N - 1$ clock periods, where N is the number of delay stages in the register. Sequences of length $2^N - 1$ are termed maximal length, or m-sequences.

The code generator used in this study was designed to produce a 127 bit m-sequence. Figure (4.3) shows the chosen[10] generator configuration. The 127 bit code can be expressed mathematically as,

$$S_S = S_3 \oplus S_7 \tag{4.5}$$

where, S_S equals the serial input to the first shift register stage (S_1), and S_i equals the output of the i^{th} shift register stage.

Every possible state of an N-stage generator appears at some time during the generation of a complete code cycle, with the exception that the

[10] There are 18 possible feedback connections for a 127 bit sequence.

all zeros condition does not occur, and can not be allowed to occur. This is because all zeros on the outputs of the shift register will force it into a cleared state.

In order to prevent 'all zeros latch-up' in the shift register, an $N-$input NAND gate was used to detect this situation, and, should it arise, to force a logic 1 into the serial input to initiate generation of the m-sequence. With a clock rate of 10Mb/s, the m-sequence repeated every $12.7\mu s$.

4.2.2 PSK Driver.

The modulation scheme used was binary phase-shift keying(BPSK).[11] BPSK can be easily generated using a double balanced mixer, as shown in Fig.(4.4). The phase of the carrier is switched depending upon the polarity of the current drive at the IF port.

Since the m-sequence generator was implemented using T^2L logic, its output was unipolar(0 to 5V). The unipolar output was converted to a bipolar current drive using a diode steered current source, see Fig.(4.5). This circuit is based on a design by Turner[4.7], but has been adapted to operate from a single $\pm 5V$ supply.

The circuit operates in the following manner for T^2L signals applied to it. When the input level is at 0V, transistor Q_1 is ON, diode D_1 is ON and diode D_2 is OFF. This causes current source Q_2 to deliver 15mA to the mixer. However, when the input level is at 5V, transistor Q_1 is OFF, diode D_1 is OFF and diode D_2 is ON. As a result, current source Q_3 acts as a 30mA current sink, and draws 15mA from current source Q_2 and 15mA from the IF port of the mixer. The RF signal phase is then shifted by 180° as it passes through the mixer. The binary phase-reversals are achieved in approximately 3ns[4.7] due to the current sources forcing rapid charging of circuit capacitance.

---

[11] Since 180° phase shifts are employed this is also widely known as phase-reversal keying(PRK).

Proper adjustment of the current levels enabled any imbalance in the mixer to be compensated for, and due care was taken to minimise code imbalance whilst maximising carrier frequency suppression[4.8].

4.2.3 RF Signal Source, Power Amplifier and Antenna.

The signal source employed at the transmitter was a commercial, low-noise RF signal generator, locked to a highly stable rubidium frequency standard. The generator was set to provide a fixed frequency of 879.93MHz, and had its modulation facilities disabled.

A broadband, class-A, linear power amplifier, with a gain of 40dB provided a 3W signal level at the transmitting antenna. The antenna was a vertically polarised wideband discone, with an omnidirectional azimuthal radiation pattern, and a VSWR less than 1.5:1 over its operating band. The amplifier and antenna were coupled together via a low-loss coaxial cable[12] to maximise power transfer.

4.3 RECEIVER.

A simplified block diagram of the receiver is shown in Fig.(4.6). A bandpass filter, a dual-channel, low-noise amplifier and a mixer form the front end of the receiver. Translation to a 69.93MHz IF is effected by mixing with an 810MHz LO, which is phase-reversal modulated by an identical, but slightly slower rate(9.998MHz), m-sequence to that formed in the transmitter. By applying the m-sequence at this point, the multiplicative part of the correlation process is carried out.

The IF signal is then split into two cophasal components, and demodulated to baseband using quadrature 69.93MHz sinusoids. Low-pass filters, in each quadrature channel, complete the correlation process, producing inphase and quadrature components of the channel response. Since bandwidth reduction is inherent in this technique, recording of the demodulated baseband information, for later analysis, was easily achieved.

---

[12] Signal reception at the receiver was carried out by an identical discone antenna to that in the transmitter, and it was coupled to the receiver by the same coaxial cable, therefore, they will be omitted from the receiver discussion. type of

The various modules making up the receiver will be discussed individually in the following sections.

4.3.1 RF Front End.

The linear swept time-delay cross-correlator system can be envisaged as a 'zero-data' direct sequence-spread spectrum(DS-SS) scheme, i.e., one where only the spreading code is present. For DS-SS systems, it is known[4.8] that the worst case interferer(jammer) is a CW tone at the carrier frequency. Since this is in-band its effect can only be suppressed by 'notch' filtering. However, it is extremely difficult to produce narrow bandwidth notch-filters, at RF frequencies, which have high levels of rejection. These factors are essential to prevent the wanted signal being removed by the notch. In addition, notch filters cannot counteract wideband jammers, or hopping jammers. Fortunately, in-band interference, narrowband and/or wideband, is spread, and therefore, its effect reduced, during despreading of the transmitted information.

From Fig.(4.6) it is seen that the first element in the receiver front-end is a pre-selector filter. This is to remove strong out-of-band interference which may cause saturation of the front-end amplifiers. The filter was a 5-section, 0.05dB Chebyshev design, having a 3-dB bandwidth of $\simeq$50MHz, and an insertion loss of less than 2dB. Following the filter was a dual channel, low-noise RF preamplifier, providing 26dB of gain in each channel.

An 810MHz LO frequency was generated by a low-noise RF signal generator, locked to an identical rubidium standard to that used in the transmitter. The LO was phase-reversal modulated by an m-sequence that was identical in character to the transmitted sequence, but was produced at the slightly slower clock rate[13] of 9.998MHz. This coded signal was used as the LO to down convert the received signal to a 69.93MHz IF. However, and more importantly, by applying the slower m-sequence at this juncture the multiplicative part of the cross-correlation process is carried out, re-

[13] The layouts of the slower m-sequence generator and PSK driver were identical to those used in the transmitter.

sulting in a narrowband IF signal. The bandwidth is only 4KHz in this case; cf. Cox's[4.1] system had an IF bandwidth of 20MHz.

4.3.2 The IF Stage.

The IF signal was split into cophasal components, and applied to the RF ports of two mixers. Prior to splitting, the IF signal was amplified to overcome splitter losses and to provide adequate drive levels for the mixers.

An existing frequency synthesiser, locked to the rubidium standard, provided a 69.93MHz LO. The synthesiser was a coherent direct design, consisting of multipliers, dividers and mixers.

Two 69.93MHz quadrature sinusoids, obtained from a 90° hybrid splitter,[14] were used to demodulate the IF signals to baseband. A low-pass amplifier and a low-pass filter completed each demodulator. The amplifiers provided sufficient signal level to drive the filters, which were digital, 7-th order, elliptic lowpass types; these filters being essentially 'brick-wall' designs, providing in excess of 80dB stopband rejection at twice the corner frequency.

Corner frequency selection is made via an external clock, and the filters were 'tuned' to provide the best impulse response concomitant with the lowest cut-off frequency, and this occurred for a 3-dB bandwidth of ≃4KHz. Both filters were operated from the same clock.

The filter outputs are the quadrature components of the channel impulse response. Since bandwidth reduction to a few KHz is inherent in this sounder, there was no difficulty in recording the channel responses.

4.3.3 Synchronisation and Time-reference Generation.

In order to be able to extract accurate timing information at the receiver, both transmitter and receiver systems were locked to highly stable atomic frequency standards. Prior to each experiment the trans-

[14] Comparisons with a 1/4-wavelength cable showed negligible difference in performance, and so, the splitter was used for convenience.

mitter and receiver 10MHz m-sequence generators were connected via a 100m length of coaxial cable,[15] see Fig.(4.7). To obtain synchronism, the one-shot switch was 'thrown', causing the flip-flop to force the transmitter m-sequence into the receiver shift register. This continued until the parallel outputs of the receiver register were 1111111, at that instant the logic gates disconnect the transmitter sequence, and reconnect the feedback loop, thus maintaining the generation of the m-sequence.

Following synchronisation, the receiver sequence runs in time with that in the transmitter, but is delayed relative to it by the propagation delays in the cable and synchronisation circuit. This problem was overcome by delaying the transmitter sequence by an amount equal to the total propagation delay prior to the PSK driver. Therefore, following synchronisation, the transmitter and receiver 10MHz m-sequence generators run in simultaneity.

Since the pulse generated by the 1111111 word occurs only once during the generation of a complete code cycle, it was also used as a time reference marker for measurement of propagation delay. However, since the correlation functions at the outputs of the quadrature demodulators are time-scaled by a factor of 5000, the time reference pulses were also similarly scaled.

The channel impulse response was obtained by cross-correlating 10MHz and 9.998MHz m-sequences, therefore, synchronism between these two generators is meaningless due to the difference in clock rates. As a result, following synchronisation, the correlation functions could appear anywhere in relation to the time reference marker pulse. Therefore, the 9.998MHz shift-register was held in a clear state until synchronisation was complete. This ensured that the correlation functions and the time reference marker always had a fixed time relationship.

4.4 SYSTEM PERFORMANCE.

The following performance measures were obtained with the transmitter/receiver system connected back-to-back.

---

[15] Due to the physical separation of transmitter and receiver.

4.4.1 Dynamic Range.

The theoretical dynamic range of a STDCC system is $20\log_{10} m$, therefore, for an m-sequence length of 127 the dynamic range should be 42dB. However, due to the presence of system noise, and in the absence of interference, the measured dynamic range was 36dB.

4.4.2 Correlation Loss due to RF Filter.

The power spectral density of an m-sequence[4.9] is given by,

$$S_m(f_c) = \frac{1}{m^2}\delta(f_c) + \left(\frac{m+1}{m^2}\right)\sum_{\substack{n=-\infty \\ n\neq 0}}^{\infty} \mathrm{sinc}^2\left(\frac{n\pi}{m}\right)\delta\left(f_c + \frac{n}{m\tau}\right) \qquad (4.6)$$

where, m is the m-sequence length, τ is the m-sequence clock period and f_c is the carrier frequency. Equation (4.6) shows that the spectral density comprises a heavily suppressed carrier and a series of spectral delta functions, whose amplitudes map out the $\mathrm{sinc}^2(x)$ function. The transmitted spectrum is shown in Fig.(4.8).

Figure (4.9) shows that the autocorrelation function produced by the receiver was not perfectly triangular, but was slightly rounded. This causes a slight decrease in both dynamic range and time-delay resolution. The rounding is a result of bandpass filtering the received sequence; Fig.(4.8) shows that the transmitted spectrum extends well beyond the f$\pm$10Mhz first nulls. According to Holmes[4.9], for a 3dB filter bandwidth-chip rate product($B\tau$) of 5.0, the correlation loss is less than 0.5dB, while for a $B\tau$ value of 2.0,[16] the loss in time-delay resolution is less than 0.1 of a chip.

Therefore, overall the dynamic range was limited by system noise, and the time-delay resolution was 0.1μs to within 10%; this was confirmed by the back-to-back measurements.

---

[16] Holmes only considers the loss in time-delay resolution for the case $B\tau = 2.0$.

4.4.3 Accuracy of Frequency Standards.

In order to assess the fractional frequency difference between the transmitter and receiver frequency standards, the quadrature outputs of the sounder were observed on an oscilloscope. If perfect frequency synchronism was possible, the quadrature outputs would map out a vector with some fixed, arbitrary, phase angle. However, due to the frequency difference, Δf, between the standards, the vector rotates in the IQ-plane at a rate proportional to Δf. By maintaining one standard fixed, and by fine-tuning the other, it was possible to minimise Δf.

For his study, Cox[4.1] achieved a phase change of 360° in 10s, which corresponds to a frequency difference of $\simeq 1 \times 10^{-10}$. Using an 879.93MHz carrier frequency, a phase change of 360° in 30s was consistently achieved during this study. This corresponds to a difference of $\simeq 3.8 \times 10^{-11}$, and set a maximum time of continuous field trial operation of 44 minutes. The stability of the two rubidium standards was found to be excellent, and fine-tuning needed to be carried out only at periods of several days.

4.4.4 Phase Noise in Signal Sources.

Although there have been several studies made of the mobile radio channel impulse response(see Chapter 3), no reports have been made of the effect of phase-noise on system performance. Therefore, prior to the start of field trials, a comparative survey of several commercial RF signal generators was undertaken to assess the influence of phase-noise on the performance of the STDCC system. From this survey it emerged that the criterion for good system performance was a reasonably low value of phase-noise power spectral density close-in to the carrier. This was confirmed by comparisons with a cavity-tuned generator noted for its low phase-noise at carrier offsets greater than, or equal to, 20KHz.

The choice of suitable generators was made by observing their effect on the system outputs. The single-sideband phase-noise power spectral density of the chosen generators was at least -50dBc[17] in a 1Hz bandwidth at a carrier offset of 10Hz, and this figure was not limited by the phase-

[17] Manufacturer's quoted figures.

noise of the rubidium oscillators. Figure (4.9) shows a two second exposure of the quadrature components of the back-to-back system response, for the case when all the received energy was in the inphase channel. It can be seen that the fluctuation induced in the quadrature channel was extremely small, as was required. Overall, the dominant factor causing broadening of Doppler-spectra components is likely to be the inability to maintain a constant vehicle velocity[4.1].

REFERENCES

[4.1] Cox, D. C., "Delay doppler characteristics of multipath propagation at 910-MHz in a suburban mobile radio environment", IEEE Trans. Antennas Propagat., Sept. 1972, Vol. AP-20, No. 5, pp 625-635.

[4.2] Kartaschoff, P., "Frequency and Time", Academic Press, 1978.

[4.3] Robins, W. P., "Phase Noise in Signal Sources", IEE Telecommunications Series 9, Peter Peregrinus Ltd., London, 1982.

[4.4] Linfield, R. F., Hubbard, R. W. and Pratt, L. E., "Transmission channel characterisation by impulse response measurements", U.S. Dept. Commerce, Office Telecommunications(OT) Rep. 76-96, Aug. 1976.

[4.5] Sass, P. F., "Propagation measurements for UHF spread spectrum mobile communications", IEEE Trans. Veh. Technol., May 1983, Vol. VT-32, No. 2, pp 168-176.

[4.6] Huish, P. W. and Gurdenli, E., "Radio channel measurement and predictions for future mobile radio systems", Br. Telecom. Technol. J., Jan. 1988, Vol. 6, No. 1, pp 43-53.

[4.7] Turner, R. J., "Binary RF phase modulator switches in 3 nanoseconds", Electronics, April 26, 1973, p 104.

[4.8] Dixon, R. C., "Spread Spectrum Systems(2nd Edition)", John Wiley, 1984.

[4.9] Holmes, J. K., "Coherent Spread Spectrum Systems", Wiley, New York, 1982.

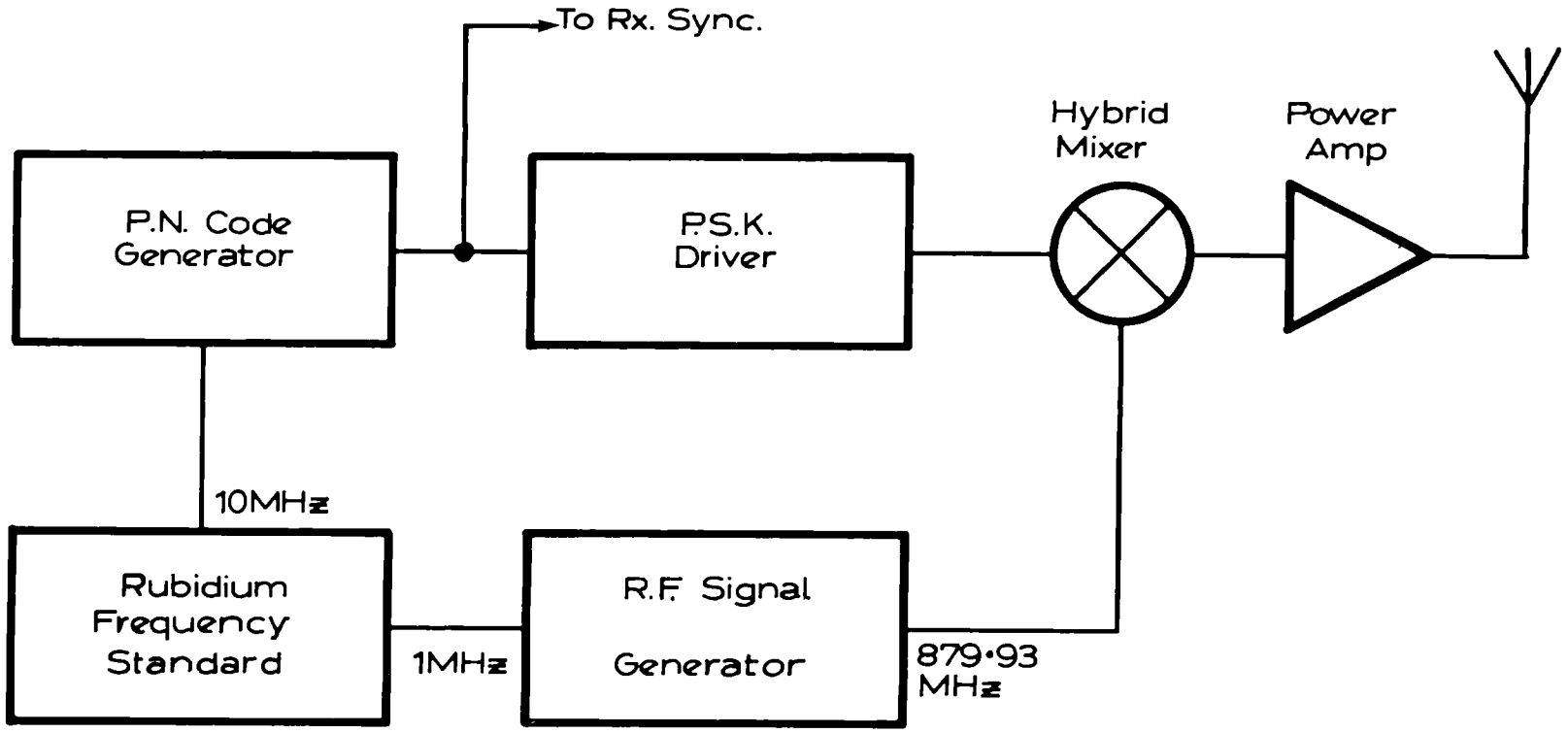

Fig. 4.1. Transmitter Block Diagram.

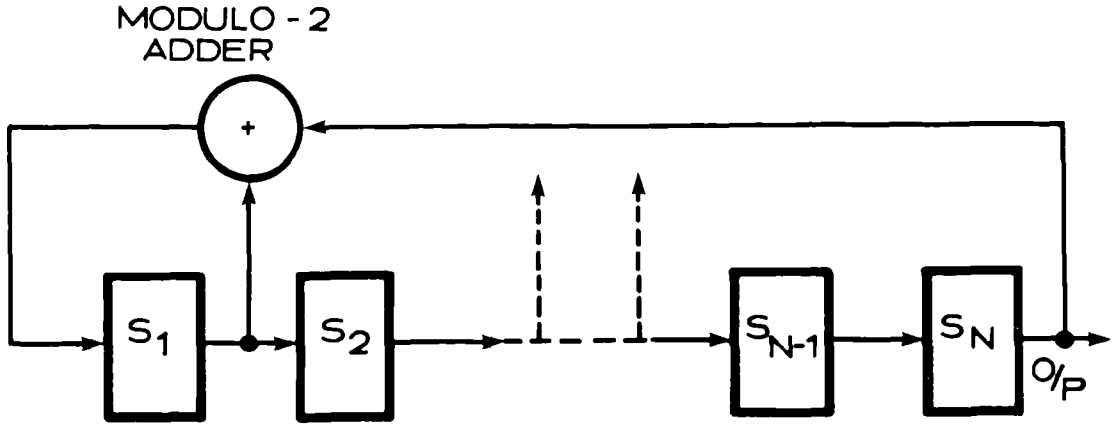

Fig. 4.2. General N-stage pseudo-random sequence generator.

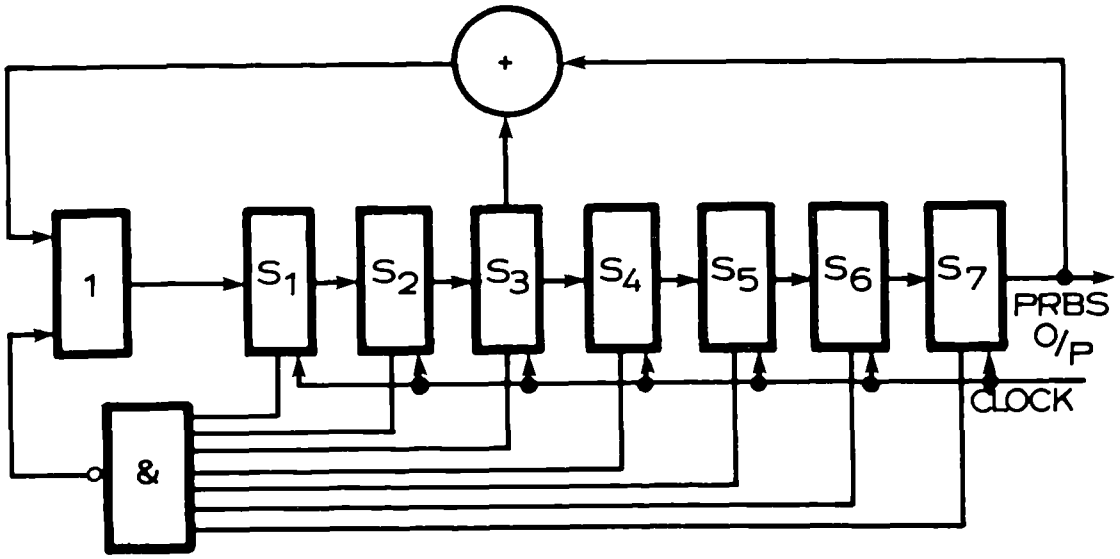

Fig. 4.3. 127-bit m-sequence generator showing NAND gate to prevent all-zero latch-up.

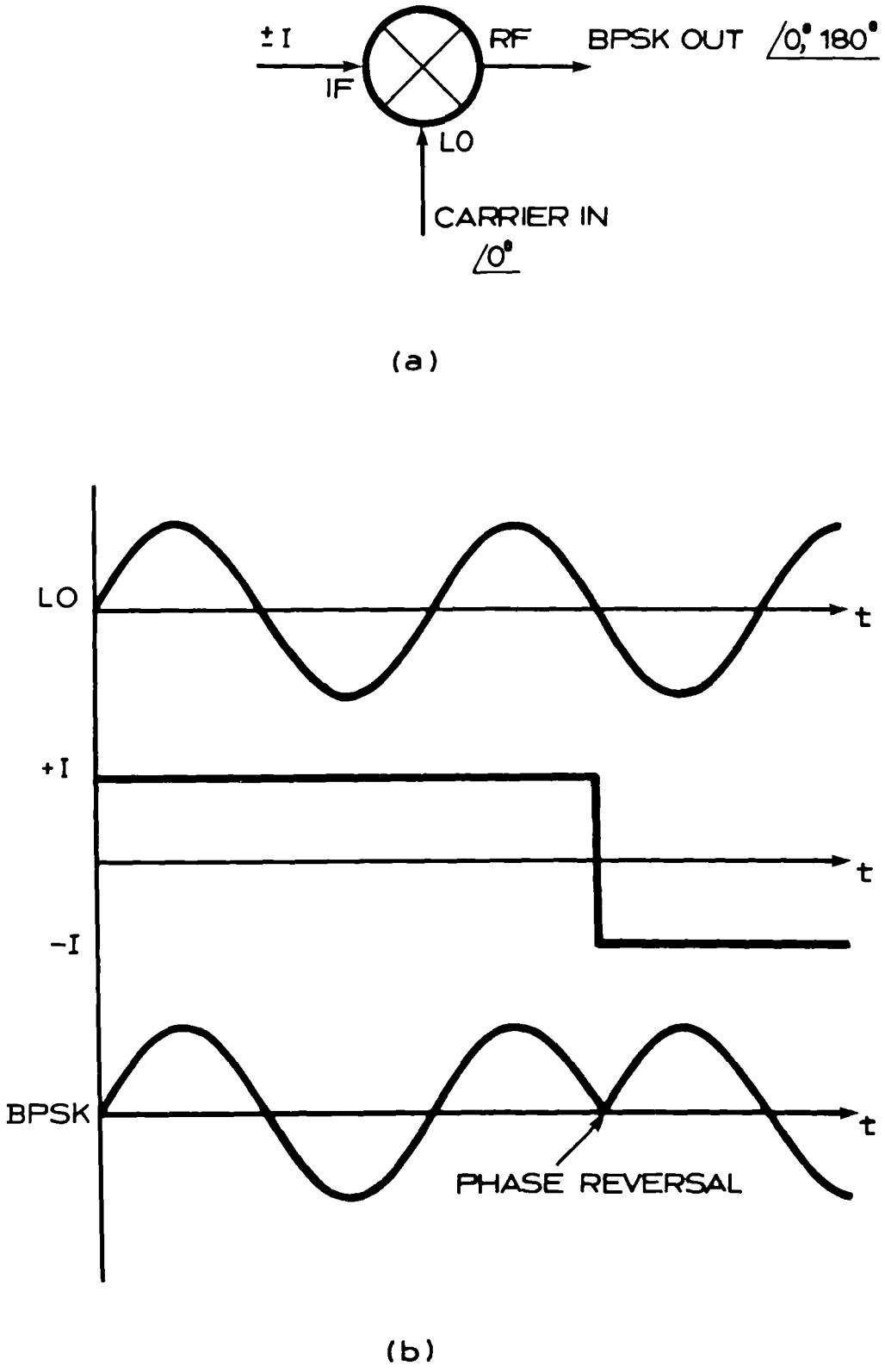

Fig. 4.4. (a) BPSK modulator; (b) Waveforms at LO, IF and RF ports of a BPSK modulator.

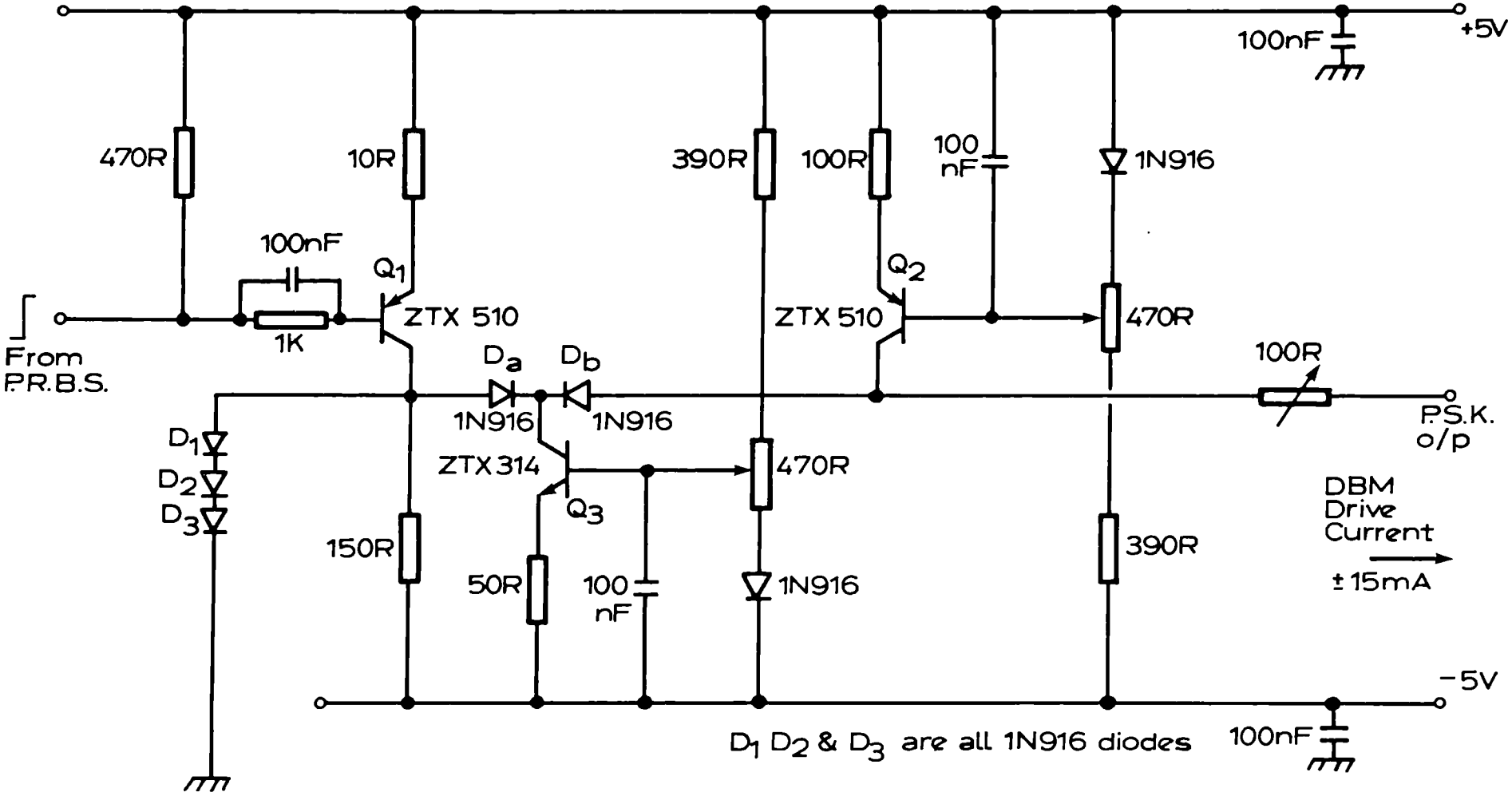

Fig. 4.5. The PSK driver circuit.

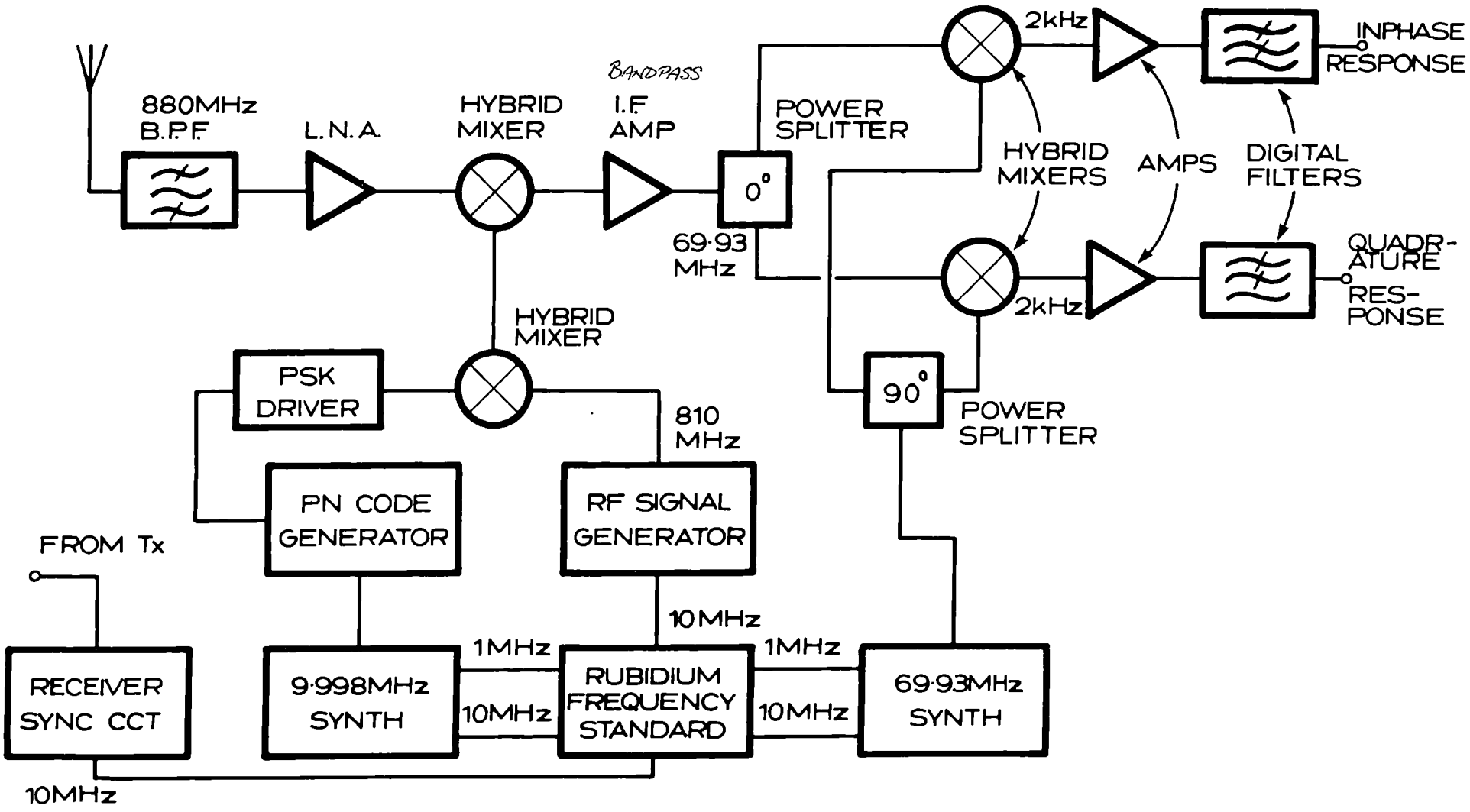

Fig. 4.6. Receiver Block Diagram.

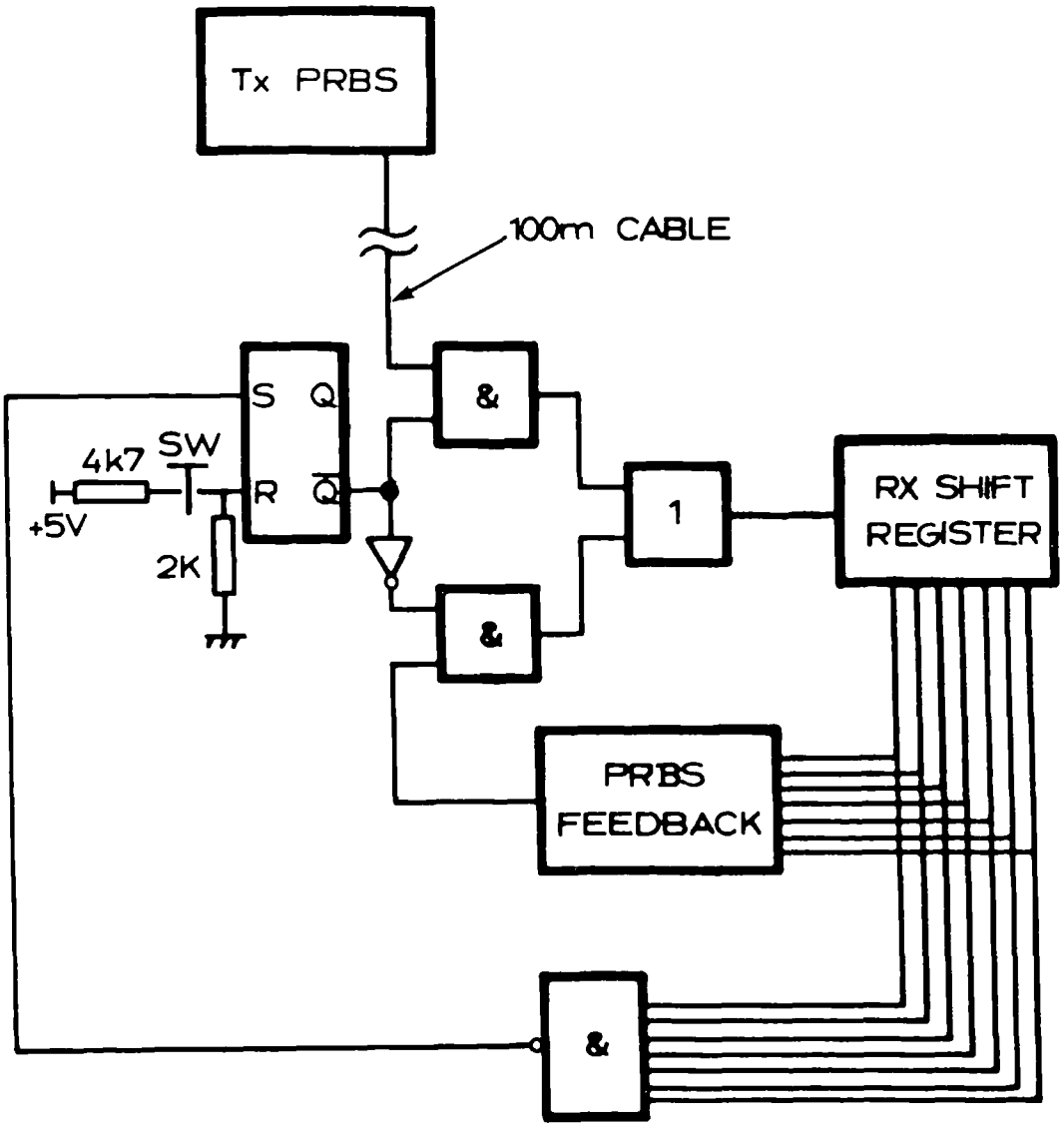

Fig. 4.7. Receiver synchronisation and time-reference generator circuit.

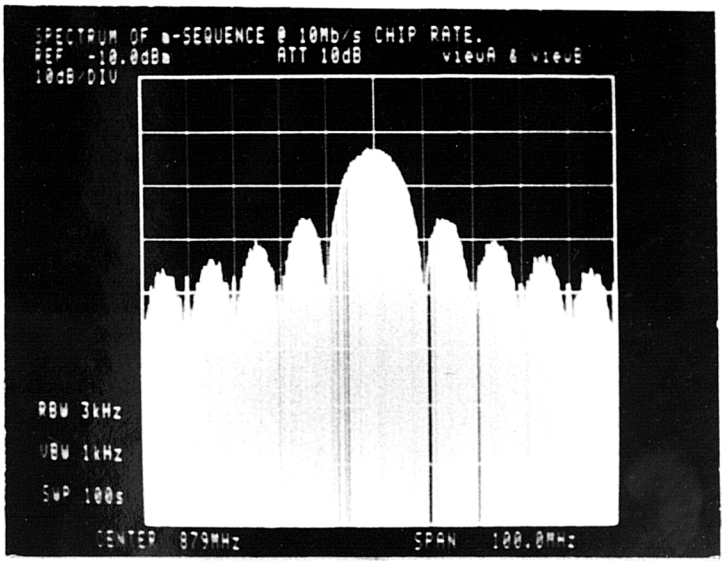

Fig. 4.8. Spectrum of the transmitted signal, showing low levels of spuriae.

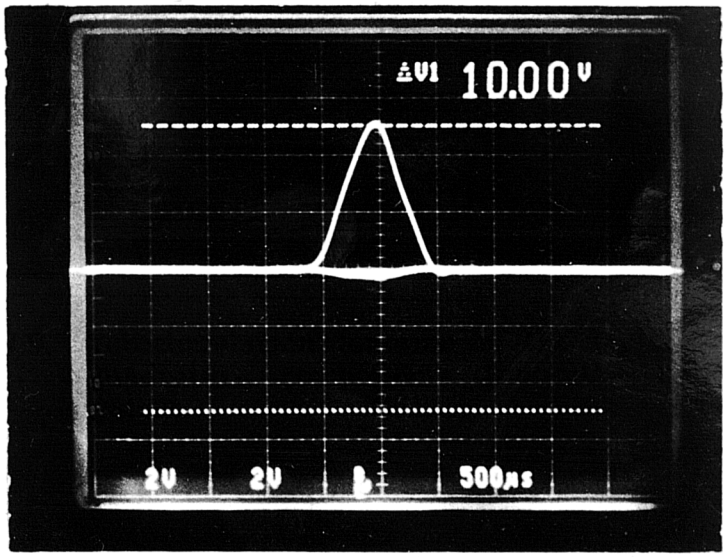

Fig. 4.9. Autocorrelation function of the Inphase and Quadrature components from the receiver system.

CHAPTER 5. DATA ACQUISITION AND DIGITISATION.

For the purpose of conducting the field trials, all the receiver equipment, described in Section 4.3, was built into a 19"-rack and installed in a conventional motor-car on resilient mountings. In addition, a 4-beam CRO and a 7-track analogue instrumentation tape-recorder were installed for signal monitoring and data collection.

Prior to the start of any experimental run, a check was made of the relative difference between the transmitter/receiver frequency standards. Provided the difference was sufficiently small, the transmitter/receiver systems would be synchronised, following the procedure outlined in Section 4.3.3. The system would then be ready to begin logging data.

5.1 DATA COLLECTION.

Following synchronisation, it was known(see Section 4.4.3) that the stability of the frequency standards would permit a maximum period of field trial operation of $\simeq$44 minutes, before re-synchronisation was necessary. Consequently, to avoid any irregularities in the measured responses, all measurement periods were kept as short as possible, and were typically 20 to 30 minutes in duration.

During the course of the experimental programme, data was recorded on to 5 channels of the tape-recorder, with a voice commentary being added on an auxiliary 'edge-track'. The data signals consisted of

(i) Inphase and Quadrature components of the channel impulse response.

(ii) time-reference marker pulses.

(iii) speed marker pulses.

(iv) a tape servo signal.

The tape-recorder was operated in wideband FM mode, providing a DC-to-5KHz bandwidth and 50dB SNR for a tape speed of 7.5i.p.s.

5.1.1 Time-reference Markers.

In order to measure propagation time-delay, a time-reference generator(see Section 4.3.3) was implemented in the receiver. As outlined above, prior to the commencement of data acquisition, the transmitter/receiver systems were synchronised. Following synchronisation, the transmitter and receiver 10MHz m-sequence generators run in simultaneity. Therefore, the outputs of the time-reference generator and the quadrature demodulators have a fixed time relationship. By recording this at the start of an experimental run, and by observing the difference in the time relationship during the measurement period, an accurate assessment of the propagation time-delay was realised.

In addition, the time-reference marker pulses are extremely accurate, since they are derived from a rubidium atomic standard. Therefore, they were used to initiate sampling of the quadrature channel responses, during data conversion(see Section 5.2.1). This technique is considerably more accurate than using an external pulse generator for initiating the sampling.

5.1.2 Speed Marker Pulses.

To ensure that Doppler-shift information could subsequently be extracted from the measured responses, it was essential for the vehicle to be driven at a constant speed. Also, since a low speed was required (< 6 m.p.h.), the vehicle's speedometer could not be relied upon to provide accurate speed information. Overcoming this problem required the fitting of a slotted-disk to the propeller-shaft of the car. Speed marker pulses were then produced as the rotating slotted-disk interrupted an opto-isolator.

The task of the driver, in attempting to maintain a constant sub-6 m.p.h. vehicle speed, was made easier through the use of three indicator lamps on the dashboard. The centre lamp illuminated when the car was

within 10% of the required speed, while the left and right lamps illuminated when the car was travelling too slowly, or too quickly, respectively. Both the required speed and the 'go/no-go' window could be adjusted, to cater for various transmission frequencies or accuracies as required.

5.1.3 Tape Servo Signal.

Owing to the mobile nature of the experimental programme, there may be times when inaccuracies might occur in the speed control of the tape transport. If this happens, data errors will occur, since there will not be overall tape speed constancy between recording, and subsequent replay. This problem will also occur as a result of tape stretching, or changes in humidity. To prevent this problem arising, and thereby ensuring data integrity, use was made of a function internal to the tape-recorder whereby an internally generated constant frequency signal is recorded on to one of the channels. During replay this signal controls the capstan speed, and any inaccuracies are adjusted for automatically within the recorder.

5.1.4 Voice Commentary.

During each experimental run, a voice commentary was recorded simultaneously with the data. This served two purposes, firstly, to provide archival information in the form of dates, transmitter/receiver locations, etc. Secondly, features of the surrounding topography, traffic conditions, etc., were described throughout each experiment, so that they could be assessed in terms of their effect on the received signal.

5.1.5 Dynamic Range Adjustment.

The measured dynamic range of the receiver was 36dB. Due to the presence of signal fading, shadowing and path-loss, this dynamic range appears to be limited compared with narrowband receivers which typically have dynamic ranges on the order of 80dB. However, the effect of the path-loss can be counteracted by using a manual RF attenuator in the front-end of the receiver. The attenuator can be used to optimally situate the dynamic range window for every experimental location, and during this

study each site was previewed, to determine the attenuator setting, prior to recording.

5.2 DATA CONVERSION.

All processing of the measured channel responses was undertaken on a mainframe computer. Before any processing could be carried out, however, the raw analogue data had to be digitised, and transferred to mainframe filestore. Both of these procedures will be discussed in the following sections.

5.2.1 Analogue-to-Digital Conversion.

A special purpose, dual-channel Analogue-to-Digital Convertor(ADC) card was available for this study. The card was housed in one of the full-length(16-bit) slots of an IBM Personal Computer AT(PC-AT), and operated under software control. Both ADCs were 12-bit convertors, had $\pm$ 2.5V input ranges and were configured for simultaneous sampling of the input channels.

The most convenient form of data transfer to a mainframe is by digital magnetic tape. Consequently, an 8-track digital tape transport was connected to one of the parallel ports of the PC-AT, to receive the sampled data.

The controlling software was configured to perform the following operations,

(i) If required, enable the first record(the 'HEADER') in each data file to contain archival information about that file.

(ii) Initiate data sampling using the time-reference marker pulses. When the time-reference marker first goes 'HIGH', sampling of the Inphase and Quadrature components of the channel impulse response begins. The I and Q channels were sampled once in each time-delay cell, i.e., every 0.5ms(this corresponds to 0.1μs after allowing for the STDCC time-scaling factor). Once sampling has been initiated, an internal counter, set to the m-sequence length,

is used to ensure that exactly m samples of I and Q are taken in each profile. After m sample instants the software prevents any further sampling until the next 'HIGH' time-reference marker pulse, at which time the whole process is repeated. This approach was required to overcome inaccuracies in the PC-AT's internal clock. Therefore, by periodically resetting with pulses derived from the rubidium standard, correct sampling of each profile was obtained.

(iii) Split each data sample into two 8-bit bytes, and mask-off the unwanted bits. The PC-AT has a 16-bit bus, therefore, to ensure that correct data values are read from the ADCs, each 12-bit sample is masked(logically-ANDed) with the hexadecimal word 0FFF. Also, since the tape transport requires 8-bit words, each 12-bit word was split into low and high bytes prior to tape transfer.

As a result of the sampling, the quadrature components of the channel impulse response are represented as two discrete time-sequences, $I_i(t_n)$ and $Q_i(t_n)$, where i numbers the time-delay cells(from 0 to $m-1$), and t_n numbers the profiles.

5.2.2 Transfer-to-Tape.

Following conversion, masking and splitting, each pair of double samples(low byte-high byte) were ready for transfer to magnetic tape. However, if independent samples are written directly to tape, the system operates very inefficiently, since a START/STOP operation is required for each sample. This 'threshing' behaviour was minimised by buffering the data.

Each set of samples(i.e., 4 bytes) was written to either of two buffers set up in the PC-AT. As soon as one buffer was full, samples were automatically routed to the other buffer, with no data loss. During the time that the second buffer was being filled, the first buffer was flushed to tape, thereby requiring a single START/STOP operation for each buffer full of samples. Once the buffer had been flushed, it was again ready to receive

data, so this process of alternating between the buffers repeated until all the data had been transferred to tape.

The size of the buffer was set to the largest value that was an integer multiple of $4m$, where m is the m-sequence length, and less than, or equal to, 4,095(a limit imposed by the tape transport). The buffer size for a 127 bit m-sequence was 4,064.

5.2.3 Loading Data into Mainframe Filestore.

All the data processing was carried out on IBM 308X series mainframes. Although both the PC and mainframe were sourced from IBM, they do not operate with the same character sets. The PC uses the ASCII(American national Standards institute Code for Information Interchange) set, whilst the mainframe uses the EBCDIC(Extended Binary Coded Decimal Interchange Code) set. With the exception of the tape HEADER information, this difference is irrelevant, since the data consists of binary numbers. However, a decoding routine was implemented that converted the header information into meaningful characters.

Therefore, apart from the minor problem of the header area, the tapes created by the PC are directly compatible with the mainframe, and could be easily read into storage using IBM proprietary software for tape handling. Consequently, processing of the measured channel responses could then be undertaken. However, a complete description of the processing techniques will be presented in the following chapter.

CHAPTER 6. EXPERIMENTAL DATA PROCESSING.

6.1 INTRODUCTION.

A description of the Swept Time-Delay Cross-Correlation channel sounding technique has been presented in Chapter 3, and a detailed discussion of the experimental channel sounder has been given in Chapter 4. The characterising functions presented in Chapter 2 enable a complete description of the channel behaviour to be deduced from measured quantities. However, it is extremely important to determine exactly what information is required from the measurements, and what are its applications.

Essentially, the measurements should be capable of providing information pertinent to both accurate channel modelling(i.e., simulation), and the assessment of mobile radio services(i.e., Systems Engineering). This chapter contains an appraisal of simulation and systems studies, followed by a consideration of the relevant channel descriptors and their derivation from measured responses.

6.1.1 Simulation.

A complete assessment of a mobile radio system(or a particular aspect of it) can only be achieved by measuring the system 'in situ'. This is expensive, time-consuming and precludes consistent and repeatable results. These problems can be overcome, however, if an effective channel model can be formulated, which lends itself easily to simulation. By removing the RF link, researchers are able to conduct controlled experiments within the laboratory, which enables them to observe directly the effect of various system parameters on the overall system performance.

Simulators are useful for not only evaluating, and fine-tuning, the performance of existing mobile radio services, but also for assessing the effectiveness of modulation, coding, equalisation and/or diversity techniques to combat the channel impairments due to multipath. Furthermore, comparisons of the usefulness of the various channel descriptors can be

undertaken, with a view to producing an overall 'figure-of-merit' for wideband multipath channels that can be used in Systems Design.

Several models have been proposed for the simulation of narrowband propagation channels[6.1,6.2], and, although they differ in terms of their implementation, they all essentially produce the same result, namely a Rayleigh fading envelope, a random phase modulation and an approximation to the desired power spectrum. Whilst most narrowband simulators generate only the fast fading component, some also introduce log-normal shadowing to produce a more realistic approximation of the channel. Therefore, simulation in the narrowband case is a relatively straightforward procedure, and has been used extensively in the assessment of narrowband communication systems.

However, the converse is true for wideband channel simulation. Whilst most models[6.3-6.6] are derived from the Gaussian Wide-Sense Stationary Uncorrelated Scattering(GWSSUS) channel of Bello[6.7], they differ greatly in their complexity and controlling assumptions. Consequently, there is a disparity in the simulated channels, with some models being more representative of the 'real' channel than others. To overcome this drawback, characterising parameters were required that would facilitate the attainment of a representative channel simulation that was still relatively simple to implement. These parameters, and how they are deduced from measured quantities, will be described in Section 6.2.

6.1.2 Systems Design.

The task of Systems Engineers is to design communication systems that will operate effectively in the presence of multipath, interference, noise, etc. In addition, they need to know what can be done to improve the performance of existing systems. Therefore, they require channel parameters that relate to error and distortion criteria. Furthermore, the communication system has to perform adequately within the majority of its service area. Consequently, measures of the global propagation characteristics of the channel are also required.

In Section 2.7 the case was made for adopting a two-stage approach to channel characterisation. This necessitates acquisition of the relevant small-scale channel descriptors, followed by the formation of their cumulative distributions in order to assess both the variability of transmission conditions, and the likely performance of a specified system over the large-scale area. Descriptions of the small-scale parameters, their distributions, and how they are derived will be presented in Section 6.3.

6.2 CHANNEL PARAMETERS RELEVANT TO SIMULATION.

The complex, low-pass impulse response of a multipath channel can be expressed[6.8] as,

$$h(t;\tau) = \sum_i A_i(t)\delta\{\tau - \tau_i(t)\} \exp\{j\phi_i(t)\} \tag{6.1}$$

where, A_i is the amplitude of the i^{th} resolvable path, τ_i is its propagation time-delay, ϕ_i is its phase, i numbers the time-delay cells(i.e., 0 to 126) and $\delta\{\bullet\}$ is the Dirac delta function. Therefore, simulation of the channel merely requires the generation of the variables A_i, τ_i and ϕ_i. As a result of motion of the transmitter/receiver terminals, these parameters are randomly time-varying functions, and must, therefore, be described in terms of stochastic processes which do not easily lend themselves to simulation. However, application of the statistical constraints outlined in Chapter 2 relaxes this limitation, enabling descriptions of these parameters to be deduced from measured quantities.

6.2.1 Phase Distribution.

The path phases, ϕ_i, are assumed 'a priori' to be a set of mutually independent random variables which are uniformly distributed over the range $(0, 2\pi]$. The reasoning for this assumption, presented in Section 2.6.2, is so incontrovertible as to make measurement of ϕ_i unnecessary.

6.2.2 Amplitude Distribution.

Due to the limited time resolution of all practical measurement systems, the contribution to the echo power profile within a specific time-delay cell is the agglomeration of a large number of independent paths, each having a different phase. At UHF frequencies small spatial changes in the location of the transmitter/receiver terminals result in large changes in the phase of each constituent path. Consequently, the vector addition of these randomly-phased signals produces amplitude fluctuations in each time-delay cell of the echo power profile for small spatial displacements. Intuitively, one would also expect variations in the echo amplitudes due to large-scale changes in location, either as a result of range dependence, or differing propagation environments.

In view of these factors, it seems prudent to envisage the echo-path fluctuations as being separable into two distinct parts. The fluctuations can then be characterised in terms of small and large-scale signal variations in an identical manner to that adopted for narrowband propagation studies.

6.2.2.1 Separation of Small and Large-scale Amplitude Fluctuations.

The received path amplitudes can be represented as,

$$A_i(t) = s_i(t)\ell_i(t) \tag{6.2}$$

where, $s_i(t)$ and $\ell_i(t)$ represent the small and large-scale variations respectively. To separate the two components, a Moving Average technique[6.9] was used as follows.

An estimate of $\ell_i(t_n)$, at a time t_n, was evaluated from a series of N samples using the expression,

$$\ell_i^2(t_n) = \frac{1}{N} \sum_{m=-(N-1)/2}^{(N-1)/2} \{I_i^2(t_{n+m}) + Q_i^2(t_{n+m})\} \tag{6.3}$$

where, $I_i(t)$ and $Q_i(t)$ are samples of the inphase and quadrature components of the channel impulse response for the i^{th} time-delay cell($i = 0, 1, \ldots, 126$). Then using $\ell_i^2(t_n)$, it was possible to estimate $s_i^2(t_n)$ via,

$$s_i^2(t_n) = \frac{A_i{}^2(t_n)}{\ell_i^2(t_n)} = \frac{I_i^2(t_n) + Q_i^2(t_n)}{\ell_i^2(t_n)} \tag{6.4}$$

The number of samples, N, over which $\ell_i^2(t_n)$ is estimated has to be chosen large enough to ensure that no small-scale fluctuations are still present, but not so large that the large-scale fluctuations are lost in the averaging process. However, no rigid rules appear to exist for the choice of N, although averaging over approximately twenty carrier wavelengths has been used in two recent, independent, narrowband propagation studies[6.9,6.10]. The value of N used was 61, which corresponds to $\simeq$18 wavelengths at the transmitted carrier frequency.

6.2.2.2 Correlation Coefficients between Amplitude Fluctuations in neighbouring time-delay cells.

In using (6.1) to model the channel, it is not sufficient to merely calculate the distributions of the small and large-scale signal variations. Also of importance are the correlation coefficients between amplitude fluctuations in neighbouring time-delay cells. The correlation coefficients, ρ_{jk}, are given by[6.11],

$$\rho_{jk} = \frac{\sum_{h=1}^{M}(x_{jh} - \bar{x}_j)(x_{kh} - \bar{x}_k)}{\sqrt{\sum_{h=1}^{M}(x_{jh} - \bar{x}_j)^2 \cdot \sum_{h=1}^{M}(x_{kh} - \bar{x}_k)^2}} \tag{6.5}$$

In using (6.5) j and k number the time-delay cells, such that $j = 0, 1, 2, \ldots$ and $k = j+1, j+2, \ldots, j+10$. The correlation coefficients between time-delay cells with larger separations are of little consequence, and in a practical simulation only correlations between adjacent cells are likely to be implemented. Each sequence x_{jh} is composed of M points, the result of sampling M individual power profiles at time-delay cell j, and $\bar{x}_j$

is the mean value of the sequence. The correlation coefficients for the small and large-scale amplitude fluctuations are evaluated by replacing x_{jh}, x_{kh} in (6.5) by s_{jh}, s_{kh} and ℓ_{jh}, ℓ_{kh} respectively.

Equation (6.5) generates a matrix of correlation values which is confusing to interpret. To clarify the presentation of these results, the following method was adopted. Sequences of correlation coefficients with identical separations were formed, e.g. $\rho_{12}, \rho_{23}, \ldots$ would be a sequence with a separation of one(time-delay cell), $\rho_{13}, \rho_{24}, \ldots$ would be a sequence of separation two, and so forth. The mean value of a sequence is then a measure of the average correlation for a particular separation, and provided its associated standard deviation is sensibly small, the mean value can be used instead of the individual correlation values with minimal error.

6.2.3 Time-delay Distribution.

In ascribing statistical distributions to the propagation time-delays, several researchers[6.3,6.5,6.12] have conjectured that they form a Poisson sequence. However, after analysing their measurements, they discovered that the distribution of the time-delays was not consistent with a simple Poisson process. To overcome this finding a modified-Poisson sequence[6.13,6.14] was developed, which is similar to a Markov model. Whilst this refined model was better able to reproduce the features of their measurements[6.12-6.14], it is rather cumbersome to use. To avoid this shortcoming, a totally different approach was developed for this study.

With the possible exception of computer models, the propagation time-delays, for models based on tapped-delay lines, will be fixed quantities. Whilst this conflicts with the physical channel consisting of time-varying delays, it is a valid assumption for all channels of practical interest. Therefore, the presence[18] of an echo in a particular time-delay cell, at any instant of time, depends upon the resultant of the small and large-scale signal fluctuations for that time cell. Furthermore, since the small-scale amplitude perturbations have zero-means(following normalisation) for all time-delay cells, then the criteria for identifying significant propagation

[18] The term presence is used to indicate that the echo is distinguishable from the additive noise.

time-delays are simply the means(μ_i) and standard deviations(σ_i) of the large-scale amplitude fluctuations, which are given by,

$$\mu_i = \mathrm{E}[\ell_{ih}] = \bar{\ell}_i \tag{6.6}$$

$$\sigma_i = \sqrt{\frac{1}{M-1}\sum_{h=1}^{M}(\ell_{ih} - \bar{\ell}_i)^2} \tag{6.7}$$

Therefore, if only a finite number(J) of delay taps are available for the simulation, the time-delay cells corresponding to the J largest mean signals should be implemented. Alternatively, if all the mean levels were equivalent, the time-delay cells corresponding to the J largest standard deviations should be implemented, as they represent the largest variability in signal levels. Since the selection of the time-delays will, therefore, be based upon amplitude characteristics, and not a strict statistical characterisation, it appears more correct to relate to the 'distribution' of time-delays in terms of Weighting Factors for each delay tap(see Section 7.1.3).

6.3 CHANNEL PARAMETERS RELEVANT TO SYSTEMS DESIGN.

The mobile radio propagation channel has been described as Quasi-Wide-Sense Stationary[6.7,6.15], since it has been found to possess statistics that are Wide-Sense Stationary over small time and spatial intervals, whilst being highly non-stationary over much larger intervals. This has resulted in a two-stage characterisation being adopted, whereby the small-scale channel descriptors are evaluated first, followed by averages of these parameters to estimate the large-scale channel statistics. In keeping with the discussion in Section 2.7, the small-scale time and frequency-domain parameters will de described first, followed by their large-scale distributions.

6.3.1 Small-scale Characterisation.

6.3.1.1 Time-domain.

The wideband channel sounder provides a measure of the complex impulse response of the channel in terms of its Inphase(I) and Quadrature(Q) components. A power versus time-delay profile, $p(\tau_i)$, for a small segment of a street is defined as,

$$p(\tau_i) = I^2(\tau_i) + Q^2(\tau_i) \tag{6.8}$$

where, i numbers the time-delay cells, i.e., 0, 1, ... , 126. Averaging a suitable number of power-delay profiles, to remove the effects of the small-scale amplitude fluctuations, yields an average power-delay profile, $P(\tau_i)$. The average power-delay profile represents a measure of the magnitude of the echo path amplitudes within each time-delay cell.

Previous studies[6.15,6.16] have shown that, at UHF frequencies, the channel statistics are stationary over a few metres. In this study, impulse responses were obtained every 10cms of linear travel, and an average power-delay profile was generated from 64 individual responses, i.e., every 6.4m(cf. 5m[6.15] and 5.5m[6.16]), therefore,

$$P(\tau_i) = \frac{1}{64}\sum_{j=1}^{64} p_j(\tau_i) = \frac{1}{64}\sum_{j=1}^{64}\{I_j^2(\tau_i) + Q_j^2(\tau_i)\} \tag{6.9}$$

where, j numbers the individual power profiles. The average power-delay profile is a band-limited estimate of the average impulse response envelope, $\mathrm{E}[h(\tau_i)h^*(\tau_i)]$, where $h(\tau_i)$ is the complex, band-limited, bandpass impulse response of the propagation path and E[...] indicates the ensemble average[6.17].

The average delay, D, and delay spread, S, which are the first and second central moments of $P(\tau_i)$, are two time-domain parameters of practical interest to Systems Designers. In terms of measured quantities these are given by,

$$D = \frac{\sum_{i=0}^{126} \tau_i P(\tau_i)}{\sum_{i=0}^{126} P(\tau_i)} \tag{6.10}$$

and,

$$S = \sqrt{\frac{\sum_{i=0}^{126} (\tau_i - D)^2 P(\tau_i)}{\sum_{i=0}^{126} P(\tau_i)}} \tag{6.11}$$

and all the time-delays, τ_i, are expressed in terms of excess delay, i.e., the shortest delay time has been set to zero in the average power profile. The average delay causes ranging errors in phase ranging systems, whereas the delay spread places fundamental limits on the performance of wide bandwidth transmissions over non-equalised channels[6.2,6.17].

An alternative time-domain parameter that has not received as much attention as the delay spread, is the profile width, W [6.18,6.19].[19] This parameter is very simply defined as the time-delay between the outer $-X$dB points of the average power profile, where the largest echo amplitude has been normalised to 0dB. A choice of X equal to 10 appears reasonable since digital transmissions could be expected to operate satisfactorily(low BER) with a carrier-to-interference(C/I) ratio of 10dB[6.18,6.20]. Whilst other values may also be worth investigating[6.19], only the -10dB width was assessed during this study.

Since the average power was analysed as discrete samples of a continuous function, sample values may not coincide exactly with the -10dB level. Therefore, in order to obtain a more accurate estimate of W, linear interpolation, between the samples above and below the -10dB level, was performed at both ends of the profile. The width was then equal to the sum of the interpolated results, plus the integer number of time-delay cells

[19] Reference [6.19] refers to the profile width as delay interval.

between them. As a channel parameter, the profile width may well be more important than the delay spread, particularly with regard to equalised channels.

6.3.1.2 Frequency-domain.

The frequency-selective behaviour of the channel was shown in Section 2.7.1.2 to be described in terms of the autocorrelation function $R_T(\Omega)$ for a WSSUS channel. Furthermore, it was shown that $R_T(\Omega)$ is related to $P(\tau)$ by Fourier transformation. Therefore, using (2.82),

$$R_T(\Omega) = \int P(\tau) \exp\{ -j2\pi\Omega\tau\} \, d\tau \tag{6.12}$$

$R_T(\Omega)$ is known as the Frequency Correlation Function, and is a measure of the magnitude of correlation between two spaced carrier frequencies. This function is easily evaluated from the values of $P(\tau_i)$ through Fast Fourier Transform(FFT) techniques[6.21].

The coherence bandwidth, defined as the maximum frequency difference for which two signals have a specified value of correlation, is a frequency-domain parameter that is useful for assessing the performance of various modulation/diversity techniques[6.2]. However, no definitive value of correlation has emerged for the specification of coherence bandwidth. Therefore, coherence bandwidths for values of correlation equal to 0.9($B_{0.9}$) and 0.5($B_{0.5}$), the two most popular values, were evaluated from each Frequency Correlation Function. In a similar fashion to the evaluation of profile width, a linear interpolation was also used to evaluate $B_{0.9}$ and $B_{0.5}$.

The resolution in the time-domain is directly related to the m-sequence clock period, since it sets the width of the autocorrelation function, and was 0.1μs for this study. For most channels of practical interest this resolution is probably sufficient. The resolution in the frequency-domain, however, is related to the pulse repetition frequency(PRF) of the spread-spectrum sounding signal, which is defined as,

$$\text{PRF} = \frac{1}{mT} \tag{6.13}$$

where, m is the length(in bits) of the m-sequence and T is the m-sequence clock period. For $m = 127$ and $T = 0.1\mu s$ the PRF equates to 78.74KHz.

However, 127 is a prime number, and does not lend itself to FFT techniques[6.21]. To counteract this problem, a single zero-valued sample can be added to the $P(\tau_i)$ sequence prior to applying the FFT. This increases the number of points in the transform to 128, which is a power of 2 and is easily transformable. Addition of an extra sample point is reasonable for this type of study, since one of the overriding assumptions regarding the operation of the channel sounder is that all the multipath echoes have decayed within its 12.7μs time-delay window.

In his study in New York City, Cox[6.15] used a 511-bit m-sequence and a chip period of 0.1μs, which provided a frequency resolution of $\simeq$19.6KHz. The smallest values of $B_{0.9}$ and $B_{0.5}$ he reported[6.17] were 20KHz and 55KHz respectively. Obviously, the degree of confidence in these small coherence bandwidths, which are the most critical in terms of error performance, must be low. Furthermore, if the frequency resolution is insufficiently fine, detail may be lost in the estimation of the Frequency Correlation Function, resulting in erroneous values for $B_{0.9}$ and $B_{0.5}$. In essence, this is the same problem that afflicts the spaced-tone sounding technique, as detailed in Section 3.1.2. Therefore, it is obvious that a resolution of $\simeq$79KHz is clearly inadequate for an accurate frequency-domain characterisation of the channel.

One obvious method of counteracting this problem is to increase the length of the m-sequence, thereby still maintaining the same time-resolution. However, as stated in Section 4.1.5, there are penalties to be paid for adopting this approach, thus limiting the maximum practical value of m.

An alternative, and more elegant, solution is to make use of the argument, presented above, for adding a zero-valued sample to the $P(\tau_i)$ sequence prior to transformation. Since it has been assumed that all dis-

tinguishable echoes must be contained within the 12.7μs time-delay window, there is no restriction to the number of zero-valued samples that can be added to the $P(\tau_i)$ sequence. Therefore, an arbitrarily large m-sequence can be simulated by adding an appropriate number of zeros. This 'zero-padding' technique has been used extensively in Digital Signal Processing, but this is believed to be the first time that it has been applied to the characterisation of mobile radio channels.

Unlike the case where m is physically increased, the only penalty of using a large pseudo-m (i.e., $P(\tau_i)$ augmented with zeros) is the increased time of computation. For all the results presented in this study, the $P(\tau_i)$ sequence was augmented by 1,921 zeros, to produce a composite sequence of length 2,048. This provided a frequency resolution of $\simeq$4.9KHz. The value of 2,048, for the sequence length, was obtained by continually increasing the length from 128, until it was felt that the increase in computation time outweighed any further improvement in the estimates of $B_{0.9}$ and $B_{0.5}$.

6.3.2 Large-scale Characterisation.

6.3.2.1 Cumulative Distributions.

The small-scale descriptors presented above are essentially measures of the channel response at 'single' locations. Obviously, Systems Engineers must design communication systems that will operate satisfactorily in a large variety of geographical locations. Therefore, they require measures of the variability in the small-scale channel descriptors over the large-scale area. Specifically, they need to know for what percentage of locations a specific level of performance can be maintained. That is, they require the cumulative distribution functions(or just distribution functions)[6.22] of each parameter.

The cumulative distribution function is defined as follows[6.22]. The outcome, ζ, of an experiment causes a random variable X to take the value $X(\zeta)$. If the experiment is then performed n times, and the total number of outcomes such that $X(\zeta) \leq x$ equals n_x, where x is some specified value, then the cumulative distribution function, F(x), is given by,

$$F(x) = P\{X \leq x\} \simeq \frac{n_x}{n} \tag{6.14}$$

In its present form, (6.14) is intractable. Therefore, the cumulative distribution is more usually evaluated from its density function[6.22], which, for a continuous function,[20] can be defined as,

$$f(x) = \lim_{\Delta x \to 0} \frac{P\{x \leq X \leq x + \Delta x\}}{\Delta x} \tag{6.15}$$

If it is assumed that the number of outcomes that satisfy the condition $x \leq X(\zeta) \leq x + \Delta x$, where Δx is very small, is Δn_x, then,

$$f(x)\,\Delta x \simeq \frac{\Delta n_x}{n} \tag{6.16}$$

From[6.22], the cumulative distribution in terms of its density function is given by,

$$F(x) = \sum f(x)\,\Delta x = \sum \frac{\Delta n_x}{n} \tag{6.17}$$

where, the summation is for all outcomes such that $X(\zeta) \leq x$.

In the evaluation of the cumulative distributions, the Δx values were $0.1\mu s$ for the time-domain parameters, and 10KHz for the frequency-domain parameters.

6.3.2.2 Regression Relationships.

Several studies have been undertaken[6.2,6.23,6.24] to relate the average bit error rate, for transmission over a non-equalised multipath channel, to the small-scale channel descriptors. These studies have been carried out for various modulation and/or detection techniques. Therefore, the performance bounds of differing communication systems can be quickly

---

[20] The parameters $D, S, W, B_{0.9}$ and $B_{0.5}$ are all continuous functions over $(0, \infty)$, however, they must be discretised for practical evaluation of the cumulative distributions.

evaluated using the cumulative distribution function of a relevant small-scale parameter, in conjunction with its error estimating equation.

However, there may be occasions where a distribution of one parameter is available, along with an equation connecting an alternative parameter to the error rate. In situations such as this, it is convenient to have an expression which interrelates the two parameters, so that a simple substitution can be made. This is considerably easier than having to formulate the cumulative distribution of the alternative parameter. Additionally, for this substitution to be accurate there must be a strong interdependence between the two parameters.

In view of these facts, scatter plots of several pairs of small-scale descriptors, e.g., coherence bandwidth at 0.9 correlation versus delay spread, coherence bandwidth at 0.5 correlation versus profile width, etc., were produced to show their degree of correlation. A least-squares linear[21] regression[6.11] analysis on each pair of descriptors, produced their mathematical interrelationships. These relationships were then used to generate regression lines for the scatter plots.

[21] Due to their inverse relationship, a regression analysis on sequences of time and frequency variables was performed on the logarithms of the data points.

REFERENCES

[6.1] Arredondo, G. A., Chriss, W. H. and Walker, E. H., "A multipath fading simulator for mobile radio", IEEE Trans. Veh. Technol., Nov. 1973, Vol. VT-22, No. 4, pp 241-246.

[6.2] Jakes, W. C. (Ed.), "Microwave Mobile Communications", John Wiley 1974.

[6.3] Bajwa, A. S., "UHF wideband statistical model and simulation of mobile radio multipath propagation effects", IEE Proc. Part F, Aug. 1985, Vol. 132, No. 5, pp 327-333.

[6.4] Stein, S., "Fading channel issues in system engineering", IEEE J. Selected Areas Commun., Feb. 1987, Vol. SAC-5, No.2, pp 68-89.

[6.5] Saleh, A. A. M. and Valenzuela, R. A., "A statistical model for indoor multipath propagation", IEEE J. Selected Areas Commun., Feb. 1987, Vol. SAC-5, No. 2, pp 128-137.

[6.6] Chuang, J. C-I., "The effects of time delay spread on portable radio communications channels with digital modulation", IEEE J. Selected Areas Commun., June 1987, Vol. SAC-5, No. 5, pp 879-889.

[6.7] Bello, P. A., "Characterization of randomly time-variant linear channels", IEEE Trans. Commun. Syst., Dec. 1963, Vol CS-11, pp 360-393.

[6.8] Proakis, J. G., "Digital Communications", McGraw-Hill, 1983.

[6.9] Adachi, F., Feeney, M. T., Williamson, A. G. and Parsons, J. D., "Crosscorrelation between the envelopes of 900MHz signals received at a mobile radio base station site", IEE Proc. Part F, Oct. 1986, Vol. 133, No. 6, pp 506-512.

[6.10] Davis, B. R. and Bogner, R. E., "Propagation at 500MHz for mobile radio", IEE Proc. Part F, Aug. 1985, Vol. 132, No. 5, pp 307-320.

[6.11] Edwards, A. L., "An Introduction to Linear Regression and Correlation(2nd. Edition)", W. H. Freeman & Co., 1984.

[6.12] Turin, G. L., Clapp, F. D., Johnston, T. L., Fine, S. B. and Lavry, D., "A statistical model of urban multipath propagation", IEEE Trans. Veh. Technol., 1972, Vol. VT-21, No. 1, pp 1-9.

[6.13] Suzuki, H., "A statistical model for urban radio propagation", IEEE Trans. Commun., July 1977, Vol. COM-25, No. 7, pp 673-680.

[6.14] Hashemi, H., "Simulation of the urban radio propagation channel", IEEE Trans. Veh. Technol., Aug. 1979, Vol. VT-28, No. 3, pp 213-225.

[6.15] Cox, D. C., "910MHz urban mobile radio propagation: multipath characteristics in New York City", IEEE Trans. Commun., Nov. 1973, Vol. COM-21, No. 11, pp 1188-1194.

[6.16] Bajwa, A. S., "Wideband characterisation of UHF mobile radio propagation in urban and suburban areas", Ph.D. Thesis, Department of Electronic and Electrical Engineering, University of Birmingham, 1979.

[6.17] Cox, D. C. and Leck, R. P., "Correlation bandwidth and delay spread multipath propagation statistics for 910-MHz urban mobile radio channels", IEEE Trans. Commun., Nov. 1975, Vol. COM-23, No. 11, pp 1271-1280.

[6.18] Saruwatari, T., Mizuno, M., Iwama, T., Sekizawa, S., Ryuko, H., Ando. H. and Nilson, M., "Large area characterisation of impulse responses on(sic) 775MHz in mountainous terrain", COST 207 TD(87)36, May 1987.

[6.19] Huish, P. W. and Gurdenli, E., "Radio channel measurement and predictions for future mobile radio systems", Br. Telecom. Technol. J., Jan. 1988, Vol. 6, No. 1, pp 43-53.

[6.20] Lindell, F., Swerup, J. and Uddenfeldt, J., "Digital cellular radio for the future", Ericsson Review, No. 3, 1987, pp 160-168.

[6.21] Elliott, D. F. and Rao, K. R., "Fast Transforms: Algorithms, Analyses, Applications", Academic Press, 1982.

[6.22] Papoulis, A., "Probability, Random Variables and Stochastic Processes", McGraw-Hill, 1965.

[6.23] Bello, P. A. and Nelin, B. D., "The effects of frequency selective fading on the binary error probabilities of incoherent and differentially coherent matched filter receivers", IEEE Trans. Commun. Syst., June 1963, Vol. CS-11, pp 170-186.

[6.24] Gans, M. J., "A power-spectral theory of propagation in the mobile-radio environment", IEEE Trans. Veh. Technol., Feb. 1972, Vol. VT-21, No. 1, pp 27-38.

CHAPTER 7. EXPERIMENTAL RESULTS.

The results of the 880MHz wideband channel measurements, at urban locations in the City of Liverpool, are discussed in this chapter. The small and large-scale channel characteristics, pertaining to both simulation and systems studies, are presented. Where possible, the order of presentation follows that of the Experimental Data Processing, described in Chapter 6. All the results contained herein were obtained with the transmitter mounted atop a 35m high building, located in the main precinct of the University of Liverpool.

In selecting suitable measurement locations, two criteria had to be satisfied. Firstly, the safety of the trials vehicle occupants had to be guaranteed at all times; a sub-6 m.p.h. vehicle speed meant busy narrow streets had to be avoided. Secondly, the received signal strength had to be large enough to make maximum use of the receiver's dynamic range.

The term 'urban' has been used above to describe the measurement locations, only to indicate that all the field trials were conducted well within the confines of a medium-sized UK city, i.e., no measurements were taken in the outskirts or surrounding localities. Unlike earlier studies[7.1-7.4], sub-dividing the test sites into broad categories of urban, suburban, etc., was thought to be unnecessary. This is because the definitions of each category are imprecise, and therefore, open to interpretation, and more importantly, mobile radio communication systems have to be designed to operate successfully in all locations.

As a result, field trials were undertaken in as large a diversity of locations as possible, and no 'a priori' bias was given to either range, orientation(radial, tangential or oblique) or street position(mid-block or intersection). The statistics of the channel are, therefore, based upon the complete measurement programme. In keeping with the presentation in Chapter 6, the results will be discussed in terms of their relevance to either channel simulation or Systems Engineering.

7.1 SIMULATION.

In Section 6.2 it was shown how a tapped-delay line model could represent the mobile radio channel through the three random variables, A_i, τ_i and ϕ_i. Since the path phases, ϕ_i, were presumed to be mutually independent, uniformly distributed random variables(in the range $(0,2\pi]$), only the parameters A_i and τ_i were derived from measured quantities.

7.1.1 Amplitude Distribution.

The amplitude coefficients, A_i, were assumed to consist of both small(s_i) and large-scale(ℓ_i) amplitude fluctuations in a similar manner to narrowband signals(Section 6.2.2.1). Following separation, the two sequences s_i and ℓ_i were processed independently.

7.1.1.1 Small-scale Statistics.

During each measurement period the amplitudes of all the time-delayed paths were observed to fluctuate as a result of small-scale spatial displacements of the receiver. This fading of successive power delay profiles has also been reported in earlier studies[7.2,7.4,7.5]. These fluctuating power levels have been assumed to be due to the presence of unresolved paths, having random phases, adding vectorially within the receiver[7.2]. Sometimes the paths add in phase(constructively) and other times out of phase(destructively).

An identical mechanism is responsible for the short term fading observed in narrowband studies, where the amplitude fluctuations have been well approximated by a Rayleigh Distribution. Figure (7.1) shows the amplitude distributions of the first 10 paths(i.e., 1μs) in the profile, plotted on Rayleigh graph paper. A theoretical Rayleigh distribution, on graph paper scaled in this way, appears as the dashed straight line. It is clear from Fig.(7.1) that the amplitude fluctuations are generally an excellent fit to a Rayleigh distribution.

The time resolution of the system determines the maximum number of unresolved paths which contribute to the fast fading. Since a fine time resolution(i.e., high clock rate) enables more paths to be uniquely resolved,

slight departures from Rayleigh should be expected. The envelope distribution as a function of the number of paths(n) is shown in [7.6]. For $n \geq 6$ a very good approximation to Rayleigh was obtained with a small deviation for high signal levels. This is identical to the result presented in Fig.(7.1).

This result lends support to the small-scale Gaussian Wide-Sense Stationary Uncorrelated Scattering(GWSSUS) channel model proposed by Bello[7.7], where the term Gaussian means that the fluctuations at a particular delay constitute a complex Gaussian process. That is, a process that has a Rayleigh distributed envelope and a uniformly distributed random phase. Cox[7.2] generally found that his data was also consistent with the WSSUS model. However, it should be noted that he assessed the small-scale fluctuations by only considering data obtained over a few metres, where he assumed the mean would remain approximately constant. The results presented in Fig.(7.1) were obtained from 40,960 individual profiles, i.e., over 4Km of street sections, with a Moving Average normalisation having been carried out in each time-delay cell.

Although only the results of the first $1\mu s$ are presented in Fig.(7.1), a good agreement to the Rayleigh distribution was found for paths up to $2\mu s$. The distributions of paths with time-delays greater than $2\mu s$ were not determined, since the smaller mean signal levels at longer delays(see Section 7.1.3), coupled with the limited dynamic range, would not enable accurate assessments to be made. However, there appears to be no reason why Rayleigh distributions cannot be ascribed to the small-scale amplitude fluctuations of the later paths.

7.1.1.2 Large-scale Statistics.

In narrowband propagation studies, there have been instances when the small-scale envelope fading has been better described in terms of statistics other than Rayleigh, e.g., Rician, etc.[7.8]. However, there appears to be general agreement between researchers that the large-scale signal(local mean) fluctuations can be accurately modelled by a log-normal probability distribution[7.9]. That is, the logarithms of the local means vary in accordance with a normal(Gaussian) probability distribution[7.9].

The large-scale signal variations are then characterised by specifying the mean and standard deviation of the log-normal distribution.

Figures (7.2) to (7.5) show the amplitude distributions for the paths with excess time-delays between 0μs and 1.1μs. Each distribution is plotted on normal graph paper, with the signal levels plotted in dBs relative to their mean(i.e., the mean value corresponds to 0dB). A log-normal distribution on graph paper scaled in this way is a straight line, with a gradient proportional to its standard deviation. Theoretical log-normal distributions for each time-delay cell are also plotted for comparison. Figures (7.2) and (7.3) suggest that the large-scale amplitude fluctuations in the first few time-delay cells are well modelled as log-normal. However, as the value of time-delay becomes larger, see Figs.(7.4) and (7.5), the distributions begin to depart from log-normal. These departures for the later paths can again be attributed to the limited dynamic range of the measurement system. Therefore, log-normal distributions can be ascribed to the large-scale amplitude fluctuations for each time-delay cell.

Turin[7.1] reports log-normal amplitude distributions for all time-delays in his study in San Francisco, however, he used log-IF amplifiers in his receiver and, consequently, was not so limited by dynamic range. Since his measurement scheme entailed pulsing the transmitters once per second, and collecting the data photographically, it would have been impossible for him to have recorded the small-scale signal fluctuations. Therefore, it is assumed that Turin's results relate purely to the large-scale signal variations.[22] If this supposition is indeed correct, then the results presented here for the small and large-scale amplitude fluctuations would explain the apparent dichotomy between Cox's[7.2] and Turin's[7.1] observations.

For reasons that will become clear shortly, the means and standard deviations of the log-normal distributions will be discussed in Section 7.1.3.

---

[22] This appears to be alluded to in [7.10].

7.1.2 Coefficients of Correlation between Amplitude Fluctuations in neighbouring Time-Delay Cells.

7.1.2.1 Small-scale Statistics.

The average coefficients of correlation(plus and minus one standard deviation) between the small-scale amplitude fluctuations in neighbouring time-delay cells are shown in Fig.(7.6). This result clearly shows that the small-scale fluctuations in each time-delay cell are almost completely uncorrelated. Furthermore, since the standard deviations of all the sets of correlation coefficients are small, it is justifiable to use the mean values of correlation to represent each data set.

This is believed to be the first time that correlation data have been presented in this format. The fact that the amplitude fluctuations are explicitly seen to be uncorrelated unequivocally shows that the small-scale signal variations are consistent with the GWSSUS model[7.7]. While Cox[7.2] alluded to this result in his studies, based on the observation that grossly dissimilar Doppler spectra were obtained at different time-delays, he did not directly compute the correlation coefficients.

7.1.2.2 Large-scale Statistics.

The average coefficients of correlation(plus and minus one standard deviation) between the large-scale amplitude fluctuations in neighbouring time-delay cells are shown in Fig.(7.7). In contrast to the small-scale fluctuations, this result indicates a reasonable degree of correlation(0.66) between the large-scale amplitude variations in adjacent time-delay cells. Whilst the correlation coefficients for separations greater than one time-delay cell are larger than their small-scale counterparts, all the values are less than 0.5, and as such, the remaining large-scale fluctuations can be considered to be weakly correlated.

Barring the small increase in average correlation at 0.6μs separation, the trend is for the large-scale amplitude fluctuations to become more decorrelated with increasing separation between time-delay cells. This result should be expected since paths with large separations are unlikely to have similar statistics. The fact that the standard deviations are

again quite small, suggests that the sets of large-scale correlation coefficients can also be represented by their mean values.

This is believed to be, not only the first time that the large-scale correlation data have been presented in this format, but also the first time that the correlations have been computed for paths separated by up to 1μs. In his study, Turin[7.1] merely presented individual sample values of correlation for his four survey areas. Moreover, *his analysis only considered* the correlations between the first and second, and second and third paths. Bajwa[7.4], on the other hand, computed the same range of correlations, but did not analyse his data in terms of small and large-scale fluctuations. Therefore, direct comparisons with previous studies are not meaningful, however, the correlation coefficients presented by Turin[7.1] were typically 0.6, but this may be nothing more than coincidence.

7.1.3 Weighting Factors for Time-Delays.

The analysis above has shown that the amplitude fluctuations, in each time-delay cell can be well approximated as uncorrelated Rayleigh fading superimposed upon partially-correlated log-normal fading. The tapped-delay line model of the wideband channel, discussed in Chapter 6, will now be completed with the presentation of the tap weights. As described in Section 6.2.3, the weighting factors are merely the means of the log-normal variations.

The mean signal levels, plotted as a function of excess time-delay, are shown in Fig.(7.8). Enclosing the mean levels are the standard deviations of the individual log-normal distributions, i.e., at each value of time-delay the mean value, plus and minus one standard deviation, of that time cell's log-normal distribution is plotted. Figure (7.8) shows that the mean signal is approximately monotonic decreasing with increasing excess time-delay. A decreasing mean should be expected, since the path loss will, in general, increase as a function of path length(i.e., time-delay). However, it is noticeable that the mean signal level approaches an asymptotic value of -20dB relative to the peak level. This behaviour is again a function of the limited dynamic range.

Figure (7.8) is an extremely significant result, not only because it graphically presents the relative tap weights, but more importantly, when implementing the model with a limited number of taps, it explicitly indicates the most essential delays to be included for accurate channel simulation. To highlight this second point, assume twelve taps are available to the simulator. Figure (7.8) shows that the majority of significant echoes are contained between $0\mu s$ and $2\mu s$, therefore, assign six taps, for example, to cover this period. The remaining six taps may then be assigned to provide delays of $2\mu s$, $2.3\mu s$, $3.6\mu s$, $5.9\mu s$, $9.4\mu s$ and $10.0\mu s$. Although the four longest time-delays are all contained in the asymptotic region of the mean signal strength, they have been selected for inclusion because they have the largest standard deviations, and therefore, represent the time cells with the greatest variability in mean signal strengths.

Although it is conceded that using fixed time-delays in the channel simulation may conflict with the concept of the real channel, consisting of time-varying delays, it is considerably easier to use a graph like Fig.(7.8) to generate the delays than to compute them from Poisson distributed random numbers.

7.1.4 Summary of Results for Channel Simulation.

The concept of modelling the wideband mobile radio channel as a densely tapped-delay line is well known[7.7,7.8]. However, it is believed that this is the first study to derive all the coefficients necessary to produce a simple, realistic tapped-delay line model from wideband channel measurements. A brief description of the complete model, shown schematically in Fig.(7.9), now follows.

For practical reasons the number of taps available to the simulator will be rather small, possibly in the range 6 to 15. Using Fig.(7.8) the delay times, τ_i, can be selected on the basis of their mean signal strengths and standard deviations. However, if, for some reason, long delays are not required, more taps can be allocated to the shorter paths.

As shown in Fig.(7.9), the format of each delay is identical. Following the delay operation, the input signal is modulated by a complex

Gaussian process, i.e., a process that has a Rayleigh distributed envelope. Regardless of the number of delay taps and their delay times, all the Rayleigh distributions are uncorrelated. The composite signal is then multiplied with a zero-mean, log-normally distributed signal. The standard deviation for each log-normal distribution is obtained from Fig.(7.8), in addition, the correlations between the log-normals have to be included according to Fig.(7.7). However, for simplicity only the correlations between neighbouring taps need to be simulated, furthermore, if the time separation between adjacent taps is greater than 0.3μs(for example) then their log-normals can be assumed to be uncorrelated.

Finally, each delayed signal is weighted according to its mean signal strength given in Fig.(7.8), this can be achieved with either attenuators or amplifiers, depending on the reference point and the final value of signal level required. All the delayed, modulated and weighted signals are then summed to produce the simulated received signal. If the input sequence is a series of impulses then the output will be the time-varying impulse response of the simulated wideband channel.

In conclusion, this simple model is probably best understood by way of an example. Considering a twelve tap simulator, the parameters required to set up the simulated channel may be chosen to be those of Table 7.1.

In Table 7.1, the correlation coefficients relate to the log-normal distributions of the pairs of taps t_{n-1} and t_n, e.g., taps 4 and 5 have a correlation of 0.44, taps 5 and 6 have a correlation of 0.0, etc. Note that for this combination of delays, many of the correlations have been assumed to be zero to make the simulation process easier. Also, the uncorrelated, zero-mean Rayleigh distributions have not been included in Table 7.1 since they are common to all taps, and are independent of the other parameters.

The example shown here is not meant to be the definitive set up, but is merely an illustration of how the results may be used. The choice of time-delays, for example, will depend upon the proposed use of the simulator. For example, when evaluating equaliser performance, more emphasis may be placed upon later delays, to ensure at least one long delay falls

Tap No.	Time-Delay (μs)	Log-normal Std. Deviations (dB)	Correlations	Weighting Factor (dB)
1	0.0	6.14	-	0.0
2	0.1	5.69	0.66	-4.87
3	0.4	4.60	0.44	-11.38
4	0.7	5.57	0.44	-12.75
5	1.0	5.38	0.44	-14.70
6	1.6	3.75	0.0	-17.46
7	2.0	3.84	0.0	-17.85
8	2.3	5.57	0.44	-17.74
9	3.6	2.36	0.0	-19.90
10	5.9	2.30	0.0	-20.62
11	9.4	3.39	0.0	-20.13
12	10.0	3.45	0.0	-20.36

TABLE 7.1 - Example of the coefficients necessary to specify a 12-tap simulator.

into the equaliser window. Furthermore, measurements from other locations may yield a different result to that in Fig.(7.8), however, the method of selecting the channel coefficients remains unchanged.

7.2 SYSTEMS.

The parameters relevant to Systems Designers, seeking to counteract the impairments induced by time-delayed multipath, have been described in Chapters 2 and 6. Furthermore, the case was made for also applying a two-stage characterisation to these systems parameters. Therefore, the small-scale channel characteristics will be presented first, followed by their large-scale averages.

7.2.1 Small-scale Statistics.

The time dispersion in the channel is observed directly from the average power delay profile(APDP), whilst the frequency selectivity of the

channel is shown through the Frequency Correlation Function(FCF). Although the APDP and FCF, and the parameters deduced from them, are extremely important, it is felt that they are now sufficiently well known through earlier studies[7.1-7.5] as to warrant only a brief discussion.[23] In addition, the main emphasis of this study has been the derivation of channel coefficients to enable the development of a representative simulator. Therefore, only a few examples will be presented to show some interesting features, and the extremes in the measurements.

Figure (7.10) shows the APDP and FCF measured at a site $\simeq$0.5Km from the transmitter. At this location the receiver was moving along a quiet, radial road, set back $\simeq$35m from a busy road, with flat open ground in-between. Part of the opposite side of the 'quiet' road is flanked by a 4-storey block of flats, and the receiver was situated alongside its mid-point during this measurement.

The APDP shows that there is very little delay dispersion at this location, which is confirmed by the smoothly decaying FCF. This near Line-of-Sight(LOS) type response was attributed to the rather isolated measurement location, and the fact that the transmitter can be viewed from the receiver site. Whilst this channel could easily support high data rate transmissions, such channels are quite rare, and this is an example of a 'best-case' result.

Figure (7.11) shows the APDP and FCF obtained at a location 60m from that where Fig.(7.10) was obtained. In this case, the mobile receiver was in an open area with the block of flats behind it, and several large, distant buildings dispersed around it. The transmitter site could not be observed from this position, and several University buildings block the LOS path.

It is clearly seen that there are now distinct paths having excess time-delays up to 3μs. The presence of two strong echoes in the APDP, separated by up to 0.7μs, has induced an oscillation into the FCF with a periodicity of $\simeq$1.4MHz(i.e., the reciprocal of 0.7μs). This has resulted in

---

[23] A fairly exhaustive discussion of average power delay profiles, etc., is presented in [7.4].

significantly smaller values for the coherence bandwidths, and comparison of the results in Figs.(7.10) and (7.11) show how variable the channel characteristics can be over distances of a few tens of metres.

An example of severe time dispersion in the channel is shown in the APDP of Fig.(7.12). This measurement was obtained on a long(several Kms) radial road, at a distance of $\simeq$1.3Km from the transmitter. One side of this road is flat, whilst the other is banked. The buildings along this road are generally of two types, either long 3/4-storey blocks of flats, or 8/14-storey('high-rise') blocks of flats. Some of these blocks are close to the pavements whilst others are set back about 15-20m from the road. The largest block of all(20-storeys) is situated atop the bank. The highest buildings are generally distributed in a 'zigzag' fashion along the street.

Obviously the high density of large buildings has given rise to a great many echo paths, with delays up to 7μs. In addition, this result also shows that the shortest echo path is not the strongest, in fact, the two strongest echoes correspond to excess delays of 2.6μs and 3.2μs respectively. This is probably due to the shorter paths being blocked by the buildings surrounding the receiver, whilst two of the highest buildings are directly illuminated by the transmitter and give rise to strong reflections.

The presence of so many strong echoes has led to a 'collapse' of the FCF resulting in a further reduction to the coherence bandwidths. If $B_{0.5}$ is a good indicator of the channel's operating capabilities, then the current analogue cellular system(TACS), with a 25KHz bandwidth, should still be expected to operate satisfactorily at this location. However, a scheme such as the proposed pan-European System, with a 200KHz bandwidth, would not be expected to operate adequately without equalisation.[24] In this example, the oscillation in the FCF is not consistent with any two of the echo paths, but is composed of an aggregate of frequency components resulting from the interrelationships of all the strong echoes.

Figure (7.13) is an example of the most severe multipath encountered during this study. This result was obtained with the receiver moving

[24] Note, the pan-European System has been designed from the outset to operate with an equaliser.

tangentially along a 3-lane carriageway which gently rises out of Liverpool City Centre. Figure (7.13) was obtained as the receiver reached the crest of the incline, and was $\simeq$750m from the transmitter, which is itself located on high ground overlooking the City Centre.

The two carriageways, which are separated by a wide central reservation, run through a small industrial estate, made up of large, flat-roofed buildings which are set well back from the road. A 12-storey hospital and several tall University buildings are situated between the transmitter and receiver, blocking any LOS path.

Ignoring the small echoes between 3μs and 5μs which are of little consequence, this APDP is dominated by the two clusters at 0μs to 1μs and 9.5μs to 10.5μs. The shapes, and durations, of the clusters are very similar, and leads to the following interpretation. The shortest path is attenuated by intervening buildings prior to local scattering off the faces of the industrial buildings which surround the receiver. The longer path is due to the transmitter illuminating a large building in the city centre, giving rise to a strong specular signal, which is directed up the inclined street. This specular signal then undergoes local scattering from the same buildings, giving rise to a second, near identical cluster.

The presence of such a strong echo at 9.6μs has resulted in a highly oscillatory FCF, the periodicity of which is 104KHz(i.e., the reciprocal of 9.6μs). This has resulted in one of the smallest sets of coherence bandwidths, and represents the 'worst-case' for this study. At this location even the TACS system may have difficulty performing satisfactorily.

The APDP in Fig.(7.14) can be seen to be identical to that in Fig.(7.13), whereas the FCFs are strikingly different. This is because the FCF in Fig.(7.14) has been produced without zero-padding the APDP prior to applying the FFT. Even though there is a clear oscillation still present in the FCF, the limited frequency resolution, without zero-padding, has resulted in an underestimate of the channel's frequency selectivity.

This result is possibly the best example of the impact that frequency resolution has on measured quantities. Furthermore, it highlights the

problem of choosing a suitable value of frequency separation in a spaced-tone measuring system. In view of these factors, all the other results presented in this thesis were produced with zero-padding.

7.2.2 Large-scale Statistics.

The four example APDPs discussed in the previous section clearly show the enormous variability in channel characteristics that can be observed from location to location. It is because of this non-stationarity that a two-step characterisation was proposed. The second step, that of presenting the statistical distributions of the small-scale channel descriptors, is discussed in this section. The cumulative distribution functions will be presented first, followed by the regression relationships.

7.2.2.1 Cumulative Distribution for Delay Spread.

The cumulative distribution for the delay spread is shown in Fig.(7.15). The range in delay spreads is 0.1μs to 6μs, and whilst this maximum is slightly larger than previously published results for urban areas, e.g., 3μs[7.4] and 3.5μs[7.11], a considerably larger amount of data has been processed in this case, 564 average profiles versus 82[7.4] and 100[7.11]. Such extreme values though are quite rare, however, 10% of locations surveyed possessed delay spreads in excess of 3μs(cf. 2.5μs[7.11]).

The delay spread is possibly the most widely quoted parameter when describing wideband multipath channels. Its importance derives from the fact that system performance has been found to be quite strongly dependent on the delay spread, but relatively independent of the profile shape[7.12]. Therefore, through a knowledge of the delay spread it is possible to determine average irreducible error rates for various non-equalised digital transmissions[7.12,7.13].

7.2.2.2 Cumulative Distribution Function for 10dB Profile Width.

An alternative time-domain parameter is the 10dB profile width, and its cumulative distribution is shown in Fig.(7.16). It can be seen that very few values of profile width are contained in the region 3μs to 9μs. This

causes a large difference in the profile width for extreme values in the distribution. For example, the width exceeds 9μs in 10% of locations, but exceeds 2.5μs in only 20% of locations. Comparisons with other studies are not possible here, since Cox[7.2] presented only individual results, Huish[7.14] presented his results location by location, and the measurements by Saruwatari[7.15] were undertaken in mountainous regions.

The 10dB profile width is important since future systems will almost certainly be digital, and could be expected to operate satisfactorily with a carrier-to-interference(C/I) ratio of 10dB[7.15,7.16]. Furthermore, this parameter gives some indication of the window-width required to equalise the channel. This factor is of significant importance to wideband systems, such as the pan-European(GSM) scheme, which will have equalisers built into them.

7.2.2.3 Cumulative Distribution Function for Average Delay.

Figure (7.17) shows the cumulative distribution for the average delays. The average delay is related to the ranging error that would occur in a CW ranging system operating over a multipath channel[7.17]. The ranging error is given by $r_\epsilon = D.c$, where c is the velocity of light. From Fig.(7.17) it can be seen that 90% of locations have average delays less than 2.5μs. Therefore, the ranging error for these locations would be less than 750m.

Although the average delay has been quoted extensively in previous studies[7.2-7.4,7.17], it is felt that its importance is secondary to parameters such as delay spread, profile width and coherence bandwidth, and has been included here only for completeness.

7.2.2.4 Cumulative Distribution Function for Coherence Bandwidth at 0.5 Correlation.

The cumulative distribution for coherence bandwidth at 0.5 correlation($B_{0.5}$) is shown in Fig.(7.18). The range in $B_{0.5}$ is 26KHz to 4.86MHz, and the minimum value is smaller than previous reported values, e.g., 55KHz[7.11]. This should be expected, however, due to the larger values

of delay spread, and the fact that $B_{0.5}$ and delay spread are often assumed to be inversely proportional(see later). It can be seen from Fig.(7.18) that 10% of locations have values of $B_{0.5}$ less than 35KHz. Assuming that $B_{0.5}$ is a good indicator of the 'usability' of the channel, then frequency selective fading could well be a problem for the existing TACS system in approximately 10% of locations surveyed.

The importance of this parameter arises from the fact that average irreducible error rate equations have been formulated[7.12,7.13], for both digital and analogue FM transmissions in terms of $B_{0.5}$. In a similar manner to delay spread though, these again relate to non-equalised channels. Alternatively, if $B_{0.5}$ were considered to be the minimum bandwidth for which two frequencies have become decorrelated, then a graph like Fig.(7.18) could be used to determine the minimum frequency separation required to operate a frequency diversity scheme. By a similar argument it could also be used to determine the minimum hop-interval in a frequency-hopping system.

It is interesting to note from this result that $\simeq$15% of locations produce values of $B_{0.5}$ less than the 78KHz PRF of the measurement system. This further validates the case for using zero-padding in the experimental data processing. Note also that for more than 50% of locations the value of $B_{0.5}$ is less than 300KHz, which is close to the proposed bandwidth of the pan-European(GSM) system.

7.2.2.5 Cumulative Distribution Function for Coherence Bandwidth at 0.9 Correlation.

The cumulative distribution for the coherence bandwidth at 0.9 correlation($B_{0.9}$) is shown in Fig.(7.19). The minimum value of $B_{0.9}$ measured was 10KHz, which was observed in 8% of locations. If such a high value of correlation is required for satisfactory system operation, then it is obvious from Fig.(7.19) that all bar the narrowest bandwidth transmissions will require some form of equalisation.

Although $B_{0.9}$ has been regularly quoted in previous studies[7.2-7.4,7.11] it seems to be of less importance than $B_{0.5}$, and has,

therefore, been included here simply for completeness and comparison purposes.

7.2.2.6 Regression of Coherence Bandwidth at 0.5 Correlation on Delay Spread.

The scatter plot of $B_{0.5}$ versus delay spread(s) is shown in Fig.(7.20). Logarithmic axes are used due to the inverse relationship between time and frequency. The solid line is the least squares regression line fit to the logarithms of the data points, and equated to $B_{0.5} = 1/3.37s^{1.27}$, where $B_{0.5}$ is in MHz and s is in μs. Also shown, for comparison, are the regression lines of Cox[7.11], $B_{0.5} = 1/2.04s^{1.3}$, and Bajwa[7.4], $B_{0.5} = 1/1.37s^{1.42}$.

Provided the APDPs decay smoothly, it has been shown[7.12] that $B_{0.5}$ and s are inversely proportional, such that $B_{0.5} = 1/2s$. This result is often quoted[7.8,7.18] without qualification. To test the validity of this relationship against the measured data, the line $B_{0.5} = 1/2s$ is also shown in Fig.(7.20). It is clearly evident that use of $B_{0.5} = 1/2s$ would produce an overestimate of the coherence bandwidth, at large delay spreads, for each of the three cities surveyed(Liverpool, Birmingham and New York City), and large values of the delay spread(smallest values of $B_{0.5}$) are the most important for the assessment of system performance. This discrepancy is most likely due to the many APDPs(e.g., Figs.(7.13) and (7.14)) that contain significant delayed echoes, since it is these APDPs which give rise to both large s and small $B_{0.5}$.

The large scatter of points around the regression line in Fig.(7.20) indicates that the parameters $B_{0.5}$ and s are only weakly correlated. This effect was also observed by Cox[7.11] in his studies in New York City.

7.2.2.7 Regression of Coherence Bandwidth at 0.9 Correlation on Delay Spread.

The scatter plot of $B_{0.9}$ versus s is shown in Fig.(7.21). Although it is unclear how important the parameter $B_{0.9}$ is, this result clearly shows a strong interdependence between the two parameters. Cox[7.11] too observed this effect.

The least squares regression line fit to the logarithms of the data points is $B_{0.9} = 1/14.8s^{1.09}$. Since the exponent is approximately unity, a 'forced' fit to the line $B_{0.9} = 1/\ell s$ was also evaluated. The value of ℓ was found to be 14.7, and this is shown as the broken line on Fig.(7.21). Clearly the close agreement between these two lines enables the simpler 'forced' expression to be used to interrelate $B_{0.9}$ and s with minimal error.

7.2.2.8 Regression of Coherence Bandwidth at 0.5 Correlation on 10dB Profile Width.

The scatter plot of $B_{0.5}$ versus 10dB profile width(W) is shown in Fig.(7.22). The least squares regression line fit to the logarithms of the data points, $B_{0.5} = 1/2.55W^{1.05}$, is shown as the solid line, with the 'forced' fit, $B_{0.5} = 1/2.57W$, shown as the dashed line. Again, the close agreement between these two lines means that the more simple equation can be used to interrelate the parameters.

The generally tight grouping of the points around the regression lines suggests a significant degree of correlation between $B_{0.5}$ and W. This should be expected intuitively, since W is a measure of both echo strength and delay, and as was seen in Figs.(7.13) and (7.14), the presence of significant echoes induces oscillations in the FCF which results in reduced coherence bandwidths.

7.2.3 Summary of Results for Systems Design.

As detailed in Chapter 1, the main emphasis of this study has been to produce a simple, realistic channel model based upon wideband measurements. Consequently, the presentation and discussion of the systems results has been deliberately kept brief. However, their importance from a systems viewpoint should not be underestimated.

The variability in transmission conditions within a medium-sized UK city has been highlighted, which clearly demonstrates the need for formulating the large-scale distributions of the channel parameters. Although the delay spread and coherence bandwidth(at 0.5 correlation) have been the most widely quoted small-scale descriptors, it is unclear whether a single parameter provides a representative 'figure-of-merit' for wideband channels.

This is particularly true for equalised channels, and alternative parameters are emerging, e.g., as the result of the COST 207 programme, which may prove more useful. However, now that all the coefficients have been determined to enable the construction of a wideband channel simulator, laboratory evaluation of the parameters can be undertaken to determine their impact on system performance.

Provided mathematical expressions can be formulated to relate error performance to the channel descriptors, as is the case for delay spread and coherence bandwidth in unequalised channels, then use of the appropriate cumulative distribution function will enable Systems Designers to determine lower bounds on the average error rate for a specified fraction of locations. However, average irreducible error rates are only first-order approximations of the channel's performance, and work by Chuang[7.13] has shown that a more useful measure is the percentage of time that the channel gives rise to a particular error rate.

Use of the regression relationships enables simple substitution of parameters provided they are reasonably correlated. This could prove useful for comparing results from different locations, or when an error rate equation is only available for an alternative parameter. Furthermore, if a 'forced' regression can be found that is nearly identical to the 'true' regression, then use can be made of the simpler expression with only minimal error.

REFERENCES

[7.1] Turin, G. L., Clapp, F. D., Johnston, T. L., Fine, S. B. and Lavry, D., "A statistical model of urban multipath propagation", IEEE Trans. Veh. Technol., Feb. 1972, Vol. VT-21, No. 1, pp 1-9.

[7.2] Cox, D. C., "Delay doppler characteristics of multipath propagation at 910-MHz in a suburban mobile radio environment", IEEE Trans. Antennas Propagat., Sept. 1972, Vol. AP-20, No. 5, pp 625-635.

[7.3] Cox, D. C., "910MHz urban mobile radio propagation: multipath characteristics in New York City", IEEE Trans. Commun., Nov. 1973, Vol. COM-21, No. 11, pp 1188-1194.

[7.4] Bajwa, A. S., "Wideband characterisation of UHF mobile radio propagation in urban and suburban areas", Ph.D. Thesis, Department of Electronic and Electrical Engineering, University of Birmingham, 1979.

[7.5] Young, W. R. and Lacy, L. Y., "Echoes in transmission at 450 megacycles from land-to-car radio units", Proc. IRE, March 1950, Vol. 38, pp 255-258.

[7.6] Schwartz, M., Bennett, W. R., and Stein, S., "Communication Systems and Techniques", McGraw-Hill, 1966.

[7.7] Bello, P. A., "Characterization of randomly time-variant linear channels", IEEE Trans. Commun. Syst., Dec. 1963, Vol CS-11, pp 360-393.

[7.8] Stein, S., "Fading channel issues in system engineering", IEEE J. Selected Areas Commun., Feb. 1987, Vol. SAC-5, No.2, pp 68-89.

[7.9] Papoulis, A., "Probability, Random Variables and Stochastic Processes", McGraw-Hill, 1965.

[7.10] Suzuki, H., "A statistical model for urban radio propagation", IEEE Trans. Commun., July 1977, Vol. COM-25, No. 7, pp 673-680.

[7.11] Cox, D. C. and Leck, R. P., "Correlation bandwidth and delay spread multipath propagation statistics for 910-MHz urban mobile radio channels", IEEE Trans. Commun., Nov. 1975, Vol. COM-23, No. 11, pp 1271-1280.

[7.12] Jakes, W. C. (Ed.), "Microwave Mobile Communications", John Wiley 1974.

[7.13] Chuang, J. C-I., "The effects of time delay spread on portable radio communications channels with digital modulation", IEEE J. Selected Areas Commun., June 1987, Vol. SAC-5, No. 5, pp 879-889.

[7.14] Huish, P. W. and Gurdenli, E., "Radio channel measurement and predictions for future mobile radio systems", Br. Telecom. Technol. J., Jan. 1988, Vol. 6, No. 1, pp 43-53.

[7.15] Saruwatari, T., Mizuno, M., Iwama, T., Sekizawa, S., Ryuko, H., Ando. H. and Nilson, M., "Large area characterisation of impulse responses on(sic) 775MHz in mountainous terrain", COST 207 TD(87)36, May 1987.

[7.16] Lindell, F., Swerup, J. and Uddenfeldt, J., "Digital cellular radio for the future", Ericsson Review, No. 3, 1987, pp 160-168.

[7.17] Cox, D. C. and Leck, R. P., "Distributions of multipath delay spread and average excess delay for 910-MHz urban mobile radio paths", IEEE Trans Antennas Propagat., Mar. 1975, Vol. AP-23, No. 2, pp 206-213.

[7.18] Proakis, J. G., "Digital Communications", McGraw-Hill, 1983.

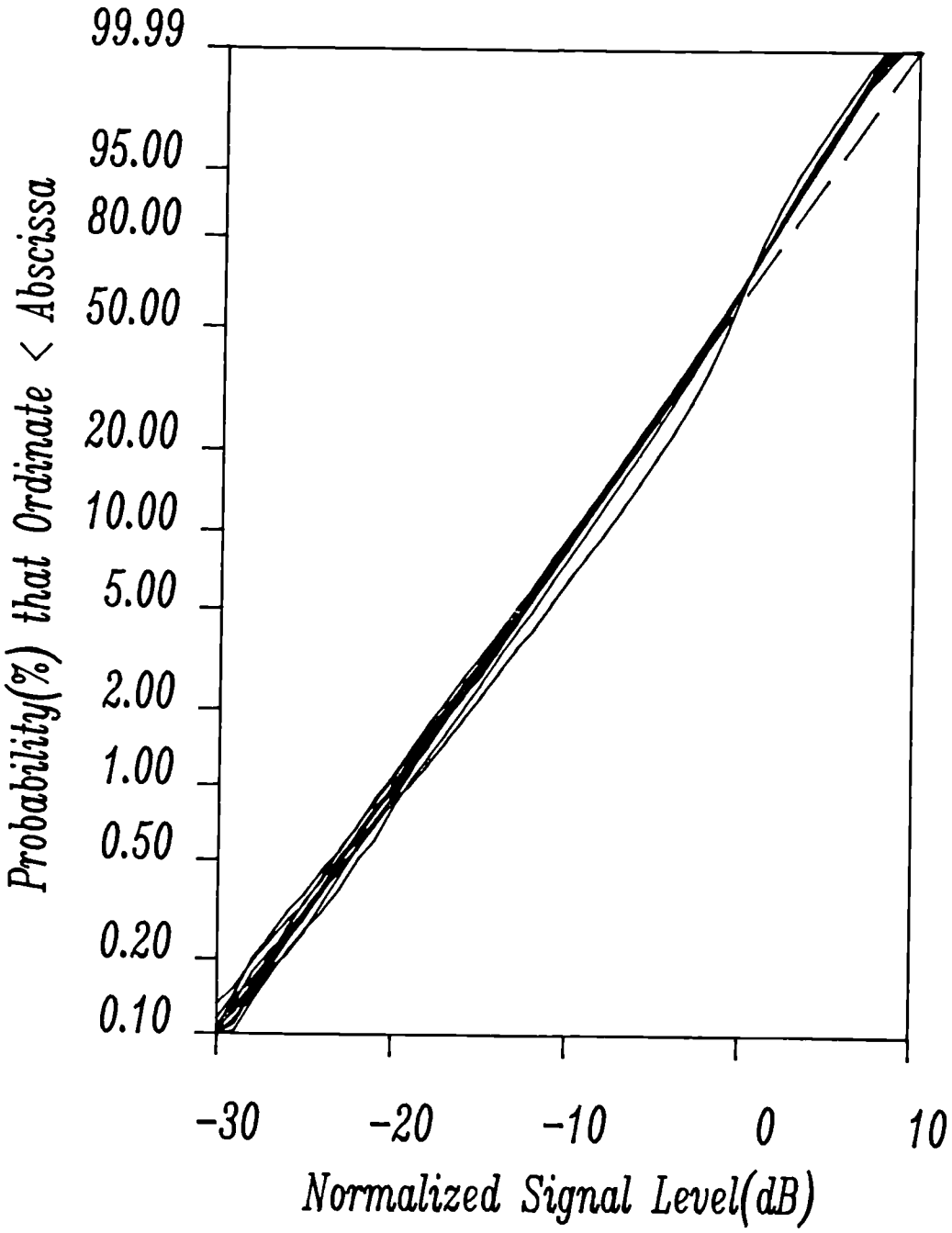

Fig. 7.1. Small-scale amplitude distributions of the first 10 paths(i.e., 1μs).

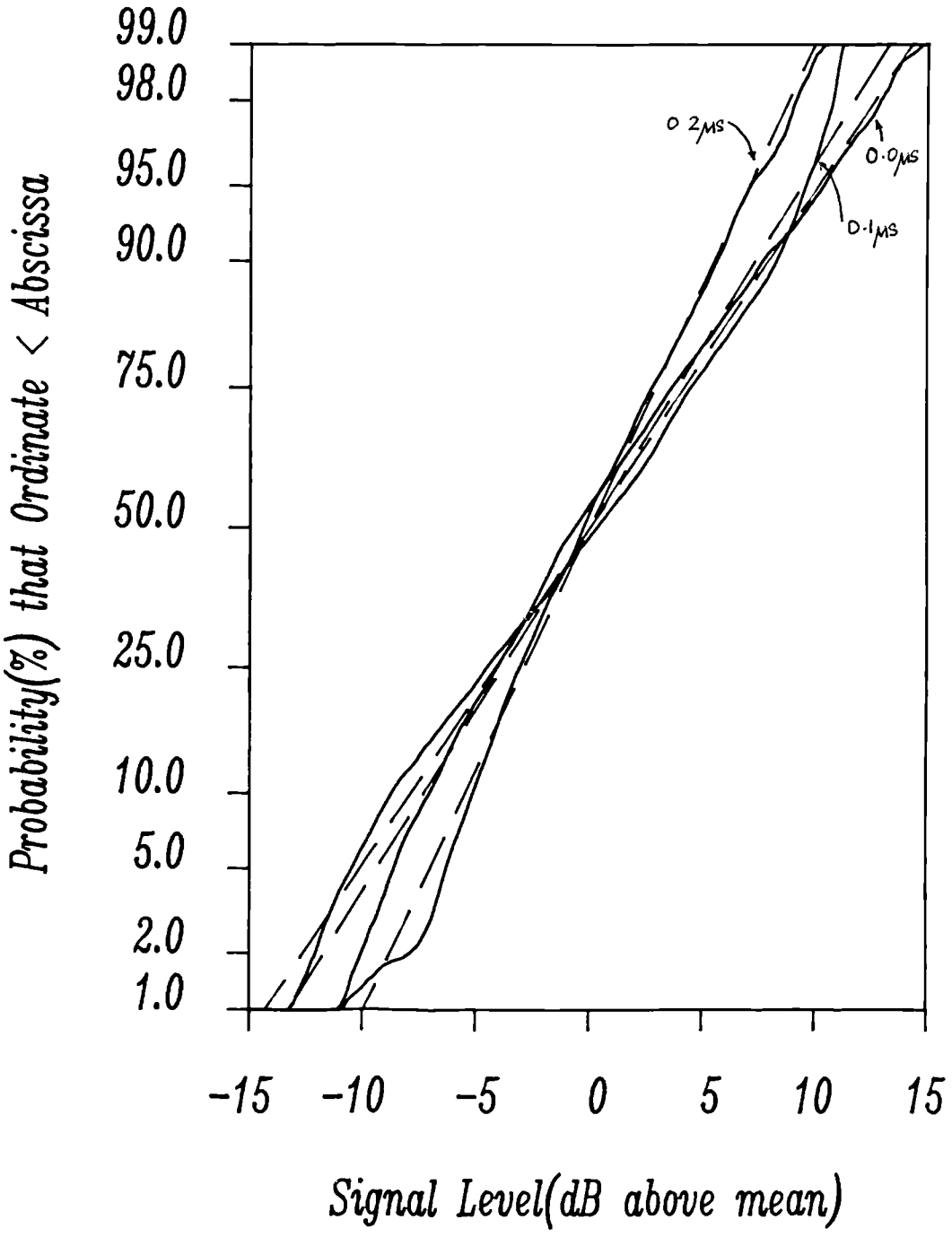

Fig. 7.2. Large-scale amplitude distributions of the paths with excess delays $0\mu s$, $0.1\mu s$ and $0.2\mu s$.

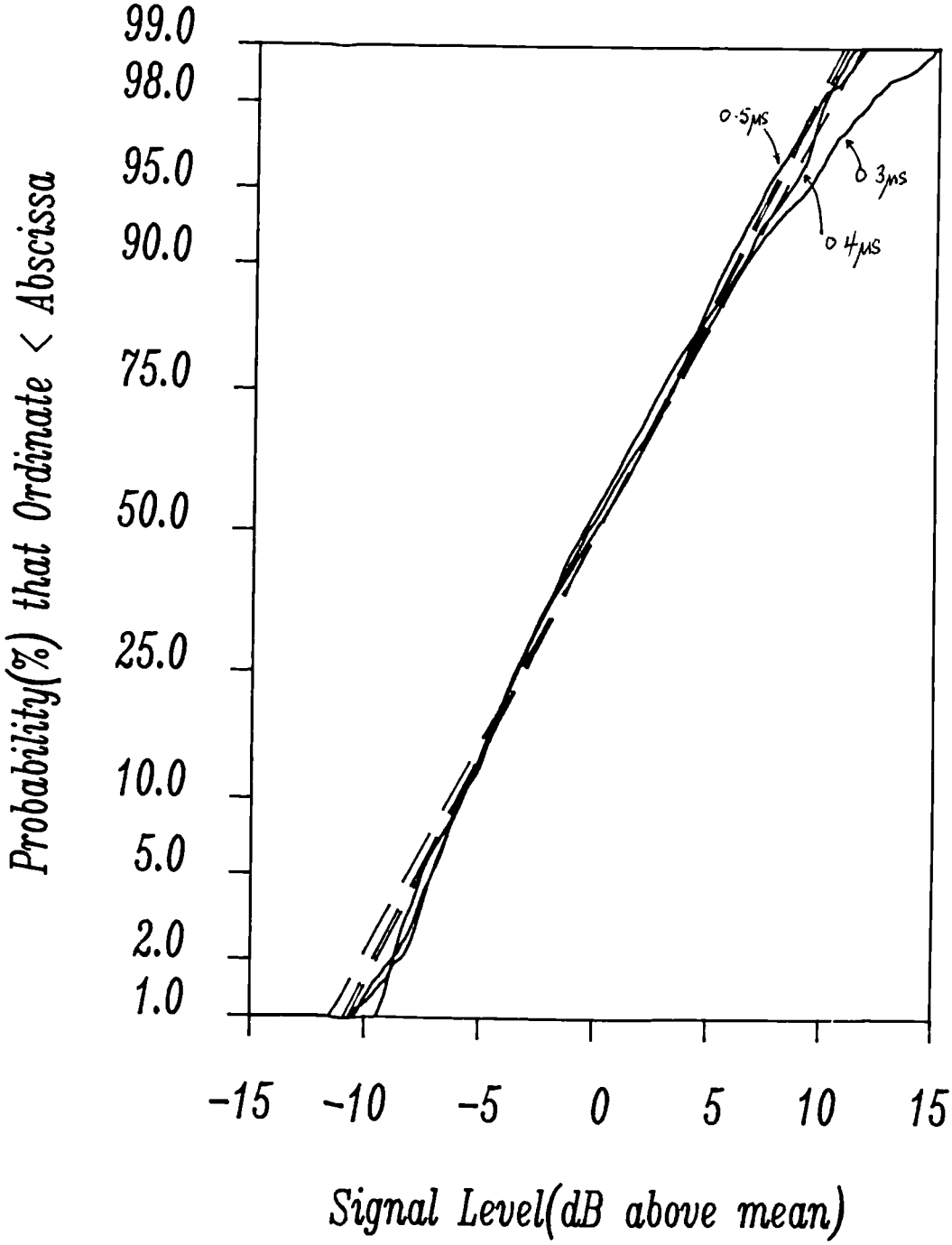

Fig. 7.3. Large-scale amplitude distributions of the paths with excess delays $0.3\mu s$, $0.4\mu s$ and $0.5\mu s$.

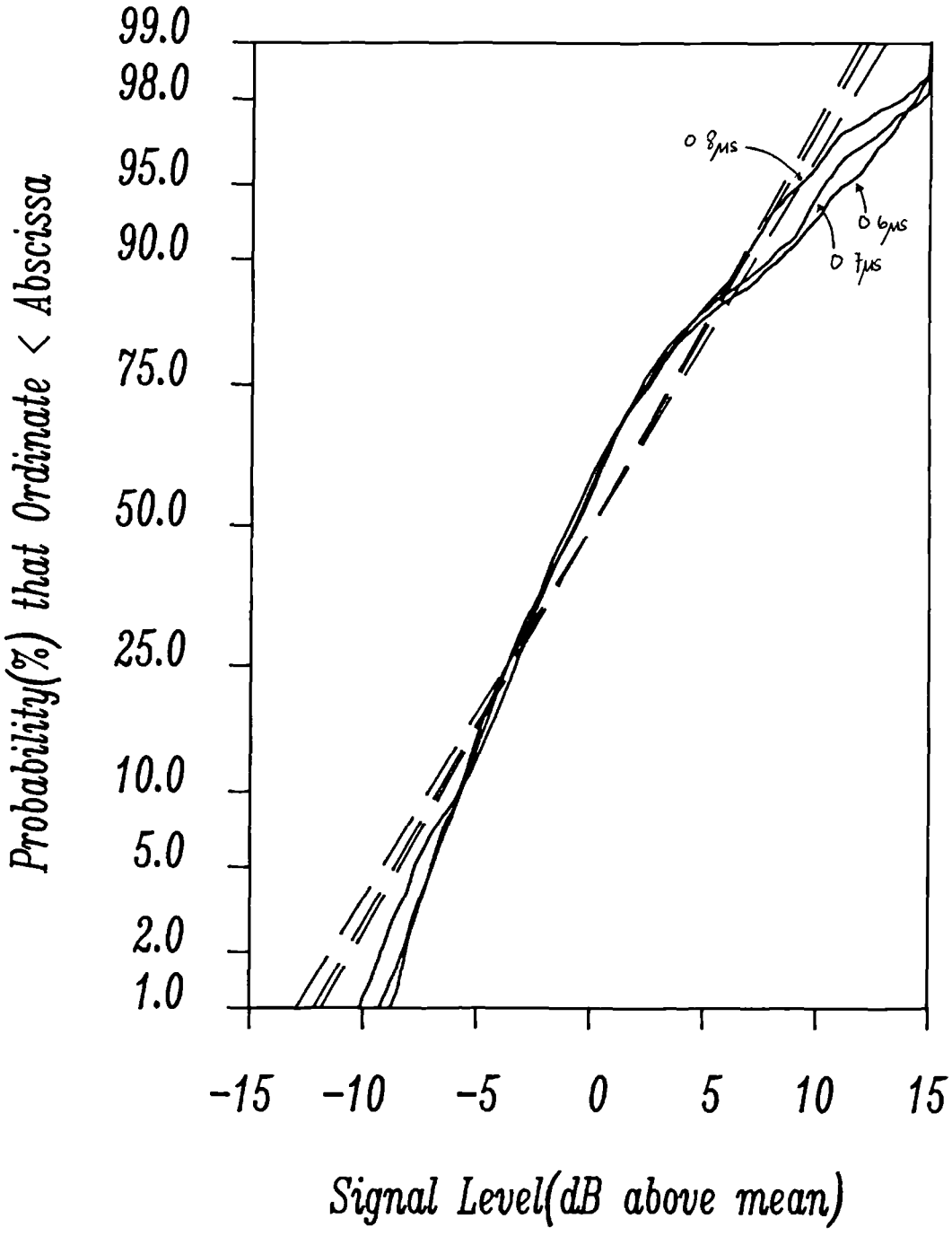

Fig. 7.4. Large-scale amplitude distributions of the paths with excess delays $0.6\mu s$, $0.7\mu s$ and $0.8\mu s$.

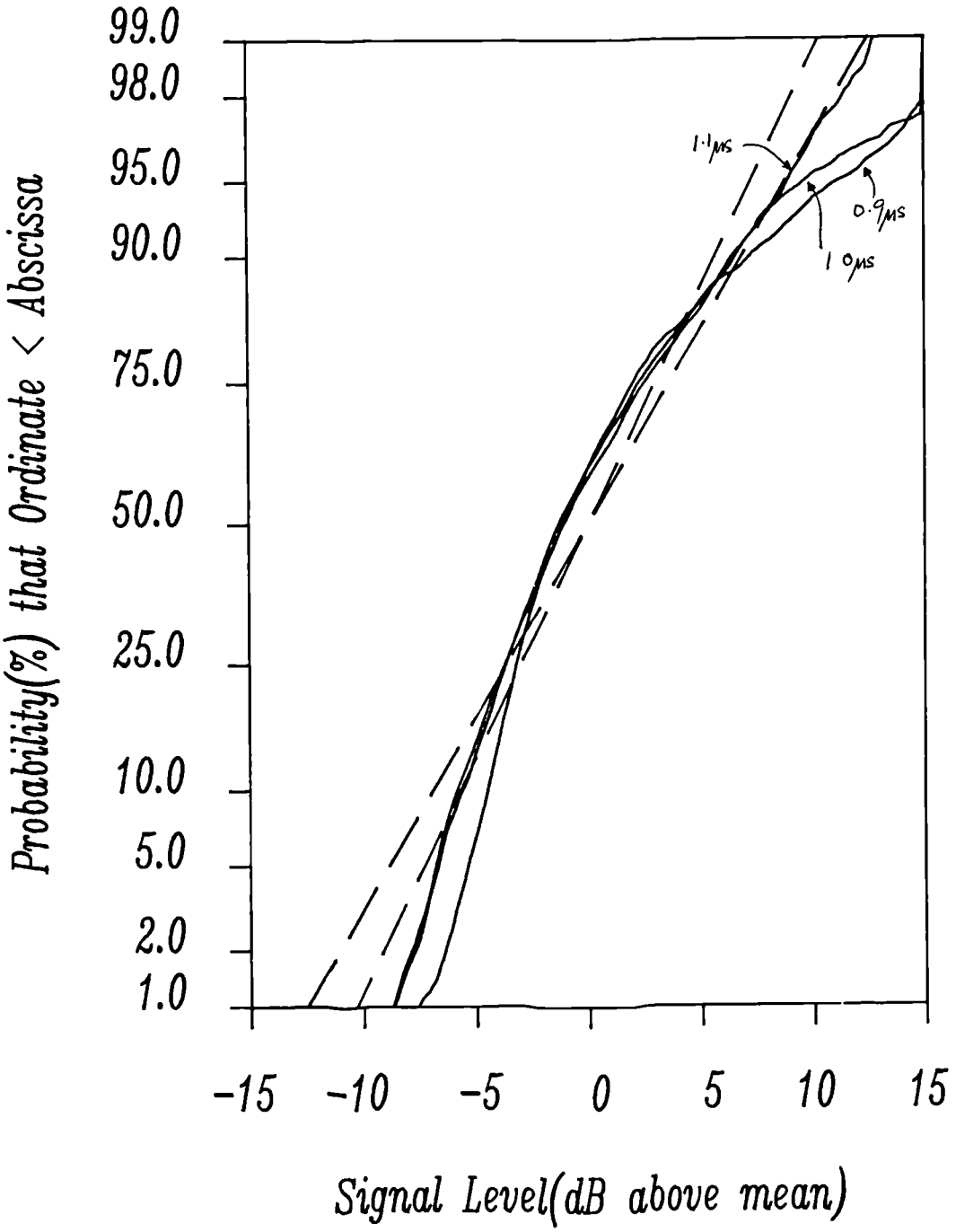

Fig. 7.5. Large-scale amplitude distributions of the paths with excess delays $0.9\mu s$, $1.0\mu s$ and $1.1\mu s$.

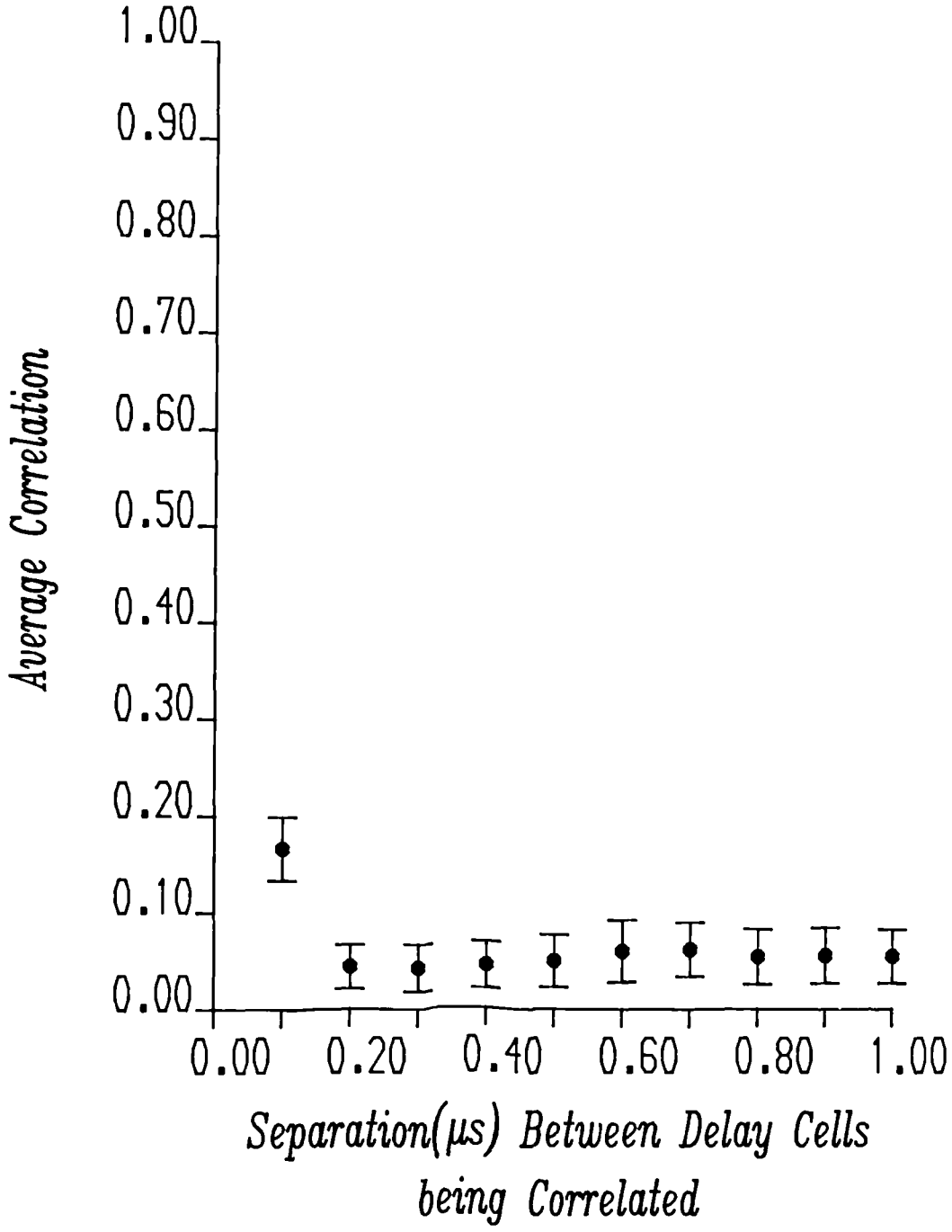

Fig. 7.6. The average coefficients of correlation between the small-scale amplitude fluctuations in neighbouring time-delay cells.

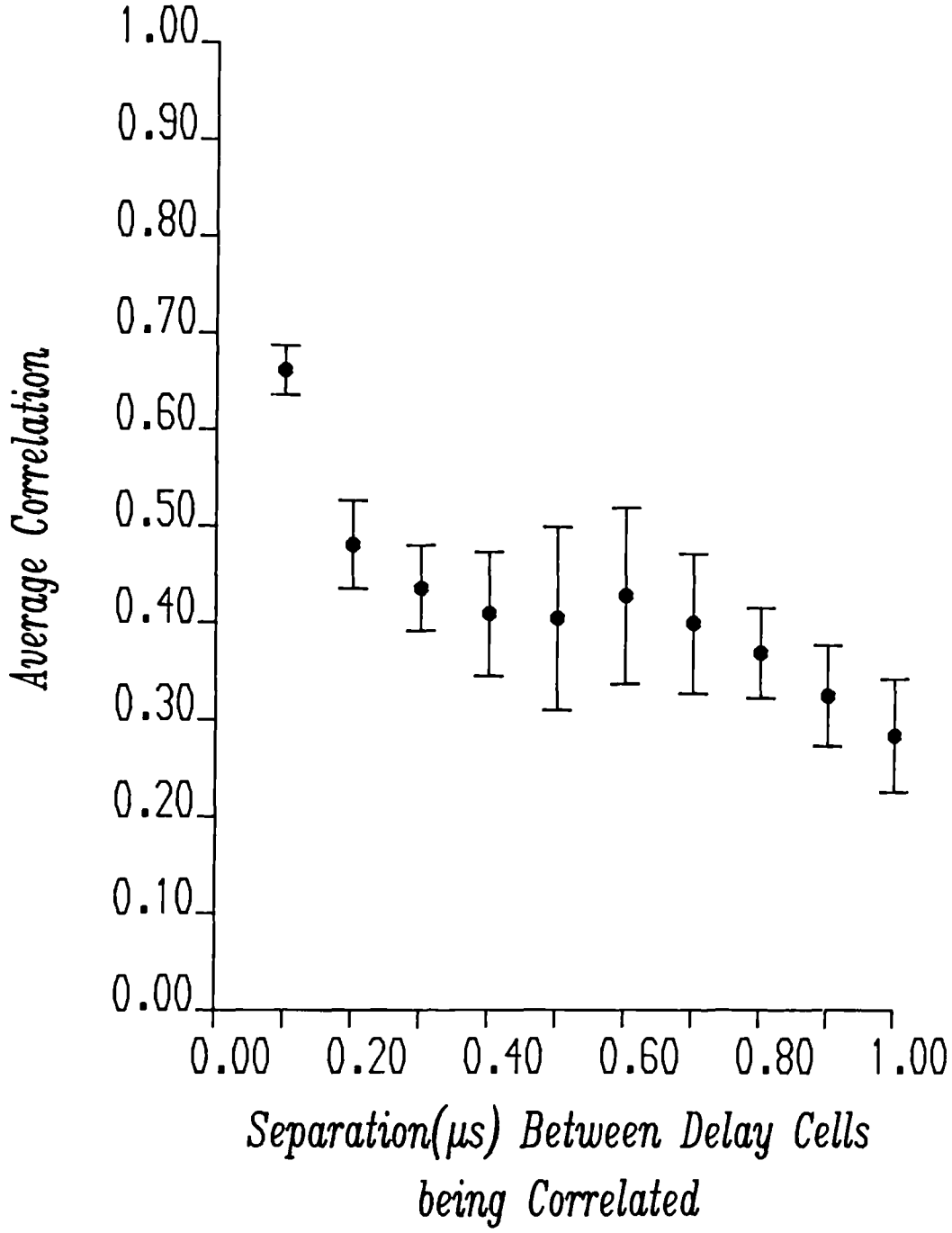

Fig. 7.7. The average coefficients of correlation between the large-scale amplitude fluctuations in neighbouring time-delay cells.

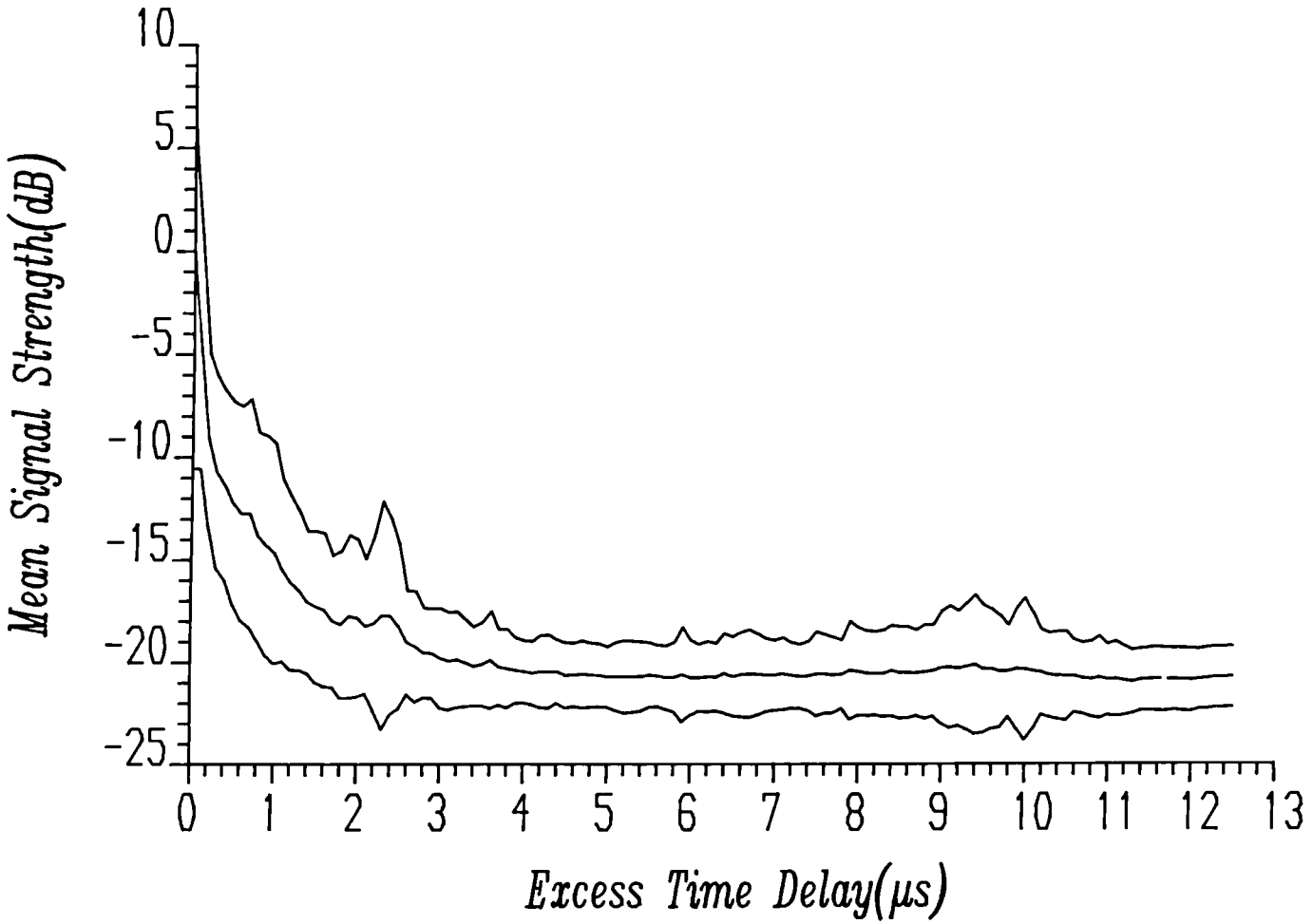

Fig. 7.8. The large-scale mean signal strength(i.e., weighting factor) versus excess time-delay.

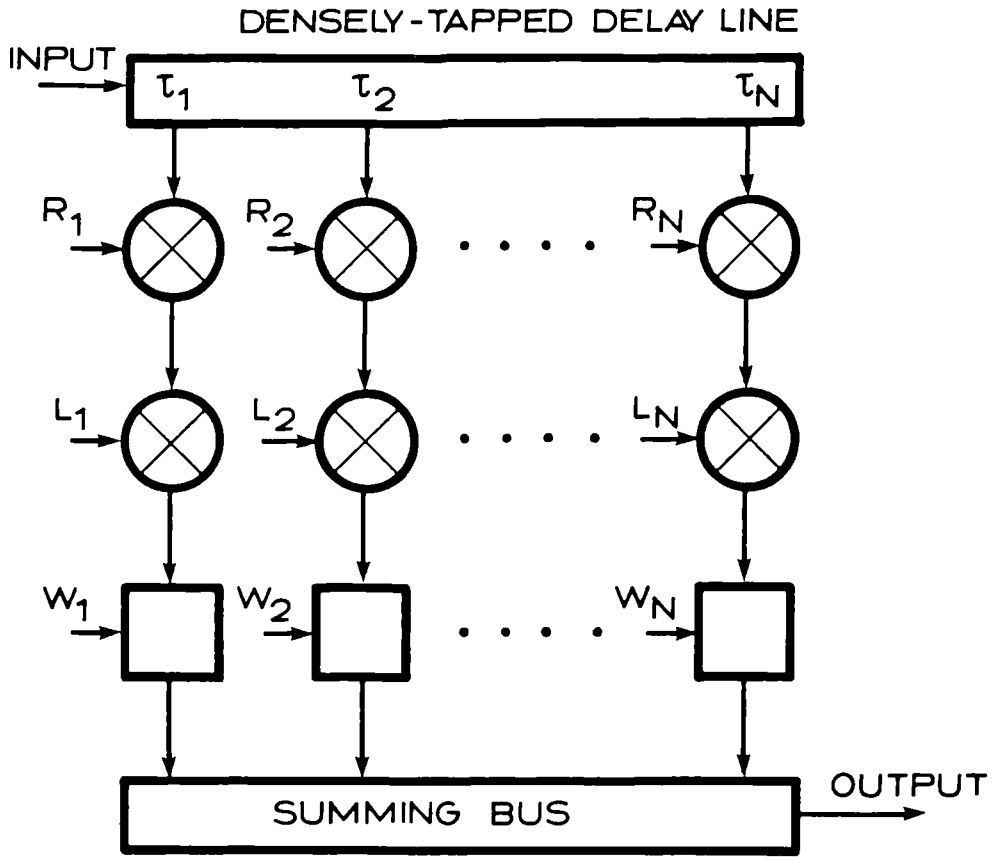

$R_1, R_2, \ldots, R_N$	Independent, zero-mean, complex Gaussian modulators.
$L_1, L_2, \ldots, L_N$	Zero-mean log-normal modulators with standard deviations selected according to Fig.(7.8), and correlations selected according to Fig.(7.7).
$W_1, W_2, \ldots, W_N$	Weighting factors for each tap selected according to Fig.(7.8).

Fig. 7.9. Schematic of the tapped-delay line simulator for wideband multipath channels.

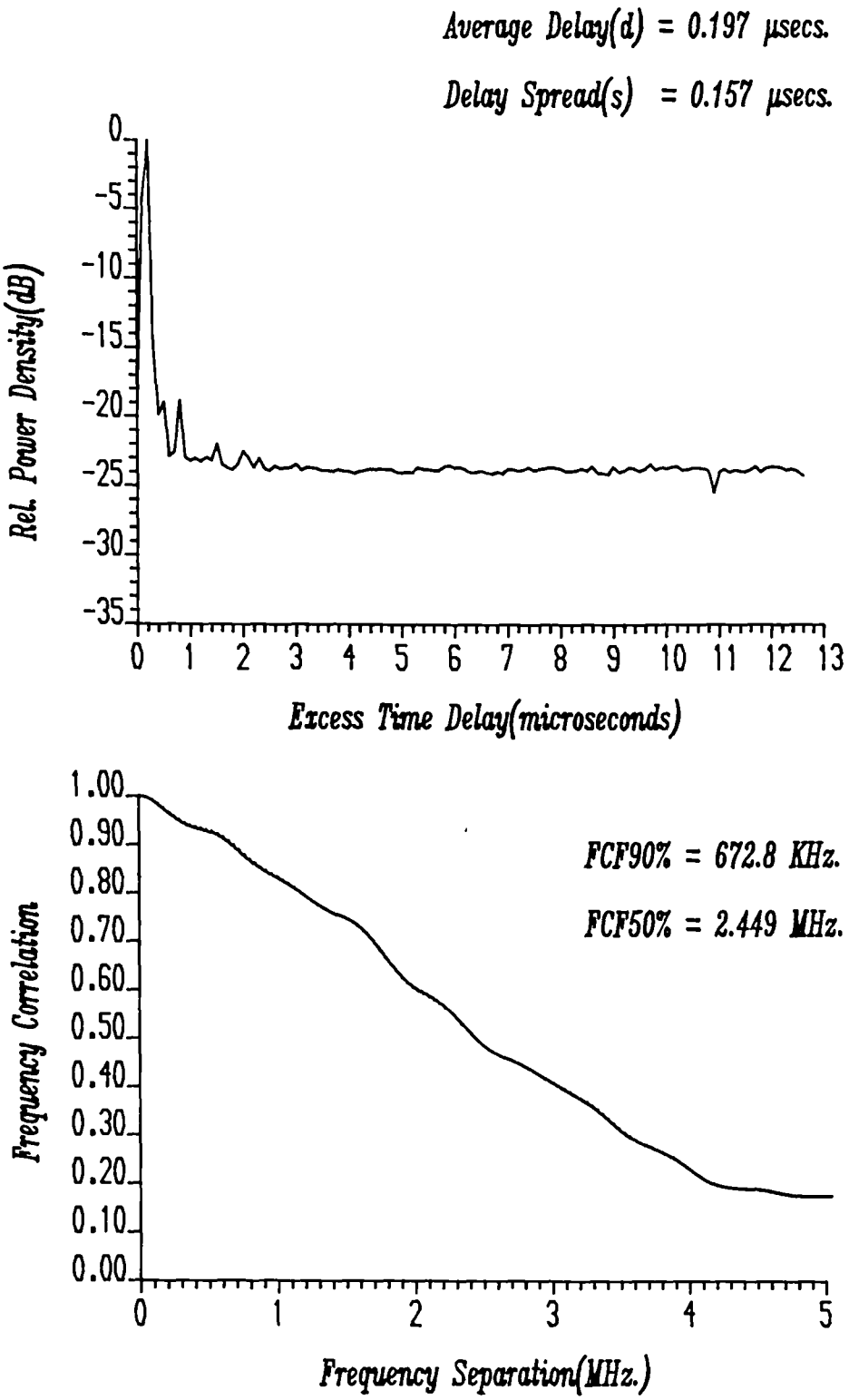

Fig. 7.10. Typical average power delay profile and frequency correlation function for a near LOS transmission.

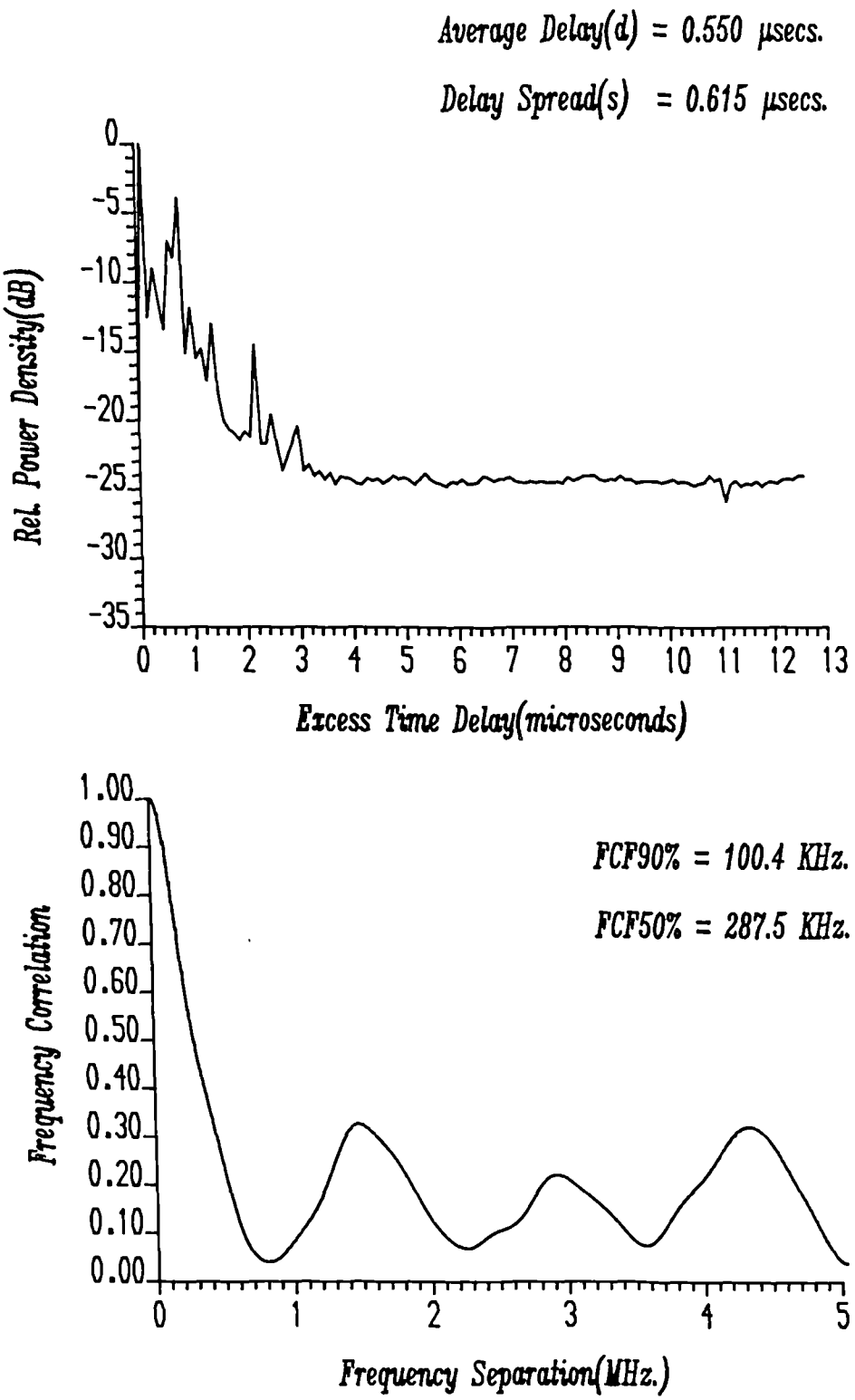

Fig. 7.11. Typical average power delay profile and frequency correlation function showing the variability in transmission conditions within a few tens of metres.

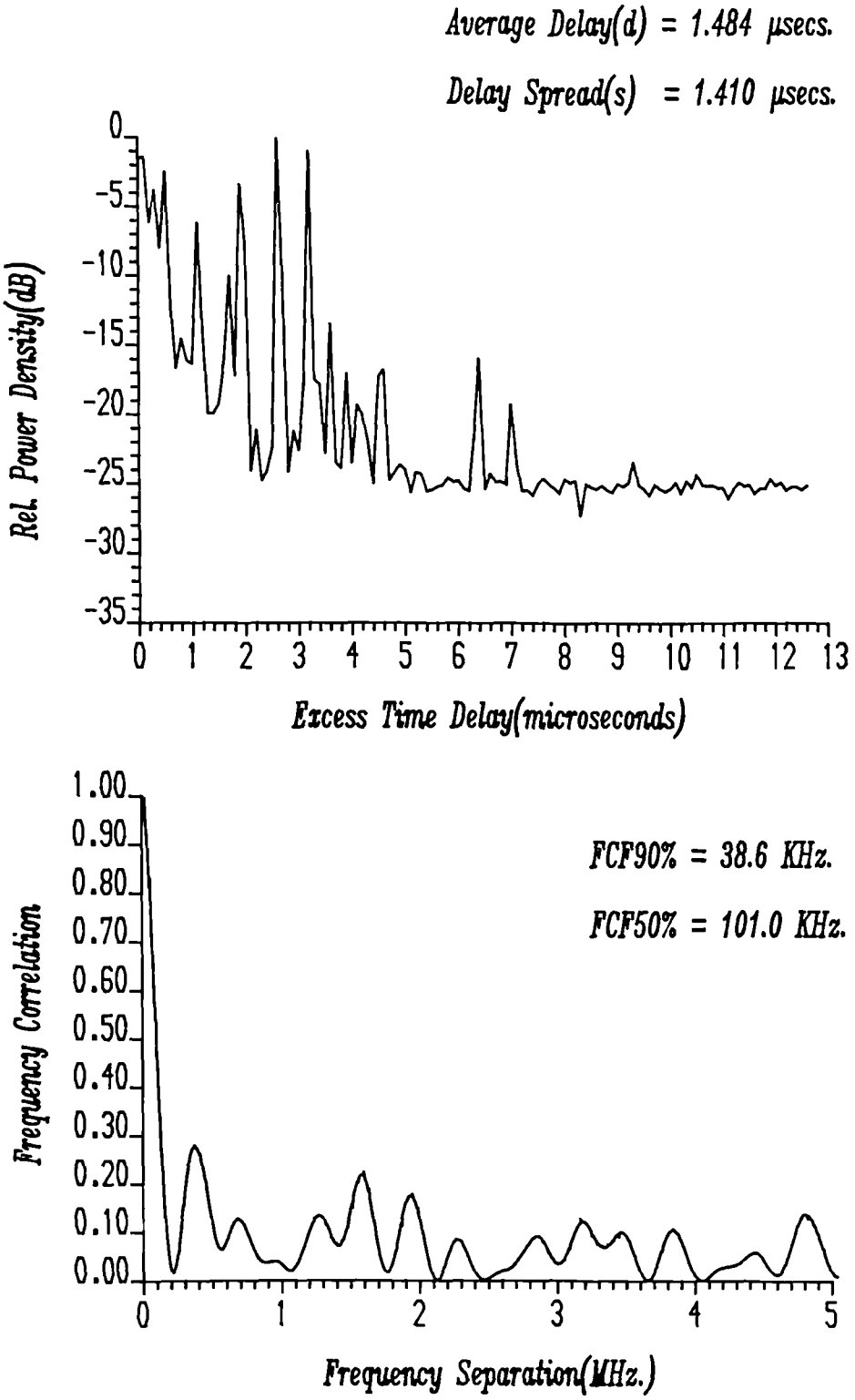

Fig. 7.12. Typical average power delay profile and frequency correlation function showing severe multipath dispersion.

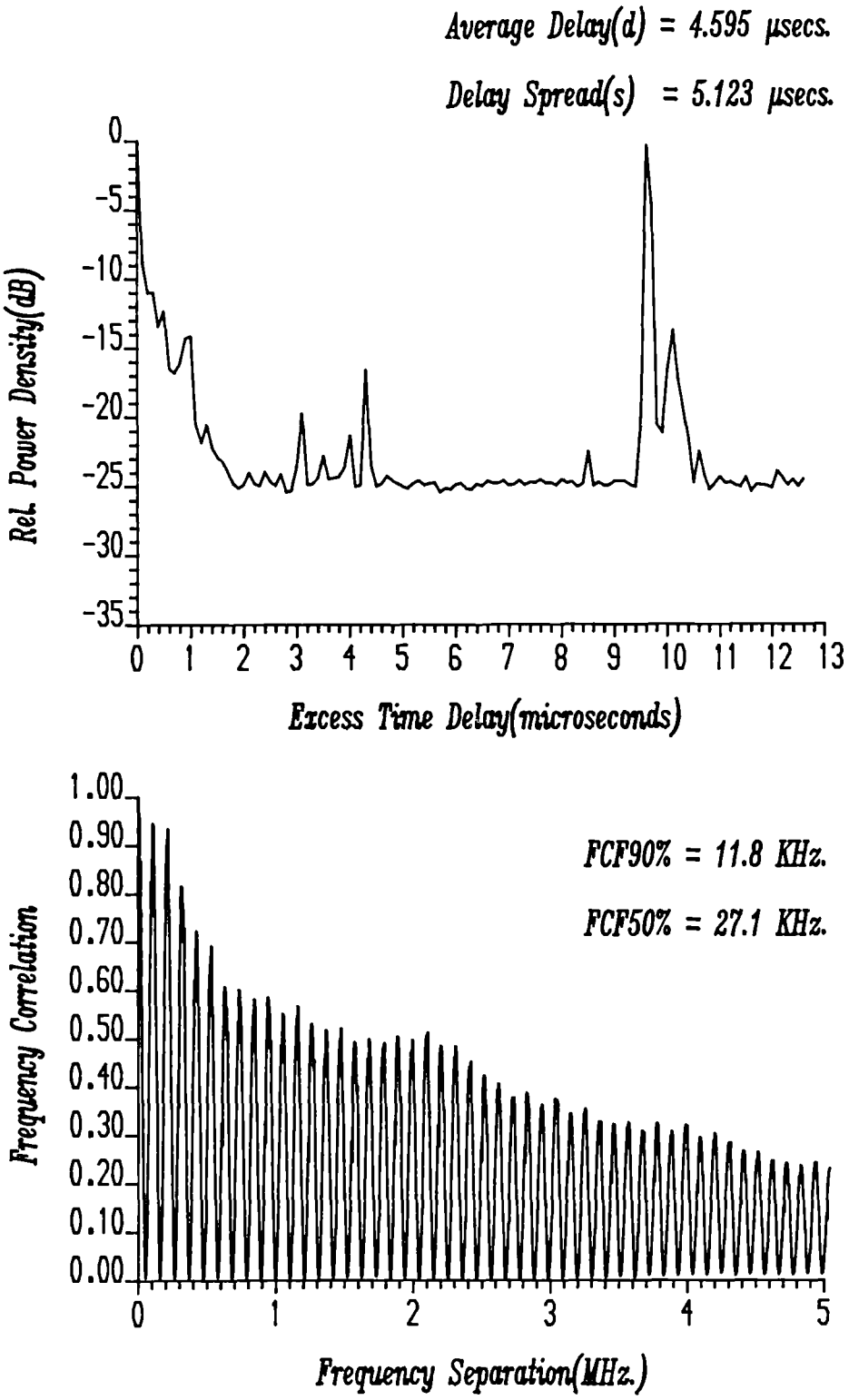

Fig. 7.13. Typical average power delay profile and frequency correlation function showing the most severe multipath dispersion.

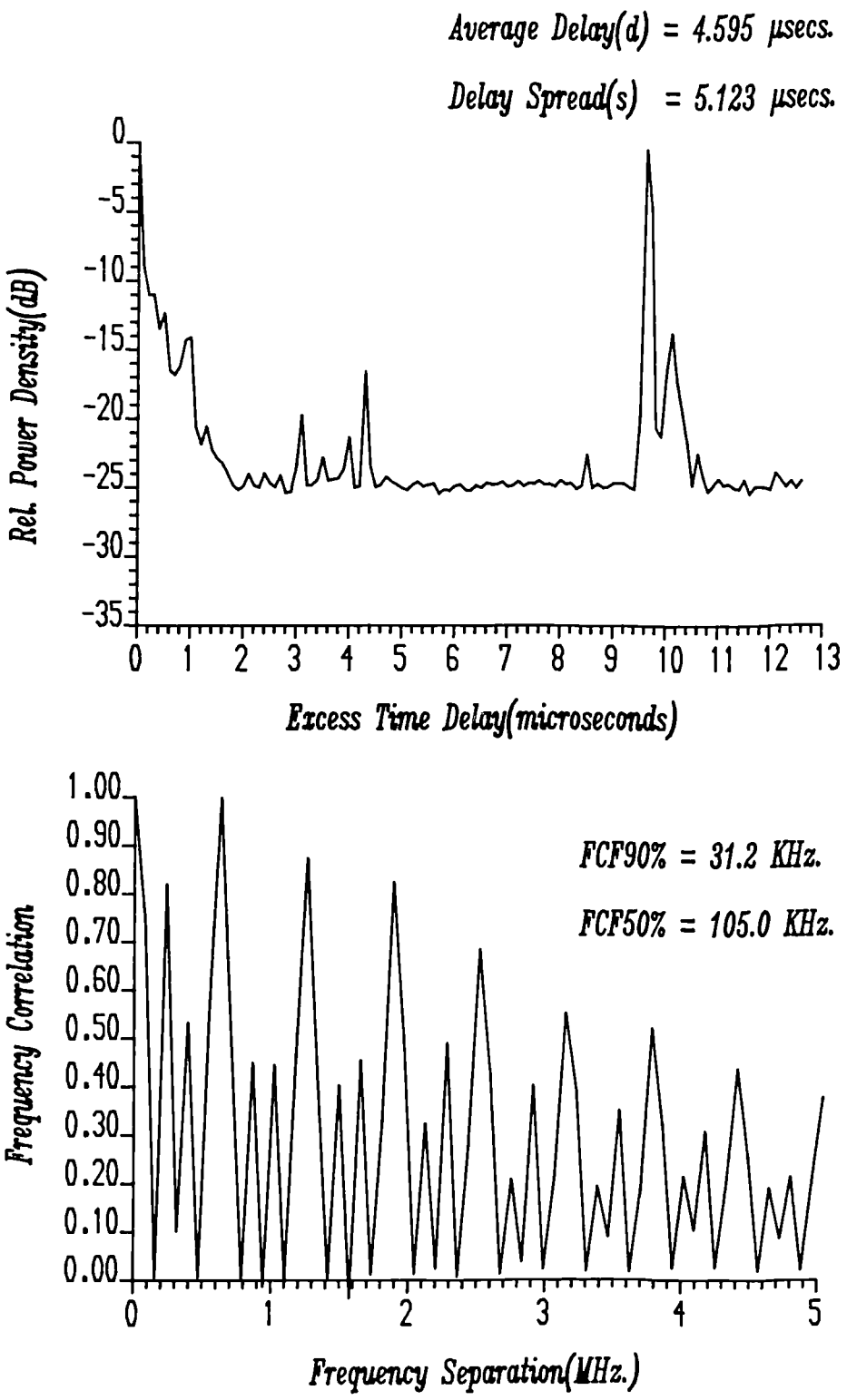

Fig. 7.14. Frequency correlation function of the average power delay profile of Fig.(7.13) produced without zero-padding to emphasise the problem of limited frequency resolution.

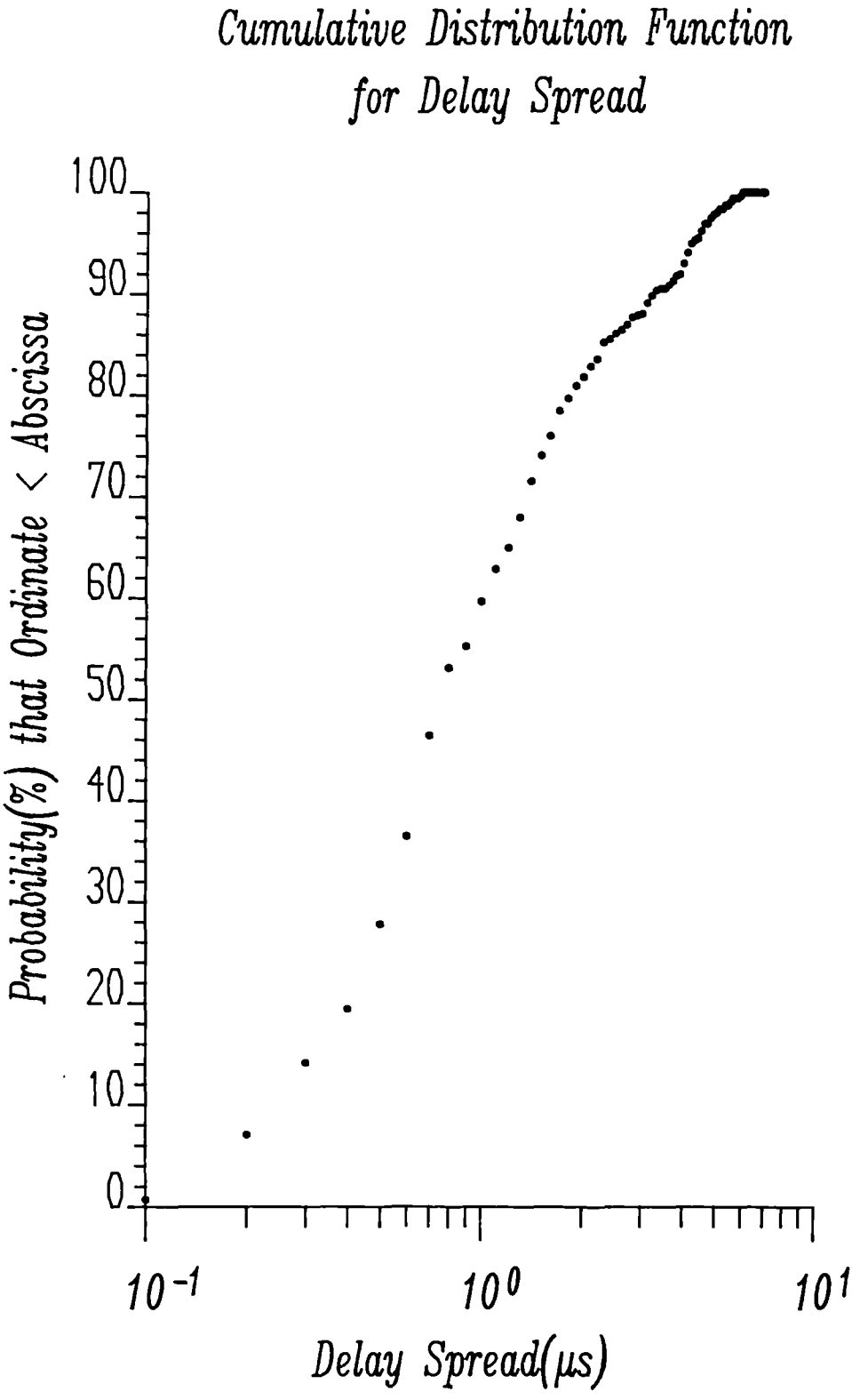

Fig. 7.15. Cumulative distribution function for the delay spreads.

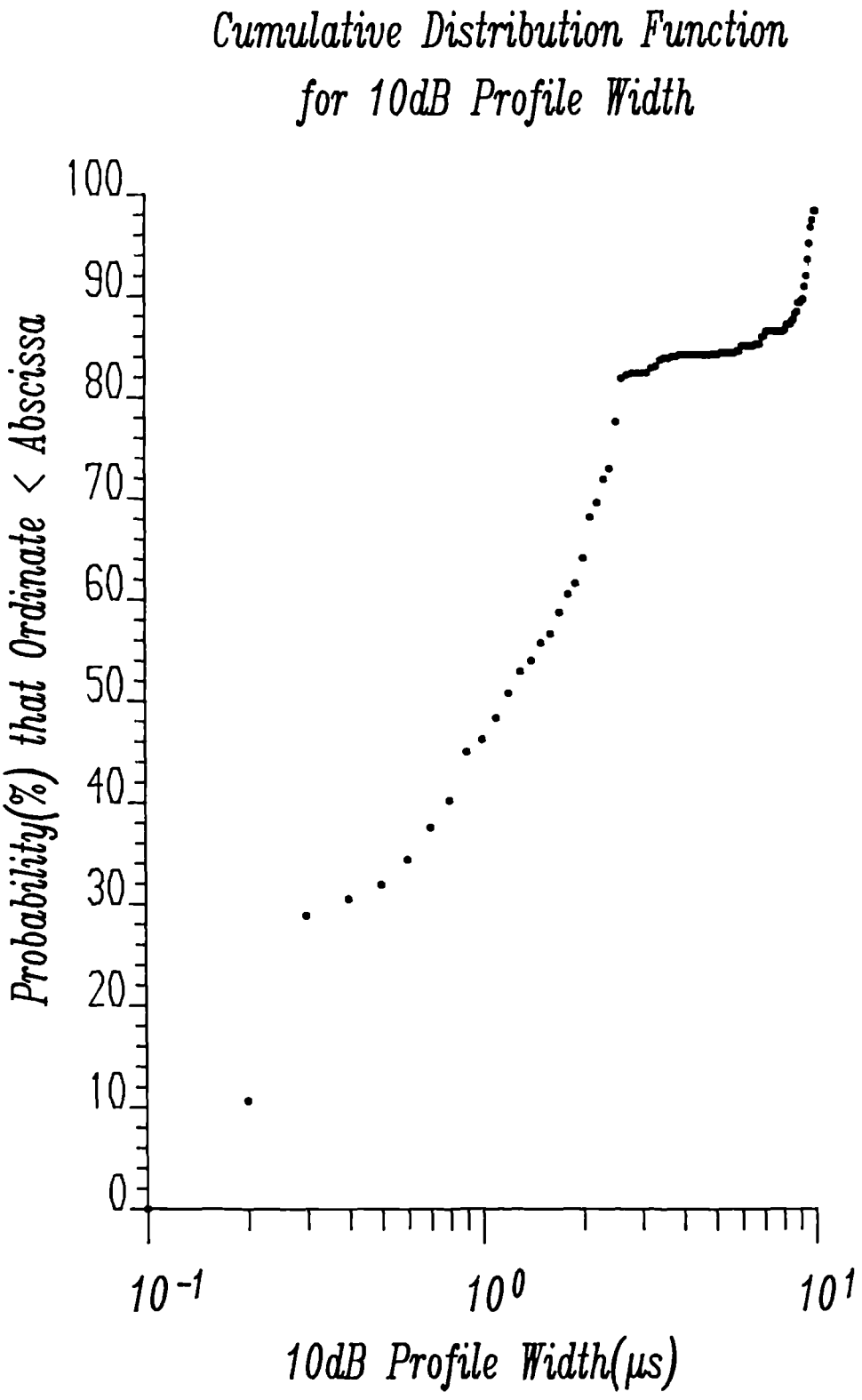

Fig. 7.16. Cumulative distribution function for the -10dB profile widths.

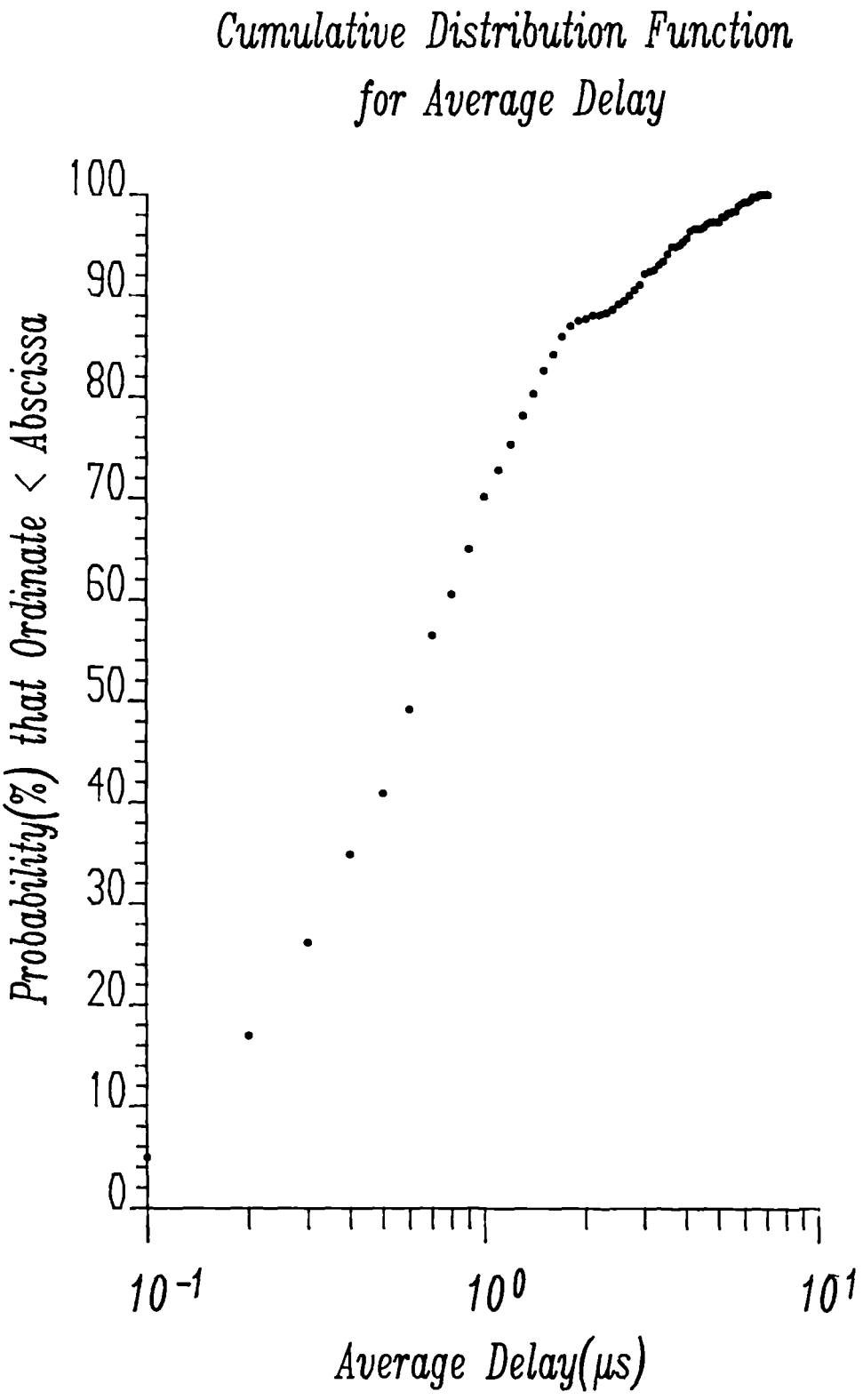

Fig. 7.17. Cumulative distribution function for the average delays.

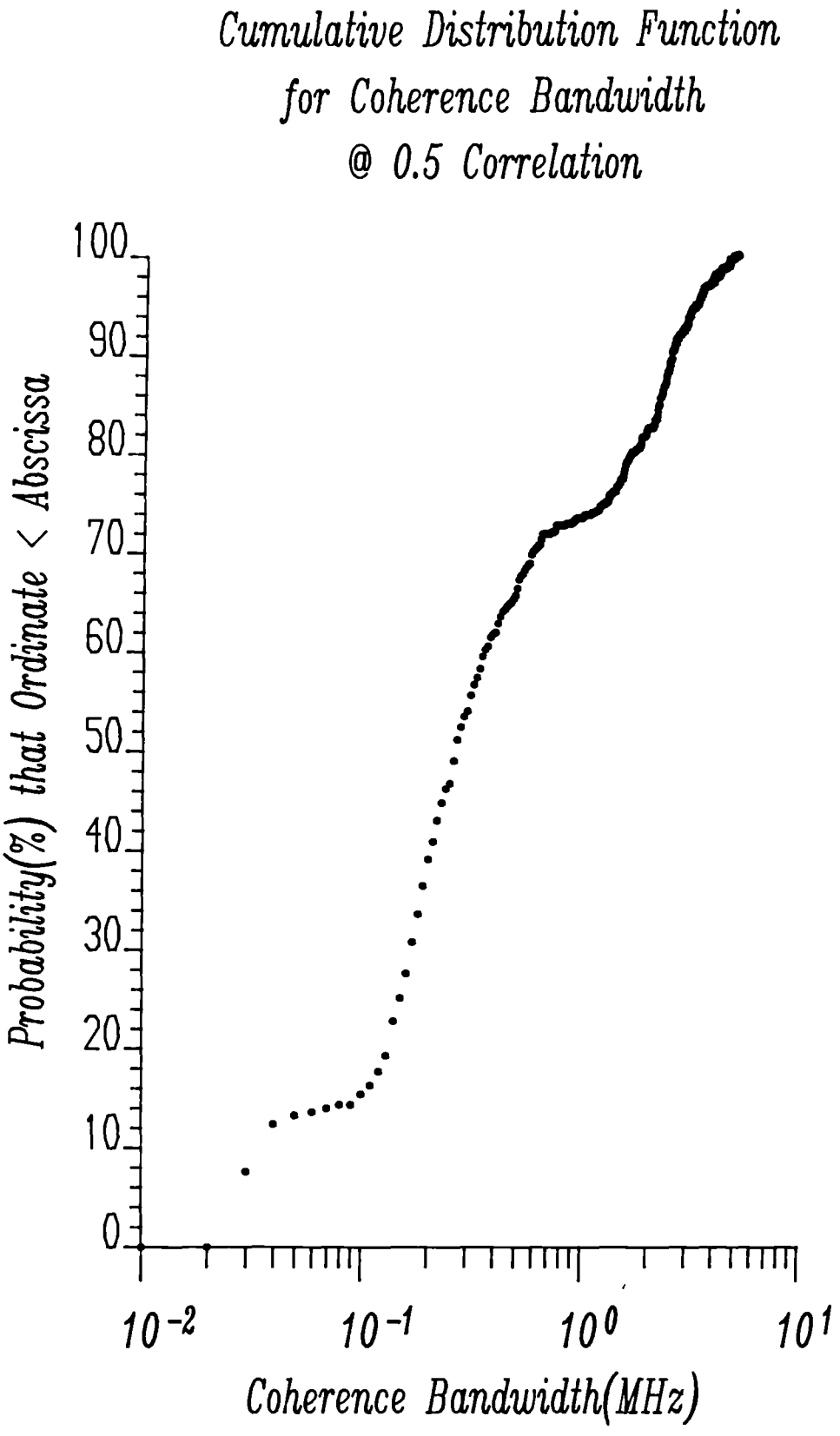

Fig. 7.18. Cumulative distribution function for the coherence bandwidths at 0.5 correlation.

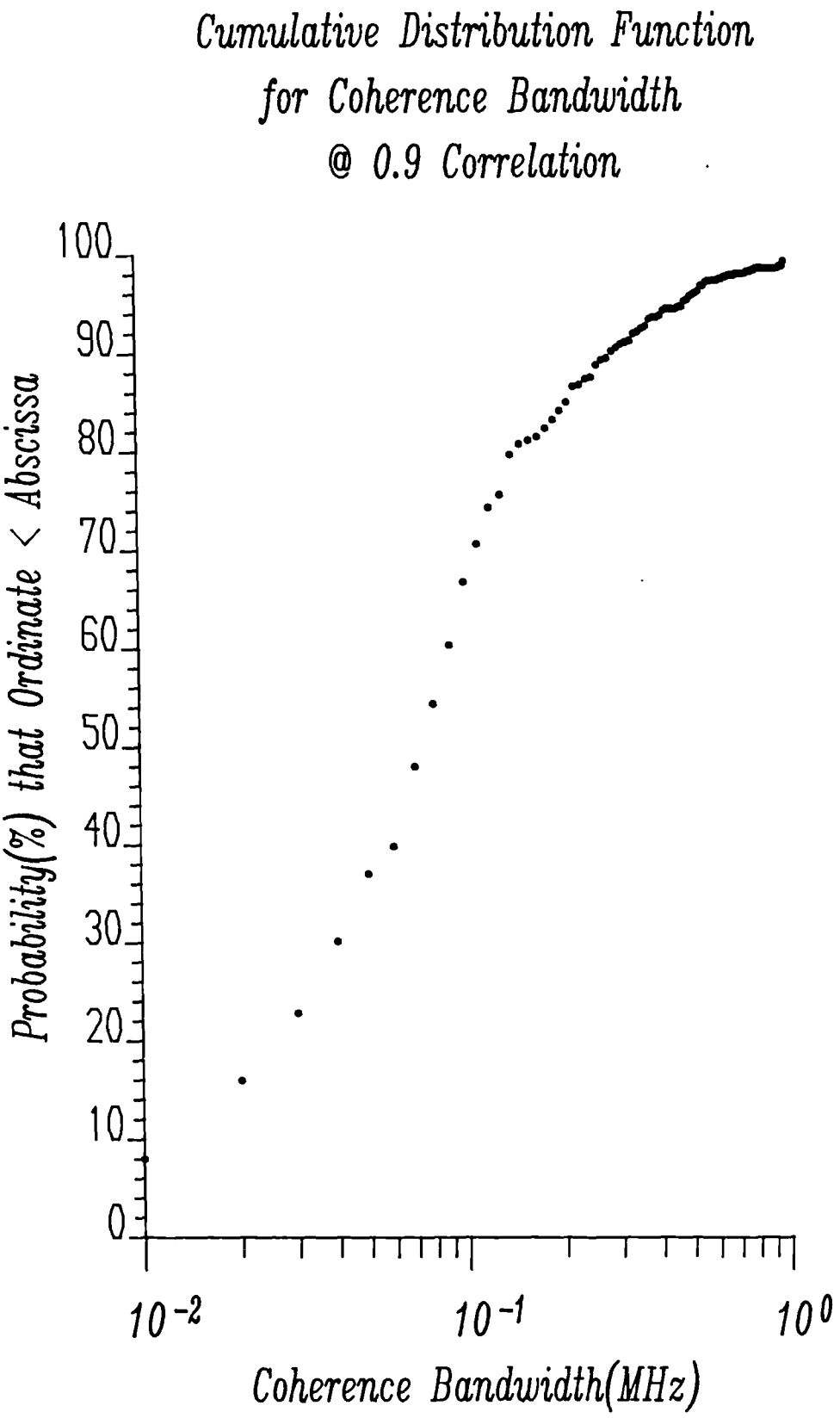

Fig. 7.19. Cumulative distribution function for the coherence bandwidths at 0.9 correlation.

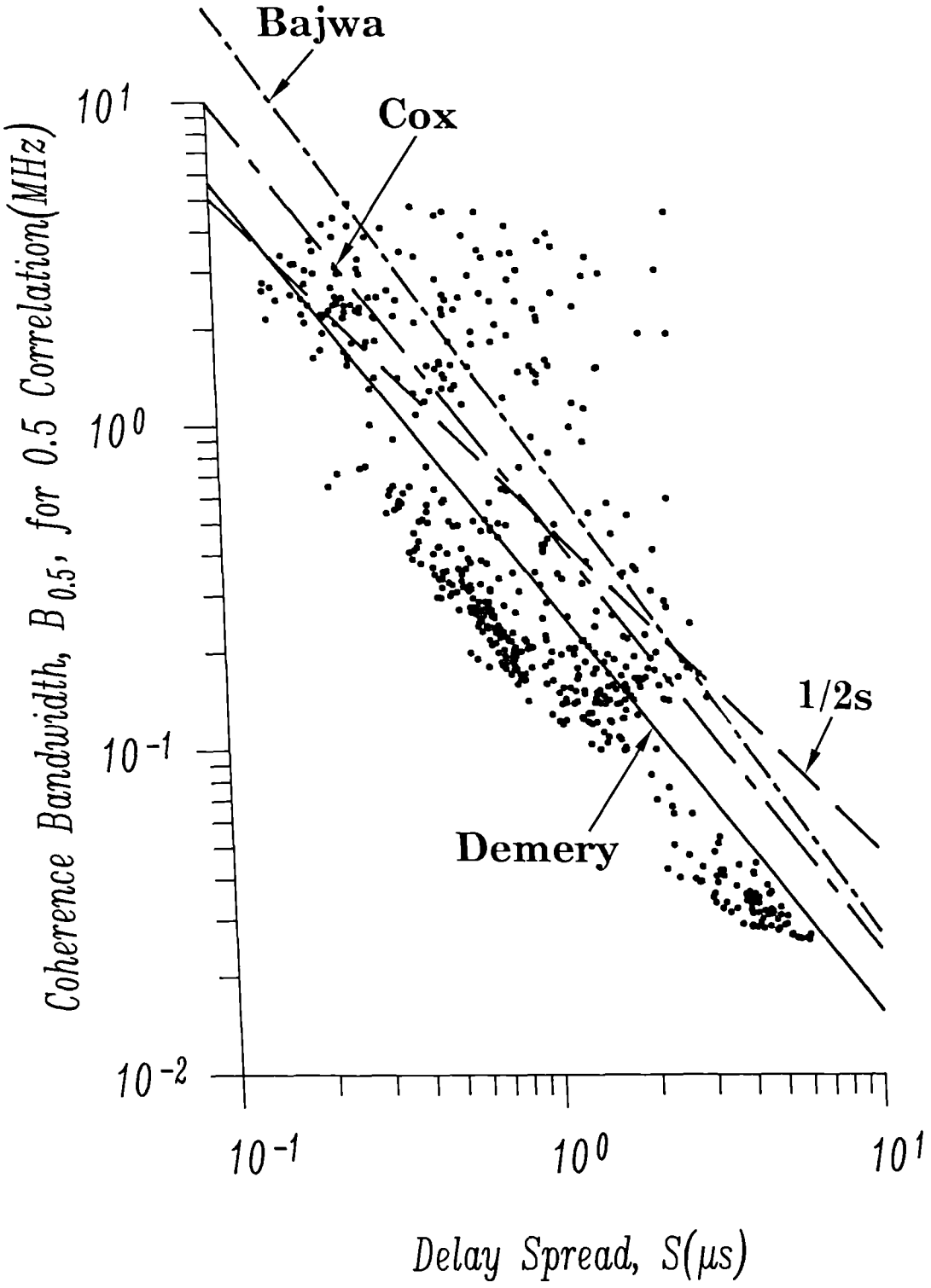

Fig. 7.20. Scatter plot of coherence bandwidth at 0.5 correlation versus delay spread.

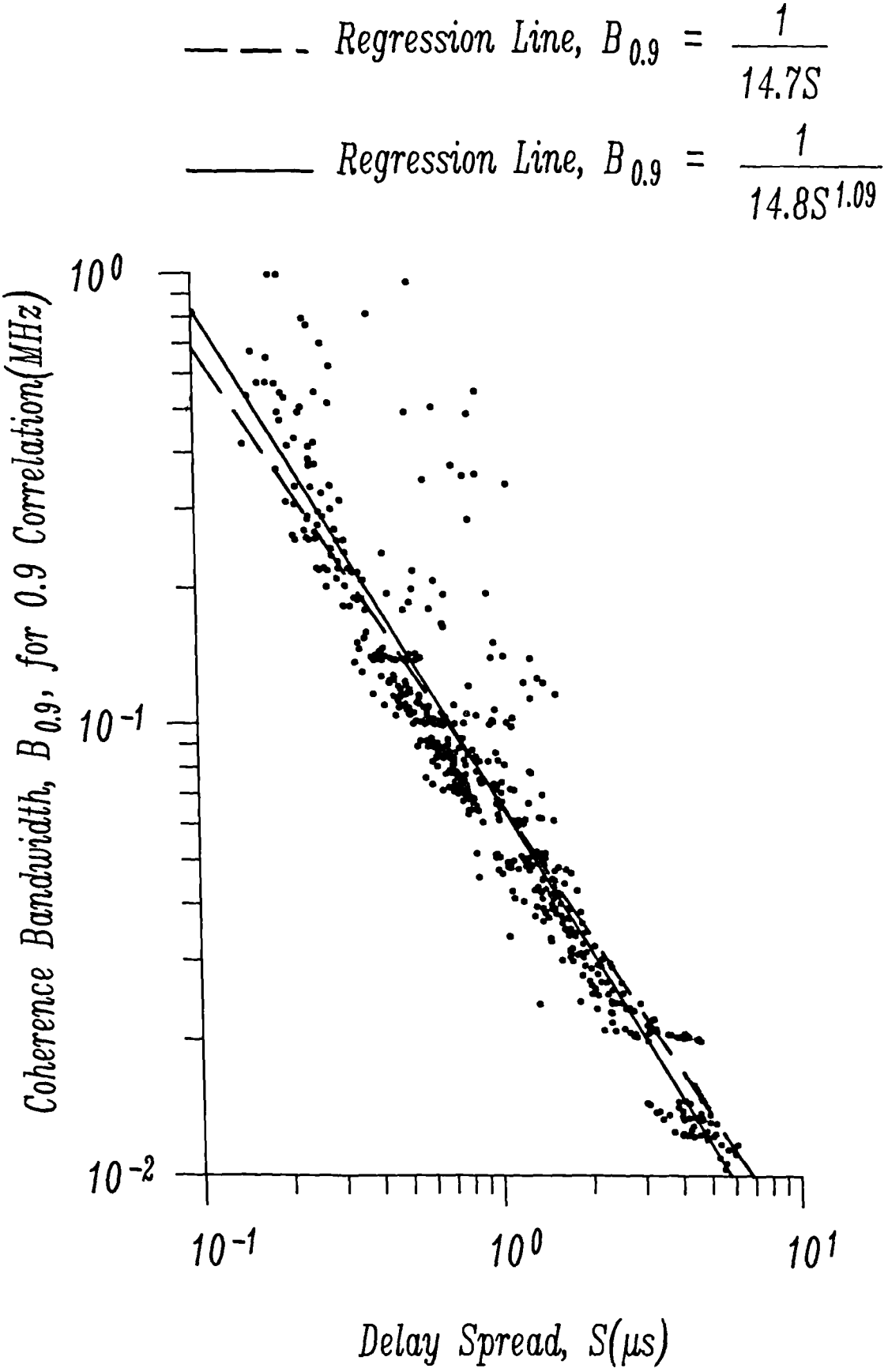

Fig. 7.21. Scatter plot of coherence bandwidth at 0.9 correlation versus delay spread.

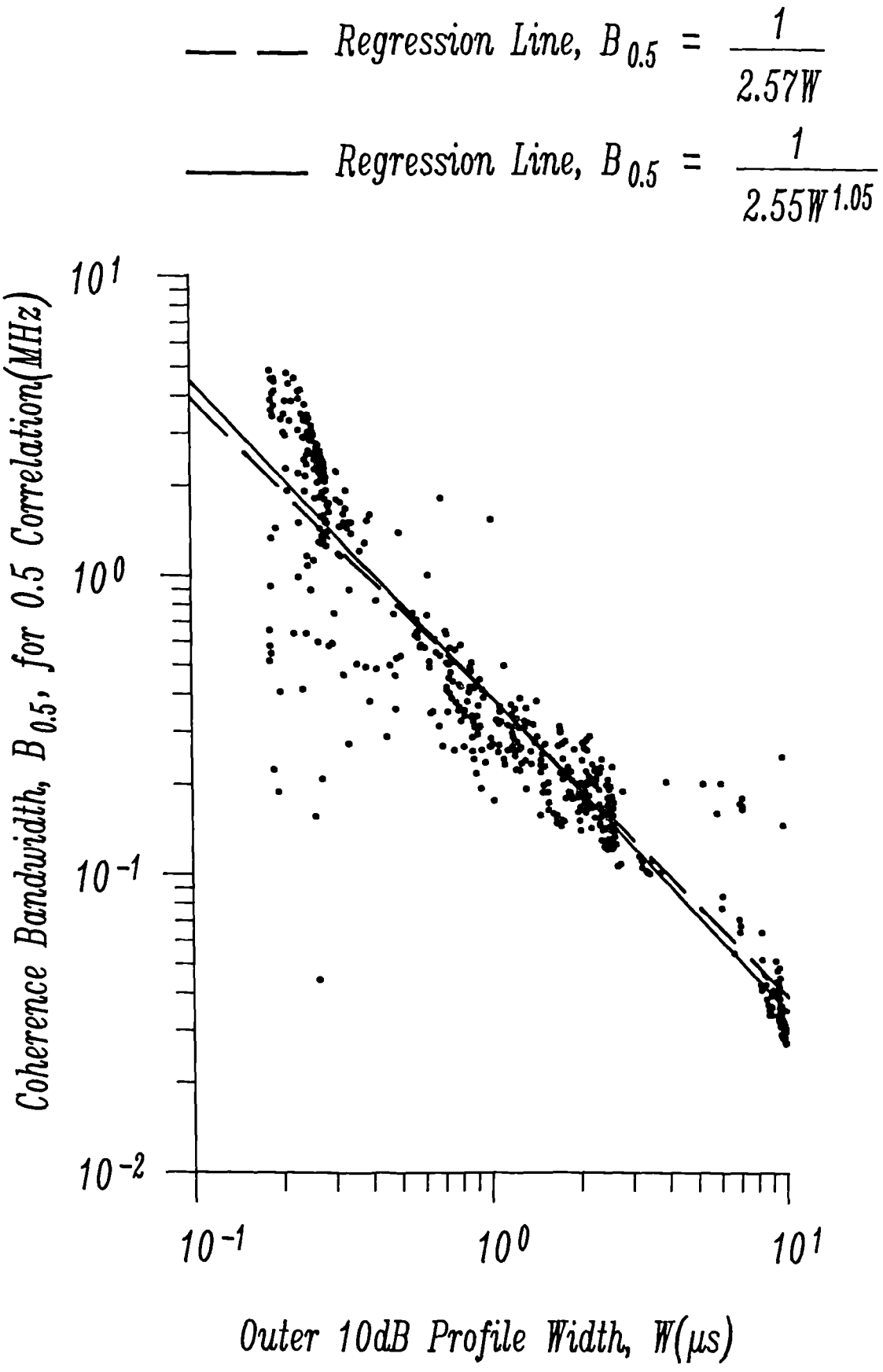

Fig. 7.22. Scatter plot of coherence bandwidth at 0.5 correlation versus -10dB profile width.

CHAPTER 8. CONCLUSIONS.

An investigation of the 900MHz wideband propagation characteristics of a medium-sized UK city has been undertaken. The main conclusions deduced from this work will now be briefly recapped. In addition, as a result of the knowledge gained during this study, some recommendations for future work will be presented.

8.1 CONCLUSIONS.

The complex bandpass impulse response of urban mobile radio channels has been measured using a Swept Time-Delay Cross-Correlator(STDCC) channel sounder. Subtle changes to the receiver layout have resulted in a sounder with a simpler, and more accurate, IF-stage than designs used in previous studies. The inherent bandwidth compression of this system makes it an attractive choice for wideband channel probing. However, the interrelationship between all the system factors, as discussed in Chapter 4, means that great care must be taken when specifying a STDCC system, if it is to produce meaningful results.

The transmission conditions at different locations were observed to be highly variable. Consequently, a two-stage characterisation was adopted for both simulation and systems studies. Although a two-stage analysis has been used in previous studies of the systems parameters, it is believed that this is the first time that a Moving Average normalisation has been applied in the processing of wideband data. As a result, all the coefficients necessary to specify a simple, realistic tapped-delay line channel simulator have been produced. In addition, analysing the data in terms of small and large-scale components could explain the dichotomy between the observations of Turin and Cox.

The small-scale signal fluctuations in each echo time-delay cell have been shown to be well modelled as uncorrelated Rayleigh fading. This result unequivocally shows that the small-scale signal variations can be characterised by Gaussian Wide-Sense Stationary Uncorrelated Scattering(WSSUS) statistics. Moreover, it validates the argument for

applying WSSUS statistics in the derivation of the small-scale systems parameters.

The large-scale signal fluctuations in each time-delay cell were shown to be well modelled by a log-normal distribution. In contrast to the small-scale fluctuations, the large-scale amplitude variations in neighbouring time-delays were found to be reasonably correlated. For a practical simulation of the channel, however, only the correlations between adjacent taps would probably be included, with the further restriction that the correlations can be assumed to be zero if the taps are separated by more than $0.3\mu s$.

The basis for selecting the tap delay times is a graph of large-scale mean signal strength, plus and minus one standard deviation, versus excess time-delay(Fig.7.8). By modelling all the log-normal distributions as zero-mean, the mean signal strengths become weighting factors for the taps. Since the number of taps in a practical simulator will be limited, the criteria for selecting the delay times are the magnitudes of the weighting factors and standard deviations, as discussed in Chapters 6 and 7. The concept of selecting the taps in this manner is considerably easier than attempting to ascribe a statistical distribution to the excess time-delays, as has been proposed in earlier studies. The simplicity of using this approach to channel simulation was highlighted by way of an example of how a 12-tap model may be specified(Chapter 7).

From a systems viewpoint, the large variability in transmission conditions, from location to location, clearly identified the need for formulating the cumulative distributions of the small-scale channel descriptors. Assessment of mobile radio system performance is possible through use of these cumulative distributions, provided there is some correlation between the channel descriptors and the error performance. However, since interest is generally confined to the tails of these distributions, caution has to be exercised in their use, because the tails are particularly vulnerable to statistical sample size fluctuations. Nevertheless, slightly more than 50% of locations surveyed gave rise to values of $B_{0.5}$ less than 300KHz. Therefore, regardless of the absolute rate of occurrence of very small coherence bandwidths, it has been incontrovertibly shown that

wideband systems, such as the pan-European(GSM) scheme, will definitely require the use of a channel equaliser for satisfactory performance. In addition, the case was made for using zero-padding in the calculation of the Frequency Correlation Function, in order to achieve sufficiently fine frequency resolution. This is particularly relevant when the average power delay profile contains significant echoes at large excess time-delays.

8.2 RECOMMENDATIONS FOR FUTURE WORK.

The main emphasis of this study has been to extract from the measurements, all the coefficients necessary to develop a simple, realistic channel simulator. As this goal has largely been achieved, a future programme should be concerned with the implementation of the model, in both hardware and software.

Due to restrictions on time, no investigation was undertaken of the second-order channel statistics, e.g., Doppler spectra, average fade durations, etc. However, simulations carried out by contributors to the COST 207 programme have shown that use of the 'classical' Doppler spectra at each tap resulted in near identical system performance. Also, the fading rate of the log-normal 'shadow-fading' is generally of the order of one-hundredth of the maximum Doppler frequency, and whilst no results have yet been published on the spectra of the log-normal shadowing, it seems reasonable to assume that it too can be modelled as the classical Doppler shape. Therefore, these factors could be used initially until the second-order statistics have been computed.

As soon as a laboratory channel simulator is available, it will be possible to assess the impact of the propagation path on the error performance of various transmission schemes. The objectives of this study should be to investigate the error mechanisms, and to formulate a 'figure-of-merit' for wideband multipath channels. Moreover, it should then be possible to assess the importance of each of the small-scale channel descriptors.

Finally, the results presented in this thesis are based solely on measurements obtained within the confines of a medium-sized UK city.

Although most future mobile radio systems will probably be introduced into towns and cities first, there will be occasions when the systems will be expected to operate in more rural areas. Furthermore, the advances in 'personal communications' means that future systems will also be expected to operate satisfactorily within buildings. Therefore, a future study should attempt to undertake measurements in these diverse locations, in order to further refine the multipath model already proposed.

To carry out these measurements successfully, changes to the channel sounder will probably be required. Certainly the dynamic range of the system should be improved, so that the fading statistics of longer paths can be unambiguously determined. Also, for measurements within buildings the time resolution would have to be improved, due to the smaller distances that exist between scatterers. However, simply increasing the clock rate of the m-sequence is not the solution, as all the STDCC parameters would need to be reassessed as discussed earlier. The measurement of the fast fading statistics may also require an increase in the rate at which the impulse response is produced, to ensure that deep fades are 'captured'. This could be achieved by varying the scaling factor in the cross-correlator, however, this will probably mean that a stepping-correlator will be required, instead of a swept-correlator, to prevent the autocorrelation function at the output becoming distorted.